**The Dissertation Committee for Damon Constantine Polioudakis certifies that this is the approved version of the following dissertation:**

# Characterizing miRNA Mediated Regulation of Proliferation

**Committee:**

Vishwanath Iyer, Supervisor

Christopher Sullivan

Haley Tucker

Edward Marcotte

Marvin Whiteley

# Characterizing miRNA Mediated Regulation of Proliferation

**by**

**Damon Constantine Polioudakis, B.A.**

**Dissertation**

Presented to the Faculty of the Graduate School of

The University of Texas at Austin

in Partial Fulfillment

of the Requirements

for the Degree of

**Doctor of Philosophy**

**The University of Texas at Austin**

**May 2014**

# Dedication

*I dedicate this work*

*to my family,*

*without all of their love and support I never would have made it this far.*

## Acknowledgements

I would like to thank my advisor Dr. Vishwanath Iyer for his wonderful guidance throughout graduate school. He has provided me with so much support and advice. His door was always open, and he was always available to his students.

I also want to thank the current and former members of the Iyer lab. Dr. Akshay Bhinge and Dr. Patrick Killion mentored me, trained me to think like a scientist, and taught me many experimental skills. Adam Morris gave me so much advice in the late stage of my graduate career, and was always there to bounce ideas off. Nathan Abell worked incredibly hard on this research, and put up with so many of our misfires and dead ends. His dedication is remarkable. Lastly, I especially want to thank Anna Battenhouse, for being so patient, being such a good teacher, and always being willing to spend time helping us. Anna keeps the lab running.

I thank my dissertation committee members: Dr. Edward Marcotte, Dr. Chris Sullivan, Dr. Haley Tucker, and Dr. Marvin Whiteley for their time and insightful comments and suggestions.

Finally, I want to thank my wonderful family. They have provided me so much unconditional support and encouragement throughout the years. My grandfather, Keith Mather, originally inspired me to seek a career in science. My mother and father have nurtured my interest in science as long as I can remember, and always encouraged me to pursue my dreams. And lastly, I especially want to thank my sister, Heather, for putting up with me for so many years and giving her time so that I could finish my studies.

# Characterizing miRNA Mediated Regulation of Proliferation

Damon Constantine Polioudakis, Ph.D.

The University of Texas at Austin, 2014

Supervisor: Vishwanath Iyer

Cell proliferation is a fundamental biological process, and the ability of human cells to transition from a quiescent to proliferative state is essential for tissue homeostasis. Most cells in eukaryotic organisms are in a quiescent state, but on appropriate physiological or pathological stimuli, many types of somatic cells may exit quiescence, re-enter the cell cycle and begin to proliferate. The ability of cells to remain viable while quiescent, exit quiescence and re-enter into the cell cycle is the basis for varied physiological processes such as wound healing, lymphocyte activation and hepatocyte regeneration, but is also a hallmark of cancer. The transition of mammalian cells from quiescence to proliferation is accompanied by the differential expression of several microRNAs (miRNAs) and transcription factors. Our understanding of miRNA biology has significantly improved, but the miRNA regulatory networks that govern cell proliferation are still largely unknown.

We characterized a miR-22 Myc network that mediates proliferation through regulation of the interferon response and multiple cell cycle arrest genes. We identified several cell cycle arrest genes that regulate the effects of the tumor suppressor p53 as direct targets of miR-22, and discovered that miR-22 suppresses interferon gene expression. We go on to show that miR-22 is activated by the transcription factor Myc as quiescent cells enter proliferation, and that miR-22 represses the Myc transcriptional repressor MXD4, mediating a feed forward loop to elevate Myc expression levels.

To more effectively determine miRNA targets, we utilized a combination of RNA-induced silencing complex immunoprecipitations and gene expression profiling.

Using this approach for miR-191, we constructed an extensive transcriptome wide miR-191 target set. We show that miR-191 regulates proliferation, and targets multiple proto-oncogenes, including CDK9, NOTCH2, and RPS6KA3.

Recent advances in determining miRNA targetomes have revealed widespread non-canonical miRNA-target pairing. We experimentally identified the transcriptome wide targets of miR-503, miR-103, and miR-494, and observed evidence of non-canonical target pairing for these miRNAs. We went on to confirm that miR-503 requires pairing outside of the canonical 5' seed region to directly target the oncogene DDHD2. Further bioinformatics analysis implicated miR-503 and DDHD2 in breast cancer tumorigenesis.

# Table of Contents

# List of Tables

## List of Figures

# Chapter 1 Introduction

## 1.1 CELL PROLIFERATION

Cell proliferation is a basic biological process, and the ability of human cells to transition from a quiescent to proliferative state is required for tissue homeostasis. The majority of cells in an adult organism primarily exist in a quiescent state that is actively maintained by various genetic programs (1, 2). The ability of cells to re-enter the cell cycle given the appropriate stimuli is vital for numerous physiological processes. Maintenance of proliferative potential is necessary for lymphocyte activation, hepatocyte regeneration, and wound healing (1-6). The transition from quiescence to proliferation of cells re-entering the cell cycle is exquisitely controlled by multiple check points and fail safe mechanisms, but is still susceptible to deregulation by disruption of the necessary pathways. Disruption of the actively maintained state of quiescence and sustained proliferative signaling are two of the basic requirements for tumorigenesis (7).

### 1.1.1 The role of proliferation in cancer

The ability to chronically sustain proliferative signaling is arguably the most fundamental trait of cancer. Cell cycle deregulation is essential for tumorigenesis. Cancer cells possess numerous other physiological abnormalities, typically resistance to apoptosis, angiogenesis, and invasion and metastasis; however, cancer is often considered to be foremost a disease of the cell cycle (7). The pathways that control proliferation in normal cells are generally perturbed in cancer (7, 8). Many cell cycle regulators that control reentry and progression through the cell cycle are altered in cancer cells, and a number of cancer driver genes are direct regulators of the cell cycle (7-9). Specifically, the transition to G1 is deregulated in many cancers, allowing cancer cells to avoid entering quiescence and halting proliferation (4).

### 1.1.2 Primary human dermal fibroblasts as a model for proliferation

Primary human dermal fibroblasts are an excellent model to study the genetic pathways that regulate the transition from quiescence to proliferation. Primary fibroblasts

may be induced to enter or exit a quiescent state in response to exposure to or deprivation from serum containing growth factors. Fibroblast proliferation plays a central role in the wound healing process, and serum stimulation of fibroblasts produces a genetic program similar to that of wound healing (9). The wound response program is similar at the physiological level to cancer progression; wounding activates signaling cascades that lead to epithelial and fibroblast cell proliferation, matrix remodeling, cell migration, and angiogenesis (9). At the genetic level, many of the genes differentially expressed in fibroblasts following serum stimulation are also differentially expressed in tumor cells, associated fibroblasts, or both, and include a number of key cell cycle regulators (10). In addition, the expression profiles of proliferating fibroblasts are good predictors of cancer progression (7, 8, 10). Multiple protein coding genes and miRNAs are differentially expressed between proliferating and quiescent fibroblasts (7-9, 11).

## 1.2 miRNAs

One of the main classes of regulators that have been shown to mediate cell proliferation and tumorigenesis are miRNAs (4, 12). miRNAs are short, noncoding RNAs that post-transcriptionally regulate gene expression. They are ubiquitous regulators of multiple cellular pathways and biological processes such as metabolism, immune defense, development, differentiation, proliferation, and apoptosis (9, 13, 14). miRNAs are predicted to regulate ~50% of all human protein coding genes (14). miRNAs have been shown to be involved in numerous pathologies, such as cardiovascular disease, viral diseases, and cancer development (15-17). There are currently over 1,800 human miRNAs reported in the miRNA database miRBase (18). miRNAs are hypothesized to function by subtly regulating the expression of numerous targets; although the changes in expression for each individual target are generally small, the coordinated regulation of multiple targets is thought to have strong phenotypic effects.

### 1.2.1 Biogenesis

In the standard miRNA biogenesis pathway, long primary miRNA (pri-miRNA) transcripts are typically produced by RNA polymerase II, although some are products of

RNA polymerase III (19). Roughly one third of known miRNAs are located in introns of protein coding genes and are co-transcribed with the host gene (19). Primary transcripts contain an ~60-90 nucleotide hairpin structure that is the pre-miRNA (20). The pre-miRNA is released from the pri-miRNA in the nucleus by cleavage catalyzed by the RNase III endonuclease Drosha (20). The pre-miRNA is exported from the nuclease by Exportin 5, and further cleaved by the RNase III endonuclease Dicer to produce an ~22 base pair RNA duplex composed of the eventual mature miRNA paired to the miRNA* strand (20). One of the two strands of the RNA duplex is loaded into the Argonaute-2 (Ago2) protein, a core component of the RNA-induced silencing complex (RISC) (19). There are a few miRNAs that are produced by alternative pathways that typically replace one or more of the standard precursor processing steps (21).

### 1.2.2 Mode of action

miRNAs are the targeting component of RISC, and guide binding of RISC to target transcripts by nucleotide pairing. Only one strand of the mature miRNA duplex is loaded into RISC, and is selected based on thermodynamic asymmetry of the duplex, with the strand with lower stability at the 5' end being incorporated into RISC (22). miRNAs direct target pairing of transcripts by pairing to sites of imperfect complementarity. The exact mechanism of miRNA target selection remains unclear; however, a set of standard rules have been experimentally established: (1) miRNA-target interactions are primarily mediated by the "seed" region, a continuous 6 to 8 nucleotide sequence at the 5' end of the miRNA that forms Watson-Crick pairing with the target; (2) regulation of gene expression is predominantly mediated through pairing to the 3' UTR of the target mRNA, and not the 5'UTR or CDS; and (3) target site context matters, efficacy greatly increases for sites located nearer the ends of 3' UTRs and in unstructured regions with greater site accessibility (23, 24). Perfect pairing of the miRNA to the target results in target cleavage, although this is rarely observed in mammals (23). Imperfect pairing, including standard seed pairing, accounts for the vast majority of miRNA-target interactions, and results in translational repression and decreased transcript stability (25).

### 1.2.3 Alternative modes of target pairing

Transcriptome wide gene expression analysis following miRNA perturbation combined with sequence conservation analysis has shown that efficacious miRNA-target pairing is mediated through perfect pairing of the seed region (23, 24, 26). More recently methodologies to profile transcriptome wide RISC occupancy have revealed extensive RISC binding to transcripts with imperfect or nonexistent seed matches (27-30). This non-canonical miRNA target pairing has been observed to occur in up to 60% of miRNA-target pairs (27). However, mediation of gene expression by non-canonical target pairing is modest at most, and observed to have no significant effect on gene expression in multiple studies (24, 29, 30). This discrepancy may be due to differences in miRNA target identification methods, reliance on target site conservation, and dependence on seed presence.

### 1.2.4 miRNAs in tumorigenesis

Multiple miRNAs may function as either tumor suppressors or oncogenes. miRNAs are located in 50% of all fragile regions or cancer associated sites, with oncogenic miRNAs mainly located in amplified regions and tumor suppressor miRNAs generally located in deleted regions (19, 31). Disruption of the miRNA biogenesis pathway typically results in tumorigenesis (32). miRNAs have been shown to regulate the function of many of the major processes involved in tumorigenesis, including proliferation, migration, invasion, and angiogenesis (16, 19). The first miRNAs shown to be involved in cancer were those composing the miR-15a/miR-16-1 cluster, which is frequently deleted in chronic lymphocytic leukemia, and targets several promoters of cell cycle progression, including CDK6, CARD10, and CDC27 (33). miR-21 is the most commonly reported miRNA to function as an oncogene, and does so in multiple cancer types including glioblastoma, hepatocellular carcinoma, prostate cancer, and breast cancer, and depending on context targets multiple tumor suppressors including p53 and PTEN (34-36).

# Chapter 2 A Myc–microRNA network promotes exit from quiescence by suppressing the interferon response and cell-cycle arrest genes

## 2.1 ABSTRACT

The transition of mammalian cells from quiescence to proliferation is accompanied by the differential expression of several miRNAs and transcription factors. However, the interplay between transcription factors and miRNAs in modulating gene regulatory networks involved in human cell proliferation is largely unknown. Here we show that the miRNA miR-22 promotes proliferation in primary human cells, and through a combination of RISC immunoprecipitation and reporter assays, we identified multiple novel targets of miR-22, including several cell-cycle arrest genes that mediate the effects of the tumor-suppressor p53. In addition, we found that miR-22 suppresses interferon gene expression by directly targeting HMGB1 and IRF5, preventing activation of IRF3 and NF-κB, which are activators of interferon genes. The expression of interferon genes is elevated in quiescent cells and their expression is inhibitory for cell proliferation. In addition, we find that miR-22 is activated by the transcription factor Myc when quiescent cells enter proliferation, and that miR-22 inhibits the Myc transcriptional repressor MXD4, mediating a feed-forward loop to elevate Myc expression levels. Our results implicate miR-22 in down regulating the anti-proliferative p53 and interferon pathways and reveal a new transcription factor-miRNA network that regulates the transition of primary human cells from quiescence to proliferation.

## 2.2 INTRODUCTION

miRNAs have emerged as important regulators of cell proliferation driving tumorigenesis, and several studies have functionally linked miRNAs and transcription factors in regulatory networks that govern cell proliferation and cancer (37, 38). The miRNA miR-22 has been reported to act as both a proto-oncogene in various cancer cell lines and a tumor suppressor in other cancer cell lines, as well as being involved in panic disorder, hypoxia signaling, differentiation, and cardiomyocyte hypertrophy (21-24). miR-22 was shown to promote cell proliferation, invasion, and survival in multiple

cancer cell types by regulating PTEN (39-41). However, miR-22 has also been demonstrated to repress proliferation by inhibiting the binding partners, MAX and MCYBP, of the oncogene Myc (42-44). In addition, miR-22 was shown to inhibit cancer progression by inducing cellular senescence (45), and to repress cell migration and invasion in ovarian cancer (46). miR-22 has also been linked to the p53 regulatory network, is a direct target of the tumor suppressor p53, and mediates p53 induced cell cycle arrest and apoptosis in colon cancer (43). Despite the broad involvement of miR-22 in tumorigenesis in various cancers, the activity of miR-22 in primary cells has not been explored.

In this study we investigate the regulation of cell proliferation in primary cells by miR-22, and identify a new regulatory network mediating the transition of primary cells from quiescence to proliferation. This network involves the activation by the oncogene Myc of miR-22, which in turn suppresses the interferon and cell cycle arrest pathways active in quiescent cells, thus facilitating their re-entry into the cell cycle. Our data reveals novel cross-talk between the p53 and Myc regulatory networks that is mediated by mir-22.

## 2.3 MATERIALS AND METHODS

### 2.3.1 Normal cell culture conditions

HeLa cells and human foreskin fibroblasts (ATCC CRL #2091) were maintained in DMEM (Dulbecco's Modified Eagle's Medium) supplemented with 10% FBS (Fetal Bovine Serum) at 37°C under 5% $CO_2$. Fibroblasts were made quiescent by first growing them under normal conditions until 40% confluent, then replacing medium with DMEM supplemented with 0.1% FBS and growing them for a further 48 hours.

### 2.3.2 Fibroblast serum stimulation

Fibroblast cell cultures were grown under normal cell culture conditions until 40% confluent. Medium was removed and cell cultures were washed 3 times with PBS (Phosphate Buffered Saline). Replacement medium was DMEM supplemented with 0.1%

FBS and 100 units penicillin-streptomycin. Cell cultures were grown at 37°C for 48 hours. Cell cultures were washed 1x with PBS. Reference cell cultures were harvested following total RNA Isolation. Replacement medium was DMEM supplemented with 10% FBS and 100 units penicillin-streptomycin. Separate cell cultures were allowed to proliferate under serum-rich conditions for time-points of 5, 10, 20, 30, 60, and 180 minutes. At the end of each of these time points, cell cultures were harvested for total RNA isolation using the TRIzol reagent (Invitrogen) according to manufacturer's protocol.

### 2.3.3 Myc overexpression

HeLa cell cultures were grown under normal cell culture conditions. 6-well plates were seeded with 1.5 x $10^5$ cells/well. Cell cultures were allowed to grow for 24 hours. Cell cultures were lipotransfected with Invitrogen Lipofectamine 2000 according to the manufacturer's protocol (for DNA plasmid transfection). Myc overexpression plasmid was purchased from Open Biosystems (MHS1010-57504, Human MGC Verified FL cDNA, CloneID = 298544). GFP co-transfection plasmid was purchased from Clontech (Vector=pEGFP-N1, Accession=U55762). Cell cultures were grown under normal cell culture conditions for 48 hours and then harvested for total RNA.

### 2.3.4 Myc knockdown

Myc-specific siRNA and negative control siRNA were purchased from Dharmacon. HeLa cell cultures were grown under normal cell culture conditions. 6-well plates were seeded with 1.5 x $10^5$ cells/well. Cell cultures were allowed to grow for 24 hours. Cell cultures were lipotransfected with Invitrogen Lipofectamine 2000 according to the manufacturer's protocol (for siRNA transfection). Cell cultures were grown under normal cell culture conditions for 48 hours and then harvested for total RNA. For serum stimulation experiments under conditions of Myc knockdown, fibroblasts were transfected with siRNAs against Myc or negative control siRNA and cells were starved into quiescence. Quiescent fibroblasts were then serum-stimulated for the indicated time points and miR-22 expression was assayed by quantitative qRT-PCR (qRT-PCR).

### 2.3.5 miRNA enrichment, labeling, and microarrays

Ambion FlashPAGE Fractionator System, Pre-cast Gels, Buffer Kit, and Clean-Up Kit were used according to the manufacturer's protocol. Invitrogen ULYSIS 546 Nucleic Acid Labeling Kit was used for the typical Cy3 sample. Invitrogen ULYSIS 647 Nucleic Acid Labeling Kit was used for the typical Cy5 sample. The kits were used according to the manufacturer's protocol. Ambion FlashPAGE Clean-Up Kits were used for removal of unincorporated dye according to the manufacturer's protocol. Labeled small RNAs were hybridized to dual channel miRNA microarrays, quantitated and normalized. The microarrays were printed in house with the v1 Ambion array probe set that includes 281 human miRNAs registered in miRBase.

### 2.3.6 Real time miRNA PCR

Quantitative real-time PCR was performed for miR-22 using Applied Biosystems TaqMan miRNA Assays according to the manufacturer's protocol.

### 2.3.7 Quantitative Reverse-Transcription PCR for interferon stimulated genes

RNA from quiescent and proliferating fibroblasts was extracted with the TRIzol reagent (Invitrogen) and reverse transcribed using random hexamers and the Superscript II system from Invitrogen. PCR was performed using the SYBR GREEN PCR Master Mix from Applied Biosystems. The target gene mRNA expression was normalized to the expression of GAPDH and relative mRNA fold changes were calculated by the ΔΔCt method.

### 2.3.8 Myc binding site detection and motif analysis

Chromatin immunoprecipitation for Myc was performed as previously described (47). ChIP-enriched DNA was sequenced by Illumina sequencing technology. Short reads from the ends of DNA fragments were mapped back to the genome using Maq. Conservation was quantified according to the mammalian conservation track from UCSC, specifically, the 17-species conservation and alignment track (phastCons17way). Conservation was evaluated for each locus through local installation of a portion of

UCSC's Genome Browser and command-line execution of UCSC toolsets (hgWiggle) that retrieved conservation metrics for a specified genomic range. The mean conservation of conserved motifs was 90% (standard deviation is 6.7%) while the mean conservation of the non-conserved motifs was 0.6% (standard deviation is 0.3%). The presence of proximal CpG islands was evaluated using the CpG enrichment track (cpgIslandExt). Conserved binding motif coordinates for Myc across the genome were obtained from UCSC's catalog of conserved binding sites for all mammalian transcription factors [TFBS Conserved]. Motif search was performed within 20 kb upstream of the miRNA start sites. For the ChIP-PCR assay, fibroblasts were starved into quiescence and then serum stimulated to proliferate. Cells were harvested 3 hours after stimulation and ChIP was performed as described above. Myc binding was confirmed using quantitative PCR performed using the SYBR GREEN PCR Master Mix from Applied Biosystems. Fold enrichment was calculated with respect to the negative control by the ΔΔCt method.

### 2.3.9 RNA oligos, transfections, and microarray analysis

miR-22 guide and anti-guide mature sequences were obtained from miRBase (http://microRNA.sanger.ac.uk/sequences/) while sequences for siRNA against GFP (control siRNA) were obtained from (48). The corresponding RNA oligos were ordered from Invitrogen or IDT and annealed in RNA annealing buffer (20 mM HEPES, pH 7.3, 50 mM KCl, 2 mM $MgCl_2$). Both the miR-22 and control siRNA oligos contain the same chemical modifications of 5' phosphate and 3' OH. The RNA duplexes were transfected at a final concentration of 100 nM using Lipofectamine 2000 according to the manufacturer's instructions. The miR-22 inhibitor and control were a miRCURY Locked Nucleic Acid (LNA) miRNA Inhibitor and Negative Control Inhibitor obtained from Exiqon and transfected at a final concentration of 10 nM using Lipofectamine 2000. Poly I:C was obtained from Sigma Aldrich and co-transfected at a final concentration of 200 ng/ml with miR-22 or control siRNA duplexes as described above. RNA from transfected cells was extracted using the Trizol reagent (Invitrogen), amplified and hybridized to in-house cDNA expression microarrays as previously described (49). Functional analysis for repressed genes was performed using the freely available online software DAVID (50).

### 2.3.10 Flow cytometry

Fibroblasts were seeded at 50,000 cells per well in 6 well plates. Cells were cultured in DMEM supplemented with 10% FBS. Cells were allowed to grow 24 hours, and then media was replaced with low serum DMEM 0.1% FBS. 8 hours after replacement with DMEM 0.1% FBS, cells were transiently transfected with miR-22 or control siRNA duplexes (100 nM final concentration). 28 hours after transfection, cells were trypsinized, washed with PBS, and fixed for 24 hours in 70% ethanol at -20°C. After ethanol fixation, cells were washed with Stain Buffer (BD Pharmingen), incubated 30 minutes with FITC Mouse Anti-Human Ki67 antibody (BD Pharmingen), washed, and resuspended in 500 μl Stain Buffer with Propidium Iodide Staining Solution (5 μg/ml) (BD Pharmingen). Flow cytometry analysis for Ki67 was done using a FACsCalibur flow cytometer and 10,000 events above threshold levels were counted for each sample (BD Biosciences). Data analysis was done using FlowJo.

### 2.3.11 Luciferase assays

Entire 3' UTRs, if possible, or at least 0.8 to 1.2 kb around the predicted miR-22 site in a 3' UTR was cloned into a Renilla vector under a CMV promoter. For CARF, we included the last exon in addition to the 3'UTR for the luciferase assays. miRNA seed site mutants were made by mutating 3 base pairs in the 6-mer seed sequence using Agilent's QuikChange MultiSite-Directed Mutagenesis Kit. Another vector containing the Firefly luciferase under a CMV promoter was used as a normalization control. HEK293 cells were plated in 24-well plates at $10^5$ cells/well and Renilla and Firefly vectors were co-transfected at 25 ng each along with 100 nM final concentration of miR-22. Control siRNA was used as a negative control. Cells were harvested 24 hours post-transfection and luciferase activity was measured using the Promega Dual Luciferase kit according to manufacturer's instructions. Fold suppression was calculated as the ratio of Renilla to Firefly values for miR-22 normalized by the mean of the Renilla to Firefly ratios for the control siRNA. For the NF-κB reporter assays, HEK293 cells were plated in 24-well plates at 1 x $10^6$ cells/well. 24 hours after plating, cells were transfected with 100 ng/well of NF- κB reporter plasmid (SABiosciences), and co-transfected with poly I:C

and miR-22 or the control siRNA. Cells were harvested 16 hours post-transfection and luciferase activity was measured as described above. For Fig. 5E and F, we performed luciferase assays using a pGL3 promoter plasmid (Promega) as previously described (51). Around 550 bp of PCR-amplified insert from each of 4 putative Myc binding sites was cloned into the vector.

### 2.3.12 Western blots

For westerns of phosphorylated and native IRF3, HeLa cells were seeded in 6-well plates at 8 x $10^4$ cells/well and co-transfected with 200 ng/ml poly I:C and miR-22 or the control siRNA. 12 hours after transfection, cells were harvested for protein analysis. Cell lysates were separated on 10% SDS-PAGE gels and proteins were transferred onto PVDF membranes. Membranes were blocked with 5% milk in TBST (25 mM Tris pH 8.0, 150 mM NaCl, 0.05% Tween-20) and probed with corresponding primary antibodies against specific proteins (phosphorylated and native IRF3: Cell Signaling Technology). HRP-conjugated secondary antibodies (Santa Cruz Biotechnology) were used to detect primary antibodies, and proteins were visualized by chemiluminescence.

For Westerns of putative miR-22 targets, primary human fibroblasts were seeded in 6-well plates at 2 x $10^4$ cells/well in DMEM supplemented with 10% FBS. 24 hours after plating, media was replaced with low serum DMEM 0.1% FBS. The media for proliferating samples was replaced with more DMEM 10% FBS. 48 hours after serum starvation, miR-22 or control siRNA was transfected at a 100 nM concentration, and proliferating and quiescent samples were lysed. Transfected cells were lysed at 12 hr, 24 hr, 48 hr, or 72 hr post transfection. Cell lysates were separated on 4-20% gradient SDS-PAGE gels (Biorad) and proteins were transferred onto PVDF membranes. Membranes were blocked with 5% milk in TBST and probed with corresponding primary antibodies against specific proteins (HMGB1: Cell Signaling Technology, IRF5: Abcam ab33478, REDD1: Abcam ab106356, TP53INP1: Abcam ab9755, p21: Abcam ab7960, CARF: ab88322, MXD4: Santa Cruz Biotechnology sc-771, MYC: Santa Cruz Biotechnology sc-764X). Actin was used as a loading control (Actin: Santa Cruz Biotechnology sc-

10731). HRP-conjugated secondary antibodies (Santa Cruz Biotechnology sc-2004 and sc-2005) were used to detect primary antibodies, and proteins were visualized by chemiluminescence. Westerns shown are for the time point that showed the strongest repression.

### 2.3.13 Ago2 immunoprecipitation

We adapted the protocol developed by Hendrickson *et. al.* (52) for immunoprecipitating Ago2-mRNA complexes. Briefly, HeLa cells were grown in 10 $cm^2$ tissue culture plates and transfected with either miR-22 mature duplexes at a final concentration of 100 nM or mock transfected. After 24 hours, 0.5 ml of lysis buffer was added drop-wise onto the cell monolayer followed by incubation at 4°C for 30 minutes. Cell lysate was collected by scrapping and cleared by centrifugation at 14,000 rpm at 4°C. Cleared lysate was then incubated with 50 µl of protein-G beads (Roche) for 3 hours at 4°C (pre-clearing). Before pre-clearing, 50 µl of the cleared lysate was removed for total RNA estimation. Pre-cleared lysate was incubated with 15 µg of Ago2 antibody (ab57113, Abcam) and incubated at 4°C overnight. The next day, 50 µl of protein-G beads were added to the lysate and incubated for 4 hours at 4°C. Beads were washed 8 times with lysis buffer and Ago2-RNA complexes were extracted by adding 1 ml Trizol reagent (Invitrogen) directly to the beads. RNA extraction was carried out as per the manufacturers instructions.

### 2.3.14 Cell counting assays

For miRNA overexpression experiments, fibroblasts were seeded at 20,000 cells per well in 6 well plates. Cells were cultured in DMEM supplemented with 10% FBS. Cells were allowed to grow 24 hours, and then media was replaced with low serum DMEM 0.1% FBS. 24 hours after replacement with DMEM 0.1% FBS, cells were transiently transfected with miR-22 or siGFP duplexes (100 nM final concentration). 0, 24, 48, 72, and 96, hours after transfection, cells were trypsinized, and counted in a hemacytometer. 5 fields were averaged for each biological replicate. For miRNA inhibition experiments, fibroblasts were seeded at 20,000 cells per well in 6 well plates.

Cells were cultured in DMEM supplemented with 10% FBS. Cells were allowed to grow 24 hours, and then transiently transfected with miR-22 miRCURY Locked Nucleic Acid (LNA) miRNA Inhibitor and Negative Control Inhibitor obtained from Exiqon (10 nM final concentration). 0, 24, 48, 72, and 96 hours after transfection, cells were trypsinized, and counted in a hemacytometer. 5 fields were averaged for each biological replicate.

#### 2.3.15 Statistical analysis

Statistical significance was estimated using a one-sided Student's t-test.

## 2.4 RESULTS

### 2.4.1 miR-22 is induced during the transition from quiescence to proliferation and promotes proliferation

Microarray expression profiling identified multiple miRNAs that are differentially expressed in primary human fibroblasts induced to transition from quiescence to proliferation by serum stimulation (Figure 2.1A). We focused on miR-22 because it was one of the miRNAs most strongly and consistently induced by serum stimulation, and bioinformatic analysis suggested that it could be transcriptionally regulated by immediate-early transcription factors (not shown). qRT-PCR for miR-22 expression after serum stimulation of fibroblasts in an independent biological replicate experiment confirmed its induction (Figure 2.1B).

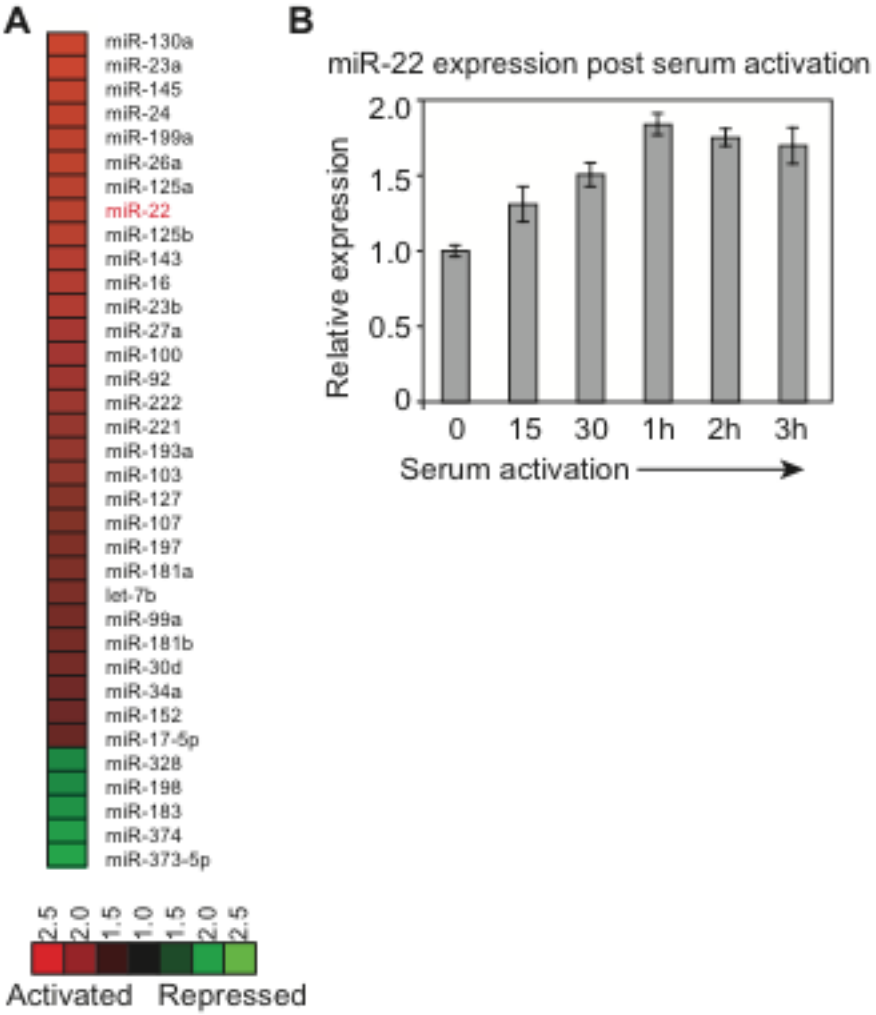


Figure 2.1 miR-22 is induced during the transition from quiescence to proliferation.

(A) Heat map showing the response of miRNAs to serum stimulation of quiescent primary human fibroblasts measured using microarrays. Ratios displayed represent the average activation across all measured time-points after serum stimulation (5, 10, 20, 30, 60, and 180 minutes). miRNAs shown were activated or repressed greater than 1.5 fold on average in serum stimulated compared to serum starved cells. (B) Independent qRT-PCR verification of miR-22 expression during the transition from quiescence to proliferation. The Y-axis indicates expression of miR-22 after serum stimulation relative to quiescence, at each of the indicated time points on the X-axis. Data shown is for a representative experiment measured in quadruplicate (mean ± s.d.).

Since miR-22 was activated during the transition of primary human cells from quiescence to proliferation, we hypothesized that miR-22 regulates proliferation in primary human cells. To test this hypothesis, we transiently overexpressed miR-22 by transfecting the mature form of the miR-22 duplex RNA into quiescent fibroblasts and assayed cell growth. Compared to the control, miR-22 transfected cells showed increased growth by cell counting assay (Figure 2.2A). Conversely, proliferating cells in which we introduced a stable antisense inhibitor of miR-22 showed decreased cell growth (Figure 2.2B). To further explore the effect of miR-22 on cell growth we assayed the expression of the proliferation marker Ki67 (53, 54). We transfected miR-22 into quiescent fibroblasts and counted cells expressing Ki67 protein using flow cytometry. miR-22 transfection significantly increased the percentage of Ki67 positive cells compared to control, indicating that miR-22 activates proliferation (Figure 2.2C). We confirmed this result by performing a biologically independent experiment where we transfected miR-22 into both quiescent fibroblasts and proliferating fibroblasts, and measured Ki67 expression by qRT-PCR. Compared to the control, miR-22 transfected cells showed elevated levels of Ki67 in both quiescent fibroblasts and proliferating fibroblasts (Figure 2.2D & 2.3). In addition, inhibition of miR-22 decreased levels of Ki67 compared to the control in cells exiting quiescence (Figure 2.2E).

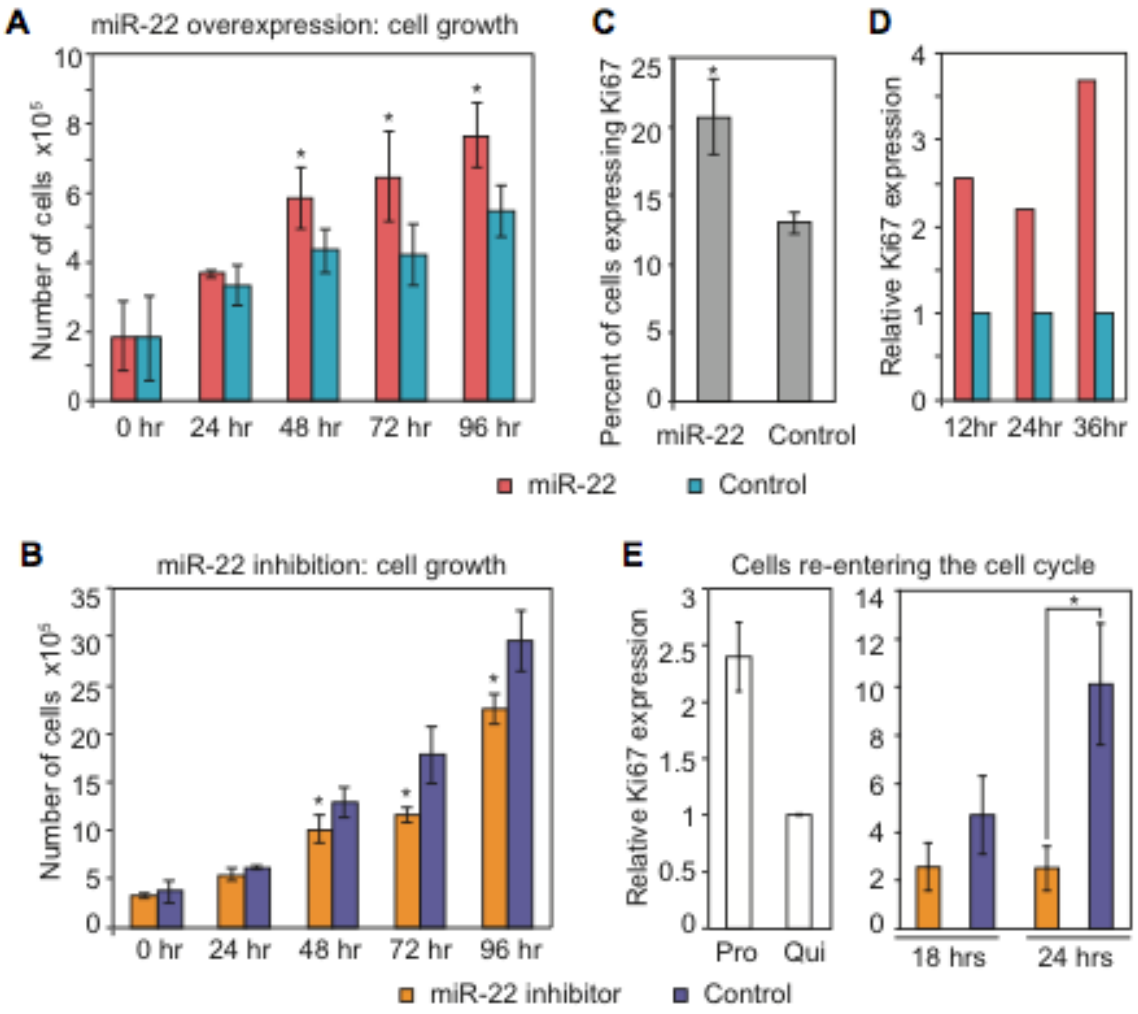


Figure 2.2 miR-22 activates proliferation.

(A) Cell growth assay following miR22 overexpression. Average cell number following miR-22 or control siRNA transfection is shown for each time point indicated. Error bars denote ± s.d., n=3. (B) Cell growth assay following miR-22 inhibition. Average cell number following transfection of a Locked Nucleic Acid (LNA) targeting miR-22 or a LNA negative control is shown for each time point indicated. Error bars denote ± s.d., n=3. (C) Flow cytometry analysis for proliferation marker Ki67 of miR-22 transfected quiescent fibroblasts. miR-22 transfected fibroblasts showed a larger population of cells expressing Ki67 compared to control siRNA transfected fibroblasts. The Y-axis shows the percentage of cells expressing Ki67. Bars are the mean percentage of cells expressing Ki67 and error bars denote the mean ± s.d, n=4. (D) qRT-PCR data for Ki67 expression in quiescent fibroblasts transfected with miR-22 duplexes compared to control siRNA. miR-22 transfected fibroblasts show elevated levels of Ki67 expression as compared to control at the indicated time points. Ki67 expression was normalized using GAPDH

Fig 2.2 continued.
mRNA levels and fold changes were normalized with respect to the control transfection. (E) Inhibition of miR-22 decreases proliferation as measured by Ki67 expression. Quiescent fibroblasts were transfected with a LNA miR-22 inhibitor or LNA control. 24 hours post transfection, cells were serum stimulated to proliferate for 18 or 24 hours prior to harvesting for qRT-PCR. Y-axis indicates relative Ki67 expression levels compared to quiescent cells. Bars indicate the normalized mean expression, and error bars denote ± s.d, n=3. Control panel depicts Ki67 expression in normally proliferating fibroblasts and serum starved quiescent fibroblasts. GAPDH was used as a control for normalizing input RNA levels. For A, B, C, and E, P-values were estimated by Student's t-test. *, P<0.05

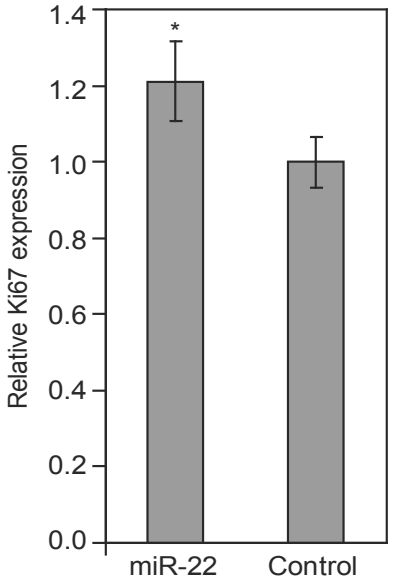


Figure 2.3 miR-22 elevates levels of Ki67 in proliferating fibroblasts.

miR-22 or control siGFP was transfected into normally growing fibroblasts, and cells expressing Ki67 above threshold levels were quantified by flow cytometry. The column graph shows Ki67 expression levels relative to the control, which was set to a value of 1.0. Bars indicate the mean, and error bars denote ± s.d., n=3. *P*-values were estimated by Student's t-test. *, P<0.05.

### 2.4.2 Identifying miR-22 targets by microarrays

To identify the downstream targets of miR-22 in proliferating fibroblasts, we overexpressed miR-22 by transfecting miR-22 duplexes and then analyzed gene expression using microarrays, relying on the fact that miRNAs frequently cause down regulation of their mRNA targets (15, 55). In order to investigate whether this approach

was able to identify miR-22 targets, we analyzed the 3' UTRs of genes that were down regulated following miR-22 transfection for enrichment of the miR-22 seed match sequence. We also performed the same experiment and analysis in HeLa cells. In both cell lines, 6-mer matches to nucleotides 2-7, the miR-22 seed region, were significantly enriched in genes repressed when miR-22 was overexpressed ($P < 10^{-8}$ assuming a binomial model, Figure 2.4A & B). Thus, genes whose mRNAs were down regulated in response to high levels of miR-22 contained a significant proportion of direct targets of miR-22.

In addition to conducting gene expression profiling following miR-22 overexpression in proliferating cells, we also transfected miR-22 duplexes into fibroblasts that were rendered quiescent by serum deprivation, and analyzed the resulting gene expression changes and corresponding seed enrichment as described above. Although there was a significant enrichment of seed matches to the 5' end of miR-22 in the 3' UTRs of the repressed genes ($P < 10^{-4}$ assuming a binomial model, Figure 2.4C), the magnitude of this enrichment was much lower than that observed for genes that were repressed by miR-22 during proliferation, suggesting that many mRNAs down regulated by miR-22 in quiescent cells may be indirect targets.

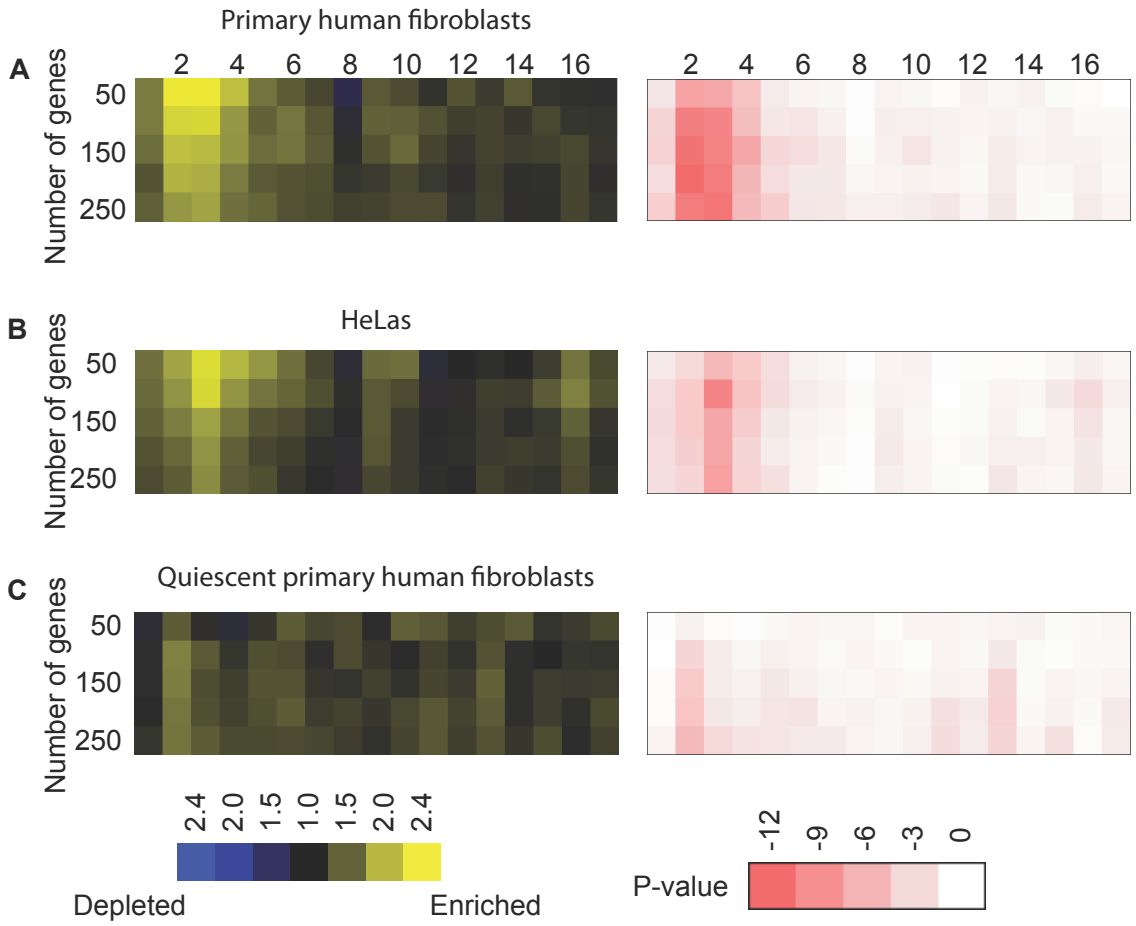


Figure 2.4 Seed match enrichment.

Seed match enrichment among miR-22 targets identified by expression profiling in (A) proliferating fibroblasts, (B) HeLa cells, and (C) quiescent fibroblasts. Left panels indicate enrichment and right panels indicate significance of enrichment for each cell type. Gene expression was assayed using cDNA microarrays after miR-22 transfection. Genes were ranked in descending order in cumulative sets of 50 from most strongly repressed to least repressed, and miR-22 seed match enrichment in the 3' UTR of genes in each set was calculated. The vertical axis shows cumulative gene sets from 50 most strongly repressed, to 250 most strongly repressed. Enrichment was calculated for each consecutive 6-mer along the miRNA, with values displayed in yellow indicating enrichment and blue indicating depletion. Background frequencies for each seed were estimated from the 3' UTRs of all genes represented on the array. P-values were calculated as described in the text assuming a binomial model. The $\log_{10}$ of the *P*-value is plotted as indicated by the pink color scale. Each value on the horizontal axis indicates the start position of a 6-mer from the 5' end of the miRNA. 6-mers starting at positions 2-4 were significantly enriched over background.

### 2.4.3 miR-22 inhibits genes involved in cell-cycle arrest

miR-22 overexpression repressed several cell cycle related genes, suggesting miR-22 may regulate proliferation through repression of cell cycle arrest genes. From the miR-22 overexpression and gene expression profiling experiments we selected genes for further analysis that were cell cycle related, repressed by miR-22 overexpression, and contained miR-22 target sites. Of these genes, TP53INP1, REDD1 (also known as DDIT4) and p21 (also known as CDKN1A) are transcriptionally activated by the tumor suppressor p53 (56-58), while CARF (also known as CDKN2AIP) enhances p53 function and induces premature senescence in primary fibroblasts (59). TP53INP1, p21 and CARF have a functional role in inducing cell-cycle arrest (58-60) while REDD1 is a DNA-damage inducible protein involved in apoptosis (57). TargetScan and RNA22 predicted REDD1, TP53INP1 and p21 as miR-22 targets. Interestingly, CARF did not show miR-22 seed sequences in its 3' UTR but showed multiple seed matches in its last exon.

To determine whether these genes were direct targets of miR-22, we used a strategy based on Ago2 immunoprecipitations (IPs) (Figure 2.5) (52, 61). Ago2 is an essential component of the RNA-induced silencing complex (RISC) that is directed to target mRNAs by the miRNA guide strand (23). Hence, changes in Ago2 occupancy on a mRNA that occur in a miR-22 dependent manner can serve to identify direct targets. We measured Ago2 occupancy of candidate target mRNAs by immunoprecipitating Ago2-mRNA complexes and quantifying enrichment of the purified transcripts by qRT-PCR. We performed parallel Ago2 IPs in HeLa cells that were transfected with miR-22 mature duplexes as well as in mock transfected cells. HeLa cells were used for the Ago2 IPs due to their greater RNA content and smaller size than human fibroblasts, resulting in much higher mRNA yield per Ago2 IP. Transcripts that showed an increase in Ago2 occupancy in the miR-22 transfected samples as compared to mock transfections were expected to be direct miR-22 targets. We measured Ago2 occupancy by qRT-PCR using GAPDH as a control. Transcript abundance in the IPs was normalized to that in an aliquot of the total RNA prior to Ago2 IP.

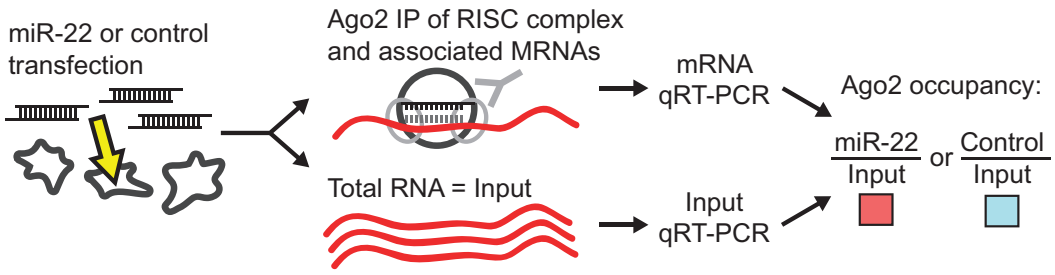


Figure 2.5 Argonaute 2 immunoprecipitation (Ago2 IP).

Ago2 forms a complex with the miRNA and the target mRNA. This complex is immunoprecipitated and the mRNA levels are quantified with qRT-PCR.

Ago2 IP confirmed REDD1, TP53INP1, p21 and CARF as direct targets of miR-22, as all four genes specifically showed increased Ago2 occupancy in a miR-22 dependent manner (Figure 2.6A), whereas other cell-cycle regulatory genes did not (data not shown). We confirmed that all four genes were directly down regulated by miR-22 using a 3' UTR luciferase reporter assay, and that miR-22 mediated repression of the 3' UTRs in the assay was dependent on the predicted miR-22 target sites in the 3'UTRs (Figure 2.6B).

The transcripts of three of these four genes (TP53INP1, p21 and REDD1) were up regulated as fibroblasts entered quiescence (Figure 2.6C). We therefore assayed whether ectopic miR-22 could inhibit these genes in quiescent cells. We transfected miR-22 into quiescent fibroblasts and assayed the changes of these three genes transcript levels by qRT-PCR and changes in protein expression by western blot. miR-22 suppressed the transcript and protein expression of the three genes in quiescent cells (Figure 2.6D & 2.6E). Protein levels of CARF were also down regulated in quiescent cells transfected with miR-22 compared to control (Figure 2.6E).

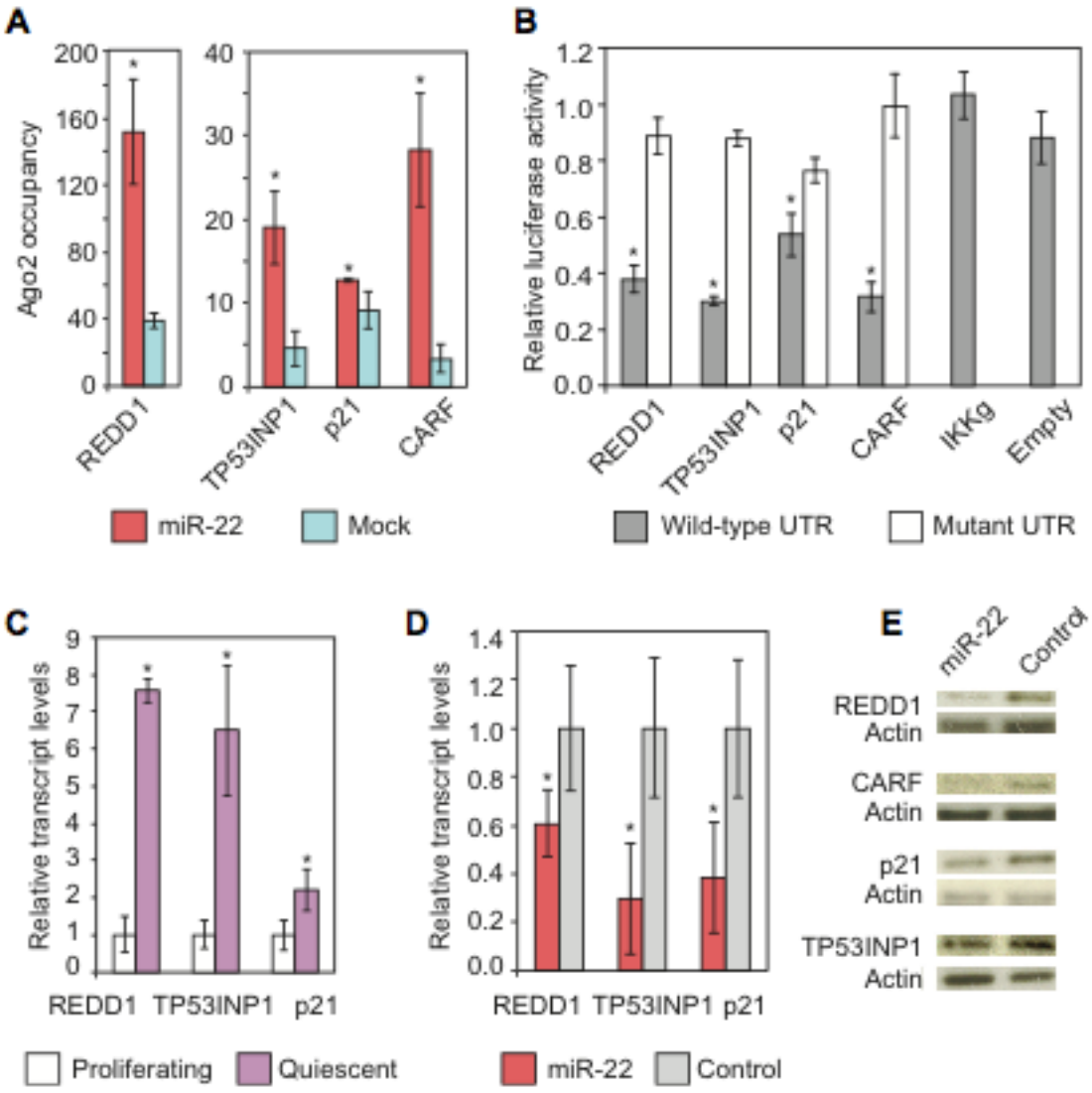


Figure 2.6 miR-22 targets genes mediating cell-cycle arrest.

(A) Ago2 immunoprecipitations identify genes mediating cell-cycle arrest and apoptosis as direct targets of miR-22. REDD1, TP53INP1, p21, and CARF transcripts show significantly higher Ago2 occupancy in miR-22 transfected HeLa cells compared to mock transfected cells. Ago2 occupancy of the target genes transcripts was measured using qRT-PCR as described in the text. The Y-axis shows fold change in mRNA levels from Ago2 IP isolated RNA normalized to input RNA, which served as the control. (B) Luciferase assays show that miR-22 directly targets the 3' UTRs of the genes indicated on the X-axis. IKKg and Empty are negative controls. IKKg was not repressed by miR-22 and Empty is the luciferase vector with no UTR. The Y-axis shows relative luciferase units from miR-22 transfected cells normalized to control siRNA transfection. For the mutant 3'UTRs, three base pairs in each 6-mer miR-22 target site in the 3'UTRs were

Fig 2.6 continued.
mutated. (C) qRT-PCR results for REDD1, TP53INP1, p21, and CARF transcripts show increased expression in quiescent fibroblasts relative to proliferating fibroblasts. Y-axis indicates fold enrichment in quiescent versus proliferating fibroblasts. (D) qRT-PCR shows miR-22 suppresses TP53INP1, REDD1 and p21 transcript levels in quiescent fibroblasts. Fold changes are denoted on the Y-axis relative to the control siRNA transfection. (E) REDD1, TP53INP1, p21, and CARF protein expression in fibroblasts was down-regulated by transfection with miR-22 compared to control siRNA transfection. For A, C, and D, GAPDH was used as a control for normalizing input RNA levels. For A, B, C, and D bars indicate the mean, and error bars denote ± s.d., n=3. *P*-values were estimated by Student's t-test. *, $P<0.05$

### 2.4.4 miR-22 targets genes that regulate the interferon response

Remarkably, 25 out of the top 50 genes identified by microarray to be down regulated by miR-22 in quiescent fibroblasts were interferon inducible genes (Figure 2.7). However, most of the interferon response genes that were repressed by miR-22 under quiescence did not show matches to the miR-22 seed sequence in their 3' UTRs (Figure 2.7), suggesting that the down regulation of the majority of these genes in response to miR-22 was occurring through an indirect mechanism.

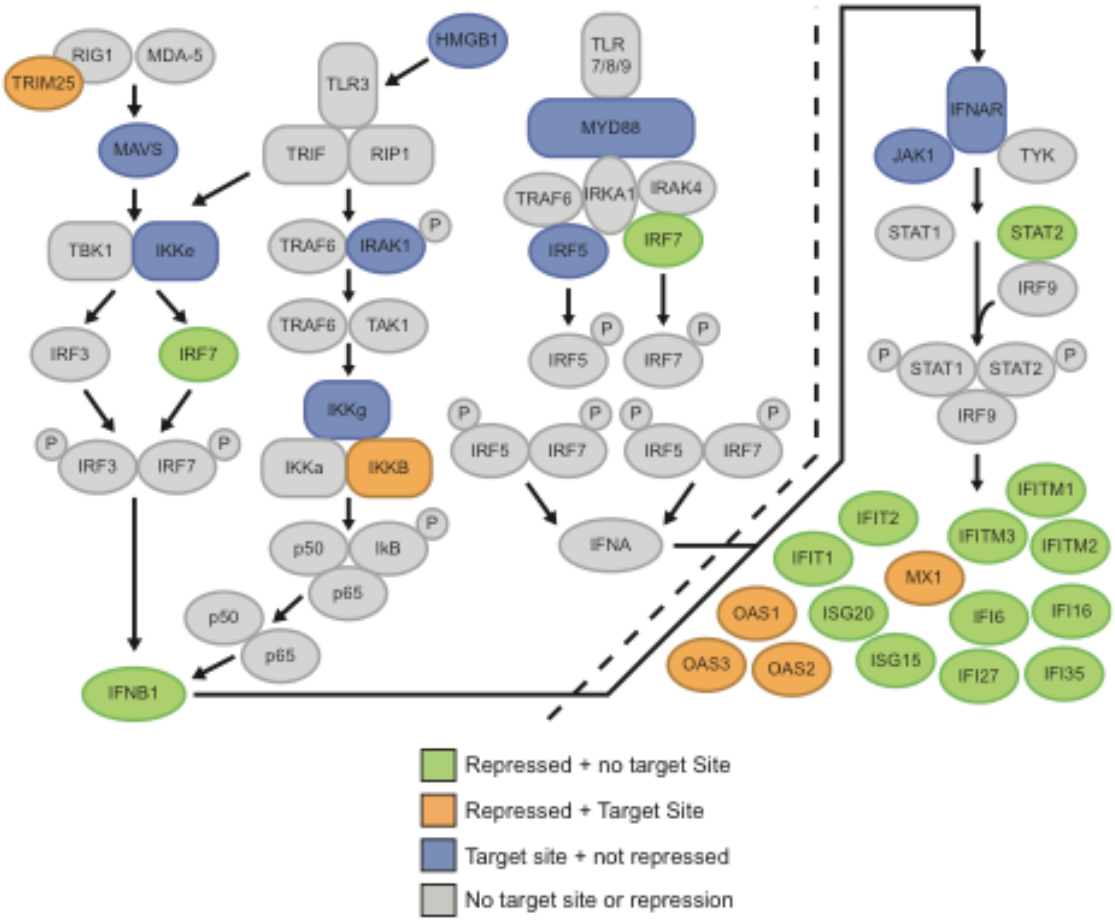


Figure 2.7 miR-22 represses genes mediating interferon suppression.

The interferon response pathway. Green indicates genes in the pathway that were repressed by miR-22 in quiescent fibroblasts but have no predicted miR-22 target sites; orange indicates genes repressed by miR-22 in quiescent fibroblasts and have predicted miR-22 target sites; blue indicates genes that have predicted target sites but were not repressed by miR-22 in quiescent fibroblasts. Genes in grey don't meet any of these criteria.

To identify the direct targets of miR-22 that mediate suppression of interferon genes, we used Ago2 IPs. We screened several candidate target genes that had established roles in activating the interferon pathway and were potential miR-22 targets based on the presence of the miR-22 seed sequence in their 3' UTRs. From this screen we identified two target genes, HMGB1 and IRF5, which showed increased occupancy by Ago2 in miR-22 transfected cells compared to control, and had established roles in

activating the interferon pathway (Figure 2.7 & 2.8A). Both HMGB1 and IRF5 have multiple miR-22 seed match sequences in their 3' UTRs, and HMGB1 was predicted to be a miR-22 target by RNA22 (62) while IRF5 was predicted to be a target of miR-22 by TargetScan (24). Other candidate genes in the interferon response pathway, which also contained miR-22 seed matches in their 3' UTRs, did not show increased Ago2 occupancy (data not shown), indicating that this assay identified specific targets. To verify that these targets identified by Ago2 IPs could be repressed by miR-22, we cloned the 3' UTRs of HMGB1 and IRF5 into luciferase reporters to assay repression by miR-22. The 3' UTRs of both genes were indeed repressed by miR-22, and introducing mutations into the predicted miR-22 target sites relieved repression, confirming that miR-22 directly targets HMGB1 and IRF5 (Figure 2.8B). Additionally, the transcript levels of both of these genes were suppressed by miR-22 overexpression in HeLa cells, and protein expression was repressed by miR-22 overexpression in quiescent primary human fibroblasts (Data not shown & Figure 2.8C). Surprisingly, neither IRF5 or HMGB1 were among the many interferon genes that showed strongly decreased expression in HeLa cells transfected with miR-22 as determined by microarray profiling (Figure 2.8). We assayed transcript and protein levels for both HMGB1 and IRF5 in proliferating compared to quiescent primary human fibroblasts by qRT-PCR and western. Only IRF5 was significantly repressed at both the transcript and protein level in proliferating compared to quiescent cells (Figure 2.8D & 2.8E).

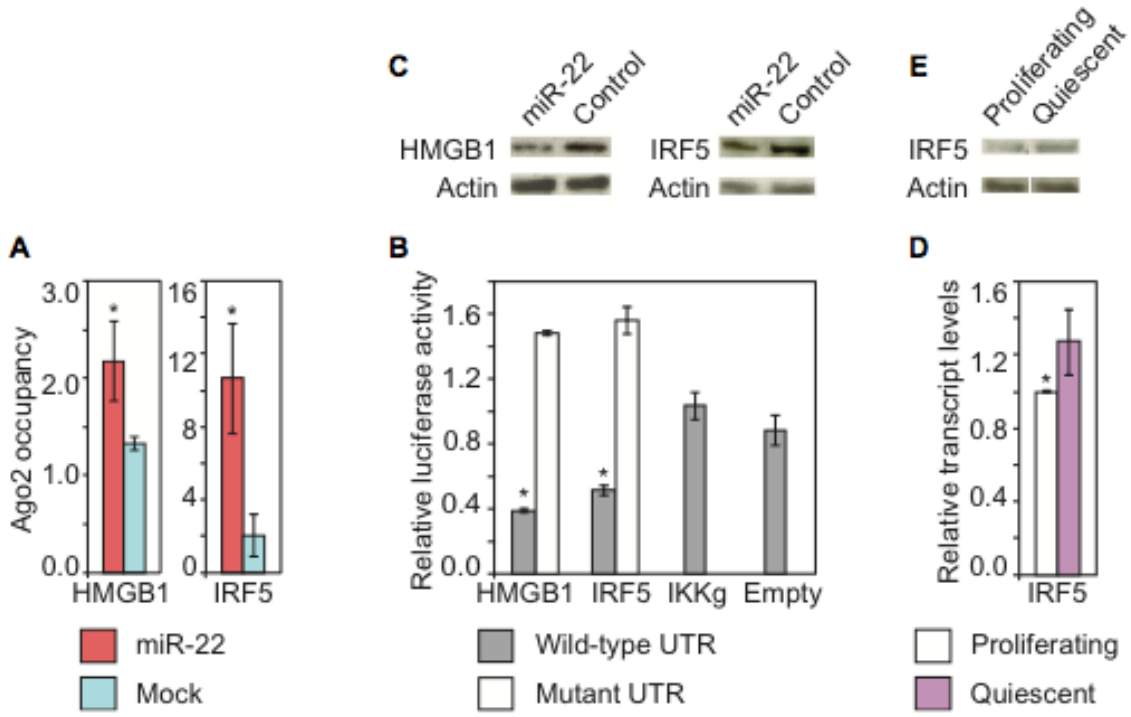


Figure 2.8 miR-22 target genes mediating interferon suppression.

(A) Ago2 immunoprecipitations identify HMGB1 and IRF5 as direct miR-22 targets. HMGB1 and IRF5 transcripts show significantly higher Ago2 occupancy in miR-22 transfected HeLa cells compared to mock transfected cells. Ago2 occupancy of the target genes transcripts was measured using qRT-PCR as described in the text. The Y-axis shows fold change in mRNA levels from Ago2 IP isolated RNA normalized to input RNA. (B) Luciferase assays show that miR-22 directly targets the 3'UTRs of HMGB1 and IRF5. The Y-axis indicates relative luciferase units normalized to the control siRNA transfection. IKKg and Empty are negative controls. IKKg was not repressed by miR-22 and Empty is the luciferase vector with no UTR. For the mutant 3'UTRs, three base pairs in each 6-mer miR-22 target site in the 3'UTRs were mutated. (C) IRF5 protein expression in fibroblasts was down regulated by transfection with miR-22 compared to control siRNA transfection. (D) Increased expression of IRF5 in quiescent fibroblasts relative to proliferating fibroblasts assayed by qRT-PCR. Y-axis indicates fold enrichment in quiescent versus proliferating fibroblasts. (E) IRF5 protein expression was increased in quiescent compared to proliferating fibroblasts. For B and E, GAPDH was used as a control for normalizing input RNA levels. For A, B, and D bars are the mean, error bars denote ± s.d., n=3. For A, B, and D P-values were estimated by Student's t-test. *, $P<0.05$.

### 2.4.5 miR-22 suppresses the interferon response

Both IRF5 and HMGB1 mediate interferon signaling pathways. IRF5 (interferon regulatory factor-5) is involved in the induction of proinflammatory cytokines in response to several different TLR (Toll-like receptor) ligands and mediates signaling downstream of the TLR7 and TLR8 pathways to activate the interferon-beta promoter (63, 64). HMGB (high mobility group box) proteins are highly represented in the nucleus and are responsible for regulating transcription and chromatin structure (65). However, HMGB1 was recently shown to act as a universal sensor for double-stranded RNA as well as DNA and stimulate the interferon pathway by activating the transcription factors IRF3 and NF-κB, which are essential components of the interferon-beta promoter "enhanceosome". Additionally, HMGB1 deficient fibroblasts (Hmgb1 -/-) show significantly impaired type-I interferon induction (66).

To establish whether miR-22 was able to functionally suppress HMGB1 and IRF5 activated interferon-signaling pathways, we examined the response of NF-κB and IRF3 to miR-22 after we artificially activated the interferon pathway using poly I:C. Poly I:C is a double-stranded RNA polymer that mimics a viral infection and induces a strong type I interferon response(67). HMGB1 and IRF5 have been shown to mediate the activation of the transcription factors NF-κB and IRF3, both of which are key regulators of the interferon response (66, 68). Using a reporter of NF-κB activation we confirmed that miR-22 inhibits NF-κB activation in response to a trigger of interferon activation (Figure 2.9A). miR-22 also suppressed IRF3 phosphorylation, a hallmark of IRF3 activation, in response to activation of the interferon response (Figure 2.9B). To further characterize miR-22 mediated suppression of interferon pathway genes, we asked whether miR-22 could suppress an induced interferon response. We co-transfected miR-22 duplexes and poly I:C into HeLa cells and harvested cells 12 hours later. Induction of the type I interferon response was measured by assaying IFNB1 and several other ISG mRNA levels by qRT-PCR. Co-transfection of miR-22 severely impaired normal IFNB1 and subsequent ISG induction by poly I:C (Figure 2.9C). These results strongly indicated that miR-22 was able to suppress the type I interferon response.

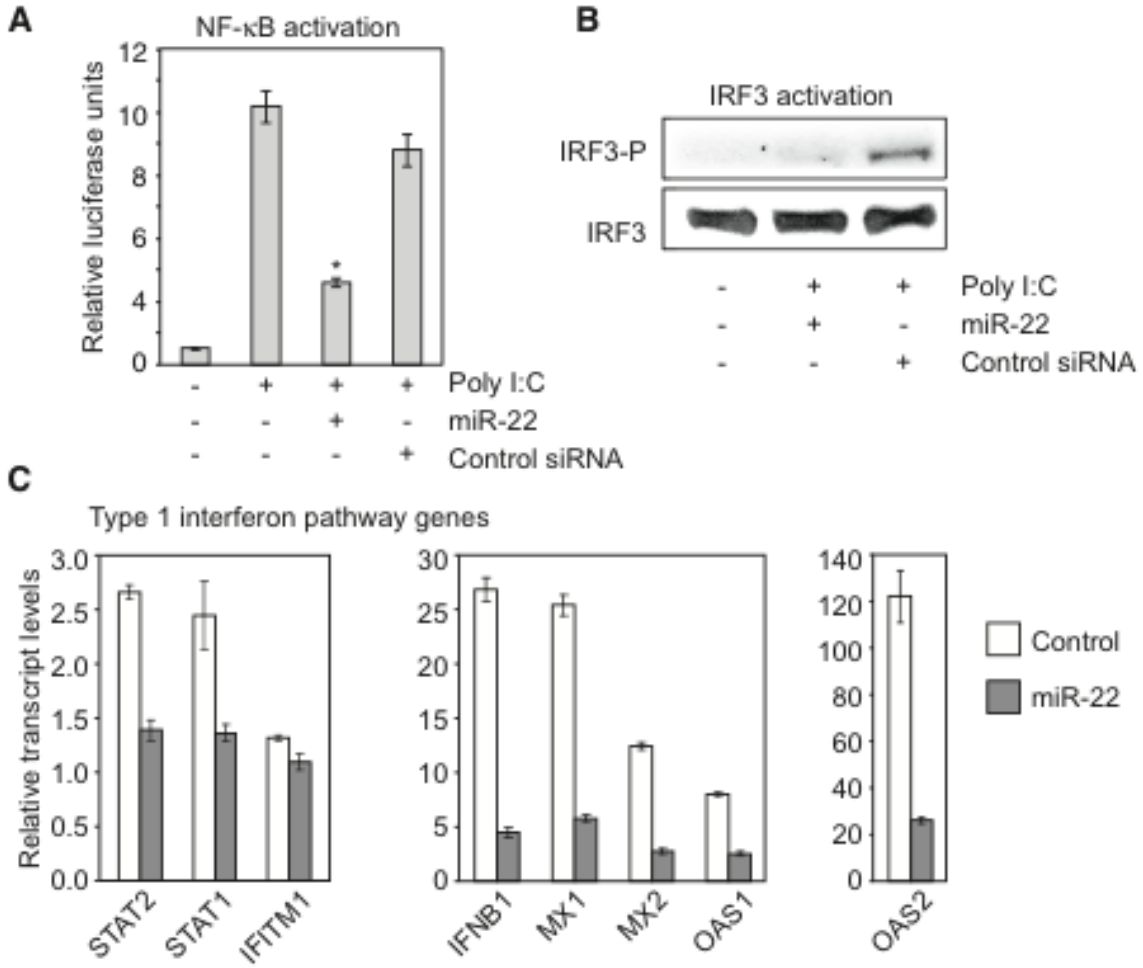


Figure 2.9 miR-22 suppresses the interferon response.

(A) miR-22 inhibits NF-κB activation as measured by reporter activity. Columns correspond to transfections of Poly I:C and miR-22 or control siRNA as indicated under the X-axis. Poly I:C was used to trigger the interferon response. Bars indicate the mean, error bars denote ± s.d., n=3. *, $P<0.05$. (B) miR-22 inhibits IRF3 activation. Western blot assay for the phosphorylated form of IRF3 shows that miR-22 prevents IRF3 activation as compared to the control. Transfections of Poly I:C and miR-22 or control siRNA were as indicated. (C) miR-22 suppresses a poly I:C induced interferon response. Poly I:C was cotransfected in HeLa cells with either miR-22 or the negative control siRNA. miR-22 suppression of the poly I:C induced interferon pathway was assayed by measuring inhibition of interferon-beta (IFNB1) and several other ISGs, using qRT-PCR. The Y-axis indicates relative transcript levels normalized to control. Data shown is a representative experiment of two biological replicates measured in triplicate, (mean ± s.d.). GAPDH was used as a control for normalizing input RNA levels.

These results combined with the observed down regulation of many interferon response genes with miR-22 overexpression in quiescent cells suggested that interferon response genes were active in quiescent cells, and that miR-22 was capable of repressing the interferon response pathway. Previous cDNA profiling studies in quiescent fibroblasts have noted that interferon response genes are activated as fibroblasts enter quiescence (69). To confirm that interferon response genes were activated under quiescence, we measured relative mRNA expression levels of interferon beta-1 (IFNB1), a key marker and inducer of the Type I interferon response, as well as several interferon stimulated genes (ISGs) in proliferating and quiescent fibroblasts. All of the interferon genes that we tested were expressed at higher levels in quiescent cells (Figure 2.10A). The interferon response is potently antiproliferative (70), and the elevated expression of interferon genes could potentially be part of intrinsic mechanisms maintaining cellular quiescence.

To verify that an active interferon response would be detrimental to proliferation, we artificially activated the interferon pathway by transfecting poly I:C into quiescent fibroblasts, then stimulated them with serum to induce proliferation and assayed expression of proliferation marker Ki67. Quiescent fibroblasts that were not treated with poly I:C showed efficient exit from quiescence into a proliferative state as measured by Ki67 expression levels (Figure 2.10B). However, poly I:C treated quiescent fibroblasts showed no change in Ki67 expression levels indicating that a heightened interferon response inhibited transition into a proliferative state (Figure 2.10B).

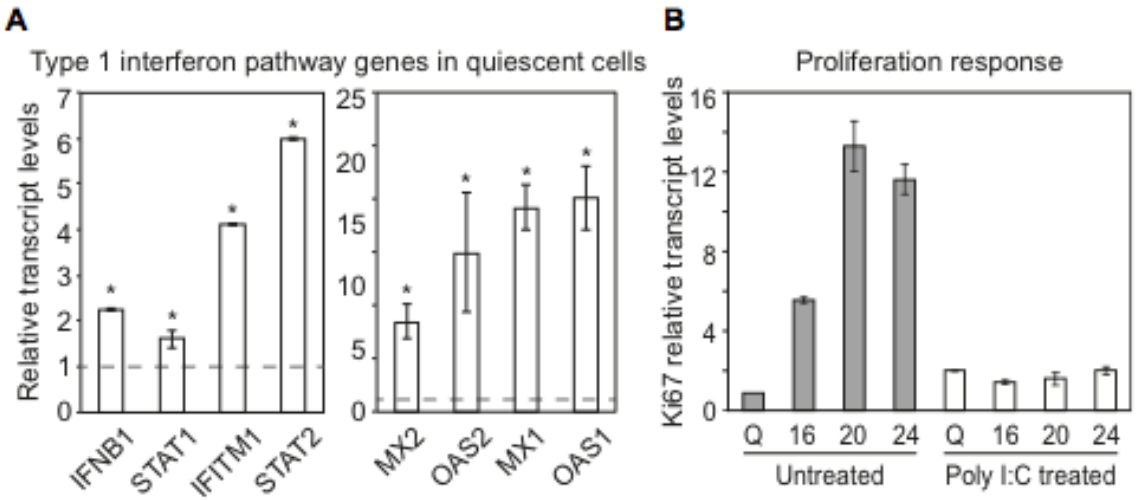


Figure 2.10 The type I interferon pathway in quiescence.

(A) The type I interferon pathway is activated in quiescent cells. The column graph shows qRT-PCR data for expression levels of IFNB1 and other ISGs in the type I interferon pathway in quiescent fibroblasts relative to proliferating fibroblasts. The Y-axis indicates relative transcript levels in quiescent fibroblasts normalized to proliferating fibroblasts. Relative transcript levels in proliferating fibroblasts are shown by the dashed line. Bars indicate the mean, error bars denote ± s.d., n=3. *, $P<0.05$. (B) Active interferon pathway impairs the transition from quiescence to proliferation. The interferon pathway was activated by transfecting quiescent fibroblasts with poly I:C, and then treated cells were serum-stimulated to proliferate. Cells were harvested at the time points indicated in hours on the X-axis. Q: quiescent fibroblasts. Cell proliferation was assayed by measuring Ki67 transcript levels using qRT-PCR. Relative Ki67 expression as indicated on the Y-axis, was calculated with respect to untreated quiescent fibroblasts. Data shown is a representative experiment measured in triplicate, (mean ± s.d.). For A and B, GAPDH was used as a control for normalizing input RNA levels.

### 2.4.6 Myc activates miR-22 during the transition from quiescence to proliferation

Interestingly, miRNA expression profiling of serum stimulated primary human fibroblasts also showed miRNAs from the miR-17-92 cluster were induced along with miR-22 during the serum stimulated transition from quiescence to proliferation (Figure 2.11A). The miR-17-92 cluster has been shown to be directly activated by the transcription factor Myc (71). To investigate whether miR-22 and other serum-stimulated miRNAs were also regulated by Myc, we first overexpressed or knocked down Myc in HeLa cells and assayed the resulting changes in miRNA levels using microarrays. miR-

22, and the known targets of Myc, miR-17 and miR-92, were activated by Myc overexpression and were repressed by Myc knockdown (Figure 2.11A). To examine Myc regulation of miR-22 in primary human fibroblasts, Myc was knocked down by siRNA in proliferating primary human fibroblasts and in primary human fibroblasts exiting quiescence. Proliferating fibroblasts with Myc knocked-down showed a significant decrease in miR-22 expression compared to control (Figure 2.11B & C). qRT-PCR for Myc expression confirmed Myc activation in response to serum stimulation of fibroblasts, at time points very similar to miR-22 induction (Figure 2.11D). This pattern of miR-22 expression in response to serum stimulation and modulation of Myc activity suggested that miR-22 may be activated by Myc.

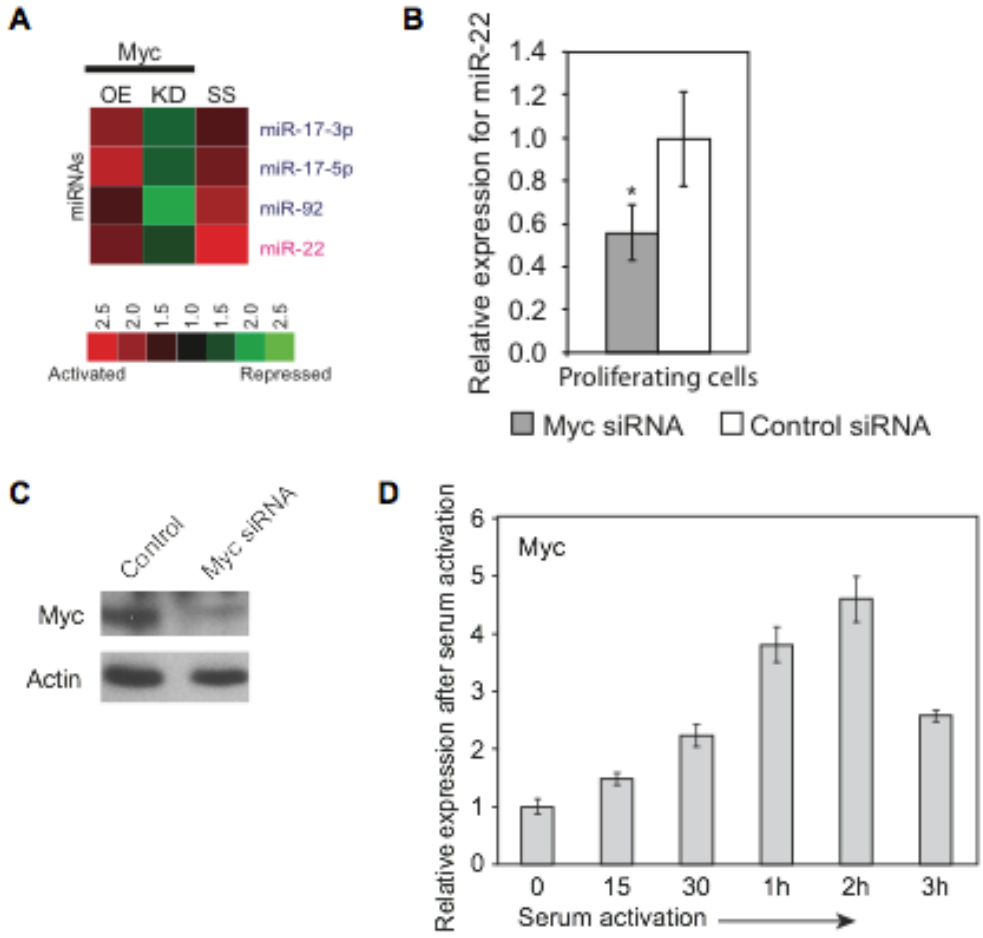


Figure 2.11 Myc activates miR-22 during the transition from quiescence to proliferation.

(A) Heat map showing the response of miRNAs to Myc overexpression (OE), and Myc knockdown (KO) in HeLa cells, and to serum stimulation of quiescent fibroblasts (SS) measured using microarrays. Ratios displayed under the SS column represent the maximum activation across all measured time-points (5, 10, 20, 30, 60, and 180 minutes) after serum stimulation. miR-17 and miR-92 are previously known downstream targets of Myc. (B) miR-22 expression is inhibited by Myc knockdown in proliferating fibroblasts. miR-22 expression was assayed by qRT-PCR in fibroblasts transfected with an siRNA against Myc or a control siRNA. Relative expression values were normalized to those obtained using the control siRNA (Y-axis). Bars indicate the mean and error bars denote ± s.d., n=3. *, $P < 0.05$. (C) Western blot of Myc knockdown by an siRNA against Myc. (D) Independent qRT-PCR verification of Myc expression during the transition from quiescence to proliferation. The Y-axis shows expression after serum stimulation relative to quiescence at each of the indicated time points on the X-axis. Data shown is for a representative experiment measured in quadruplicate (mean ± s.d.). GAPDH was used as a control for normalizing input RNA levels.

In order to investigate whether Myc directly activates miR-22 by binding to upstream *cis*-regulatory sequences, we examined genome-wide Myc ChIP-sequencing (ChIP-seq) data generated in our lab from serum stimulated fibroblasts as well as HeLaS3 and MCF7 cells (72). In all cell types, particularly in the rapidly proliferating HeLaS3 and MCF7 cells, we observed Myc binding at several sites around the predicted transcription start site (TSS) of miR-22 (73) (Figure 2.12A). Myc is known to bind its chromosomal target sites in mammalian cells, including human fibroblasts, through a DNA motif known as the E-box (48). Motif analysis of the region upstream of miR-22 revealed phylogenetically conserved E-box elements within the Myc-binding sites that we identified by ChIP-seq, many of which occurred within CpG islands (Figure 2.12A). Phylogenetic conservation of putative regulatory elements is frequently an indication of functional significance, and the genomic binding of Myc is known to be associated with the proximal presence of CpG islands (74). As an example, we verified Myc binding to one of the sites detected by ChIP-seq in an independent experiment by carrying out ChIP-qPCR in fibroblasts that were induced to proliferate (Figure 2.12B). In addition, luciferase promoter reporter assays using Myc binding regions upstream of miR-22 showed that Myc could functionally activate gene expression through one of these upstream promoter regions (L3) (Figure 2.12C). The L3 promoter region site contains two putative Myc binding site motifs (M1 and M2), but mutation of the putative Myc binding site motifs did not impair activation by Myc in the reporter assay in a consistent manner (Figure 2.12D). These results nevertheless show that miR-22 expression is responsive to Myc, and that Myc binds to the promoter of miR-22 and activates its transcription in a manner that is consistent with direct activation, both in HeLa cells as well as fibroblasts during their exit from quiescence.

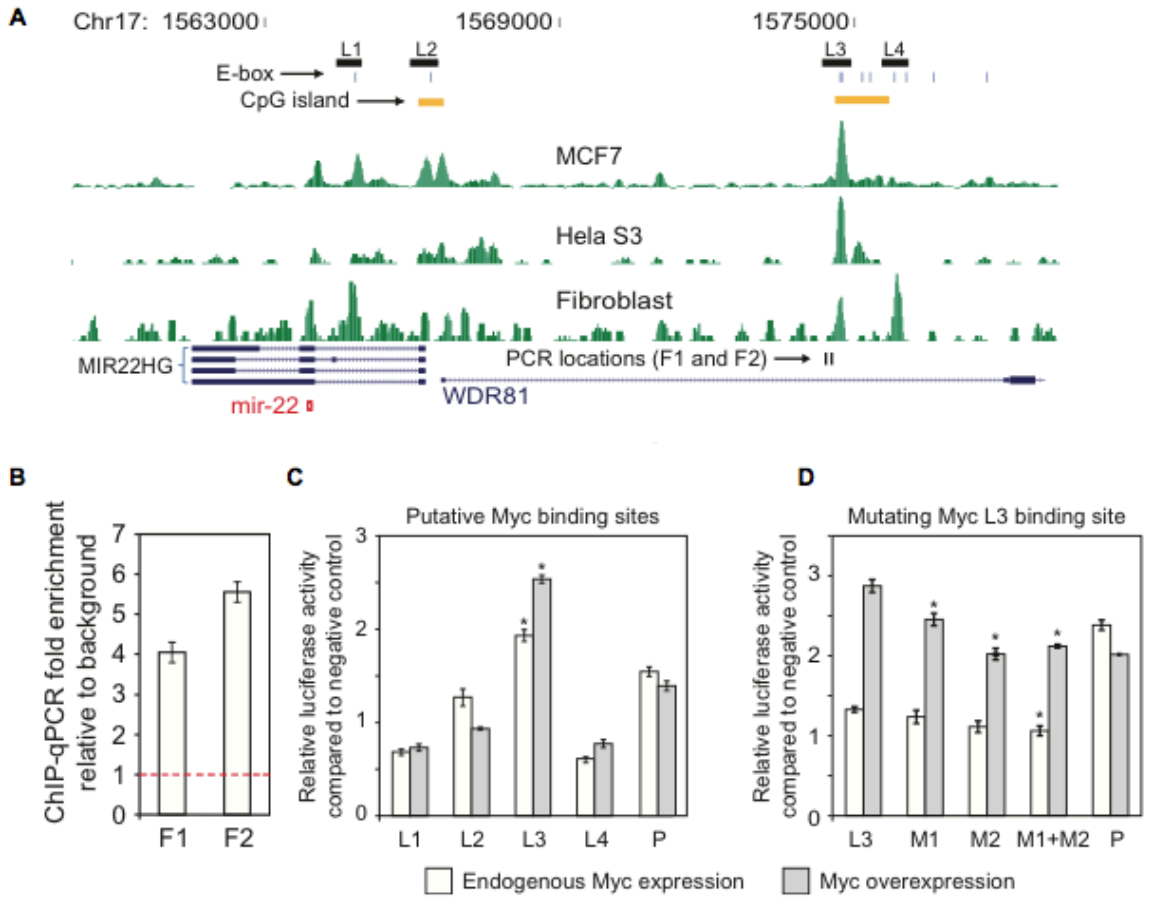


Figure 2.12 Myc binding upstream of miR-22.

(A) ChIP-seq data for Myc in HeLaS3, MCF7 and serum stimulated fibroblasts shows Myc binding upstream of miR-22. The profiles of overlapping extended ChIP-seq reads are indicated in green. Chromosome coordinates are indicated on top and genes are shown at bottom. MIR22HG refers to the primary miR-22 transcript as annotated in RefSeq, and the mature miR-22 sequence is indicated by a red symbol. Regions (L1-L4) subsequently tested for promoter activity in luciferase assays are shown by black rectangles, phylogenetically conserved E-boxes by vertical blue lines, and CpG islands and qPCR primer loci by vertical black lines. (B) ChIP-qPCR verification of Myc binding upstream of miR-22. An independent ChIP for Myc was performed in serum stimulated fibroblasts. Primers were designed to amplify two loci (F1 and F2) indicated as binding sites by ChIP-seq. Fold enrichment, indicative of Myc binding, was calculated relative to input DNA, normalized to a negative control region (Y-axis). The threshold for ChIP enrichment relative to the control is indicated by the red dashed line. (C) Promoter assays for 4 Myc putative promoter regions upstream of miR-22. L1 to L4 on the X-axis indicate cloned candidate promoter regions. P is a positive control. The Y-axis shows expression fold change of a luciferase promoter reporter normalized to a negative control vector. The

Figure 2.12 continued.
L3 region shows a significant increase in reporter activity when Myc is overexpressed. (D) Mutation of putative Myc binding sites M1 and M2 in the L3 promoter region. M1 + M2 indicates both sites were mutated. For C and D, grey bars indicate Myc overexpression and white bars indicate endogenous levels of Myc (Myc was not overexpressed). For B, C, and D bars indicate the mean and error bars denote ± s.d., n=3. For C and D *, $P < 0.05$.

### 2.4.7 miR-22 inhibits the Myc repressor MXD4

Another target of miR-22 that we identified was MXD4, a transcriptional repressor of Myc, which in turn is repressed by Myc (75, 76). We found that MXD4 transcript levels were activated and Myc levels were suppressed when cells entered quiescence (Figure 2.13A). miR-22 transfection impaired MXD4 activation and Myc suppression under quiescence (Figure 2.13B). We verified using Ago2 IP and 3' UTR luciferase reporter assays that MXD4 was indeed a direct target of miR-22 (Figure 2.13C & D). Western blot confirmed miR-22 down-regulated MXD4 expression at the protein level in primary human fibroblasts (2.13E). These results suggest the existence of a feedback loop in which Myc activates miR-22 to suppress MXD4, which causes the up regulation of Myc expression.

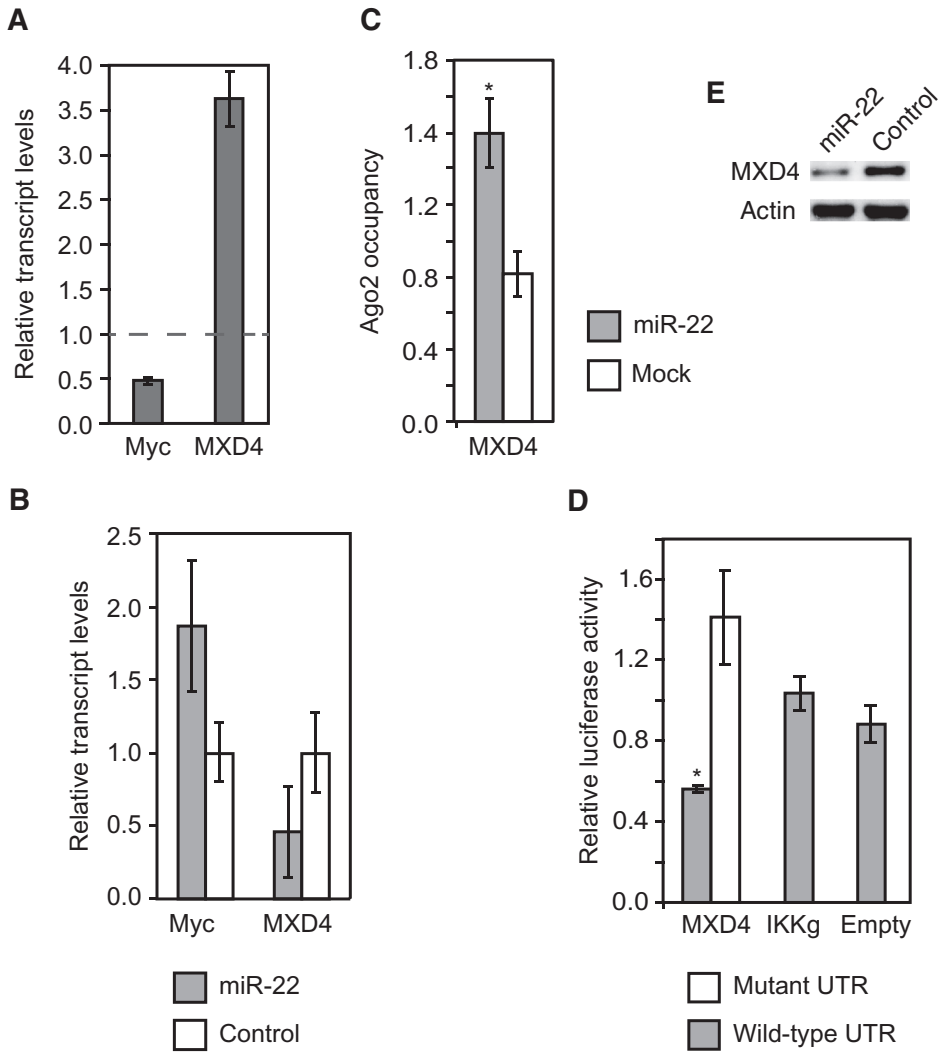


Figure 2.13 miR-22 inhibits the Myc repressor MXD4.

(A) qRT-PCR data showing MXD4 transcripts are activated while Myc transcript levels are inhibited in quiescent cells. qRT-PCR measurements of transcript levels in quiescent cells were made with respect to proliferating fibroblasts, as indicated on the Y axis. Relative transcript levels in proliferating fibroblasts are shown by the dashed line. Data shown are for a representative experiment of two biological replicates measured in triplicate. (B) miR-22 transfection impairs MXD4 activation and indirectly reduces Myc suppression in quiescent fibroblasts compared to control siRNA transfection. (C) Ago2 immunoprecipitations identify MXD4 as a direct target of miR-22. MXD4 transcripts showed higher Ago2 occupancy in miR-22 transfected HeLa cells compared to mock transfected cells. Ago2 occupancy of the target genes transcripts was measured using qRT-PCR as described in the text. The Y-axis shows fold change in mRNA levels from Ago2 IP isolated RNA normalized to input RNA. (D) Luciferase assays confirm that

Figure 2.13 continued.
miR-22 directly targets the 3'UTR of MXD4. The Y-axis indicates relative luciferase units from miR-22 transfected cells normalized to control siRNA transfected cells. IKKg and Empty are negative controls, IKKg was not repressed by miR-22 and Empty is the luciferase vector with no UTR. For the mutant 3'UTRs, three base pairs in each 6-mer miR-22 target site in the 3'UTRs were mutated. (E) MXD4 protein expression in fibroblasts was down-regulated by transfection with miR-22 compared to control siRNA transfection. For A, B, and C, GAPDH was used as a control to normalize input RNA levels. For B, C, and D bars indicate the mean and error bars denote ± s.d., n=3. *P*-values were estimated by Student's t-test. *, P<0.05.

## 2.5 DISCUSSION

Our results show a TF-miRNA network that is activated as primary fibroblasts exit quiescence and re-enter the cell cycle. The oncogenic transcription factor Myc binds upstream of miR-22 and activates miR-22 expression when quiescent fibroblasts are stimulated to proliferate. In addition, we show that miR-22 promotes proliferation in primary human fibroblasts, and we identified targets of miR-22 that include several cell cycle arrest genes, REDD1, TP53INP1, p21, and CARF, as well as MXD4 which represses Myc. Although the effect of miR-22 on the protein levels of cell cycle arrest genes was modest, moderate regulation of multiple cell cycle arrest genes may have large phenotypic effects in concert. We also found that miR-22 targets genes that mediate the interferon response, HMGB1 and IRF5, and that miR-22 repressed the interferon response.

The early activation of miR-22 we observed as cells exit quiescence and re-enter the cell cycle may be rationalized in terms of its effect on the interferon response and cell cycle arrest genes. Although the interferon response is known to be antagonistic to cell proliferation, the exact role of the interferon response genes during quiescence is unclear (70). It has been suggested that signaling pathways actively maintain cells in a viable, reversibly arrested stage (1). It is possible that high levels of interferon response genes are required for maintaining or inducing a state of cell-cycle arrest in quiescent cells. Indeed, up-regulation of interferon response genes in cells entering quiescence has been observed, and interferon has long been known to repress proliferation in fibroblasts (69, 77). Consequently, in order to exit quiescence and begin to proliferate, cells must

overcome this inhibitory influence on proliferation. When we artificially up regulated the interferon pathway under quiescence, entry into proliferation in response to serum-stimulation was severely impaired. One of the means by which cells may overcome this inhibitory effect is to use an immediate-early transcription factor like Myc to activate a suppressor of the interferon pathway, namely the miRNA miR-22 (Figure 2.14). We found that miR-22 functionally inhibits NF-κB and IRF3 activation by directly targeting and down regulating HMGB1 and IRF5, which are known activators of the interferon activation pathway, thus identifying the molecular basis of how miR-22 mediates interferon suppression. In addition, HMGB1 has recently been shown to regulate proliferation, and influences both wound healing and cancer progression (1, 76). Surprisingly, HMGB1 was not downregulated in quiescent primary human fibroblasts. However, IRF5 was downregulated in quiescent primary human fibroblasts, indicating that the interferon mediated maintenance of quiescence may only be regulated by IRF5 in primary human fibroblasts.

We also present evidence that reveals novel cross talk between the p53 and Myc regulatory networks that is mediated by mir-22. We show that miR-22 targets cell-cycle arrest pathways that are mediated by the tumor suppressor p53. IRF5 is known to be a direct target of p53 and promotes cell-cycle arrest and cell death (78, 79). IRF5 also induces senescence when overexpressed in immortalized Li-Fraumeni fibroblasts (80). Additionally, we find that miR-22 directly inhibits other pro-apoptotic and cell-cycle arrest genes such as REDD1, TP53INP1, p21 and CARF that are also direct targets of or regulate p53 (Figure 2.14). Interestingly, miR-22 itself is known to be a direct target of p53, and miR-22 determines p53-dependent cellular fate through direct regulation of p21 (43). In addition, previous studies have shown a p53-dependent suppression of Myc at the transcriptional and post-transcriptional level (81, 82). Furthermore, our data show upstream binding and activation of miR-22 by Myc. A group previously observed similar results and concluded that this indicated direct activation of miR-22 by Myc, but our further analysis of Myc binding sites does not conclusively support direct activation (44). Taken together, our data demonstrate novel interaction between the p53 and Myc regulatory networks that is mediated by miR-22 (Figure 2.14). We postulate that the

combined effect of inhibiting interferon and cell cycle arrest pathways downstream of p53 enables miR-22 to induce quiescent fibroblasts to proliferate.

Recently, other groups have reported that miR-22 acts like a proto-oncogene promoting proliferation and invasion of cancer cells by inhibiting the tumor suppressor PTEN (39-41). On the other hand, other recent studies have reported that miR-22 inhibits proliferation of cancer cell lines (not including the ones we have tested) by inhibiting MAX (42) and MYCBP (43, 44). However, we observed no inhibitory effect of miR-22 in primary cells or HeLa cells (data not shown), and in fact observed a modest activation of proliferation marker Ki67 by miR-22 in proliferating fibroblasts, consistent with our other results (Figure 2.3). We found that miR-22 indirectly up regulates Myc expression levels by inhibiting the Myc transcriptional repressor MXD4, thus participating in a regulatory feedback loop (Figure 2.14). Other groups observed inhibition of Myc by miR-22 repression of Myc binding partners MAX or MYCBP in cancer cell lines, suggesting miR-22 may activate or repress Myc activity depending on cell type (42, 44). Since haploinsufficiency of Myc leads to impairment of proliferation, a small change in Myc expression can be expected to have significant outcomes on cell cycle progression. The above results taken together raise the intriguing possibility that miR-22 may act as a switch inducing or inhibiting cellular proliferation in a context dependent manner. This study provides evidence that miRNAs up regulated during the transition of quiescent cells into a proliferative state have a defined functional role in reprogramming gene expression to enable the transition of $G_0$ arrested cells into the cycling $G_1$ stage. Furthermore, our results provide evidence of the complex interplay between transcription factors and miRNAs to transduce extracellular signals into physiological responses.

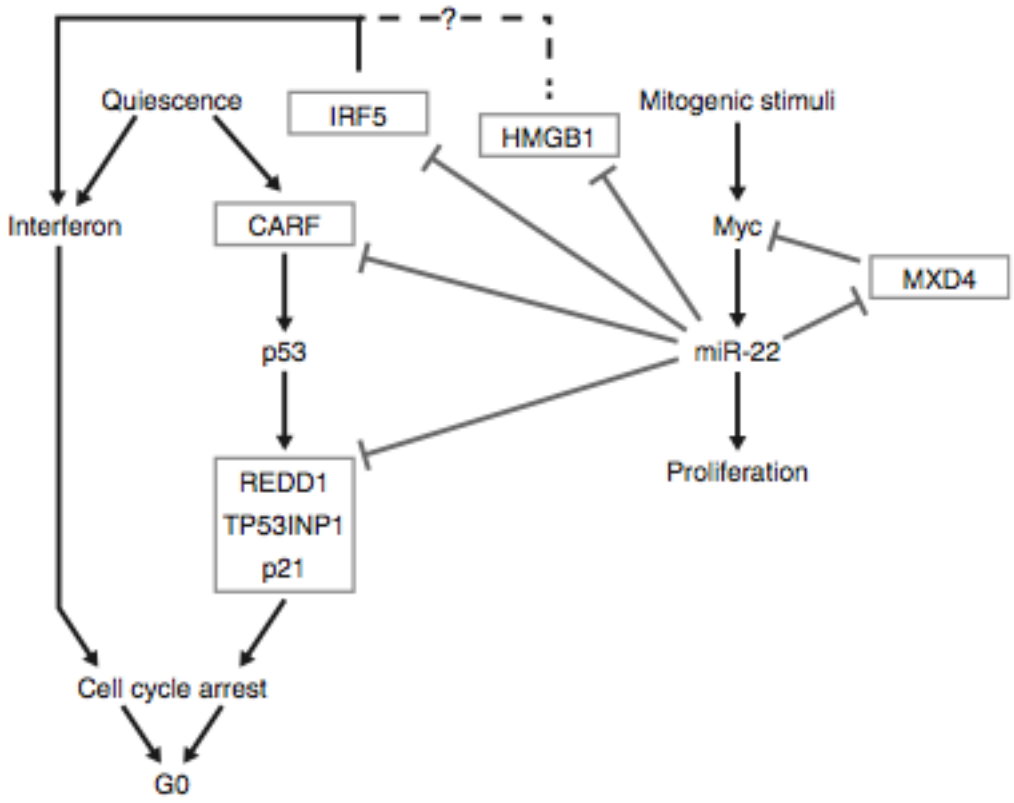


Figure 2.14 The anti-quiescence network mediated by the Myc-miR-22 pathway.

# Chapter 3 miR-191 regulates human cell proliferation and directly targets multiple oncogenes.

## 3.1 ABSTRACT

miRNAs play a central role in numerous pathologies including multiple cancer types. miR-191 has predominantly been studied as an oncogene, but the role of miR-191 in primary cell proliferation is not well characterized, and the transcriptome wide targets of miR-191 have not been experimentally determined. Here we utilized RNA silencing complex immunoprecipitations as well as gene expression profiling to construct a transcriptome wide miR-191 target set. We showed that miR-191 represses proliferation in primary human cells, and targets multiple proto-oncogenes, including CDK9, NOTCH2, and RPS6KA3. Our results provided an extensive transcriptome wide set of targets for miR-191, and demonstrated the cell type specific nature of miR-191's regulation of proliferation in non-small cell lung cancer.

## 3.2 INTRODUCTION

miR-191 has previously been shown to play a role in multiple types of cancer, including gastric, colorectal, breast, thyroid, and hepatocellular carcinoma (83-87). Proliferation related targets have also been identified for miR-191, such as CDK6 and SATB1 (88). Despite the clear link between miR-191, proliferation, and tumorigenesis, the regulation of proliferation by miR-191 has not been explored in primary cells, and transcriptome wide target identification for miR-191 has not been performed with current biochemical techniques.

In this study, we investigated the regulation of cell proliferation in primary human cells by miR-191. We experimentally identified the targets of miR-191 by conducting extensive profiling of RISC associated transcripts and gene expression profiling. GO-term enrichment analysis of these targets identified multiple genes involved in proliferation and cell cycle regulation, and we experimentally confirmed multiple proto-oncogenes as direct targets of miR-191. Finally we showed that miR-191 mediates non-small cell lung cancer (NSCLC) proliferation in a cell type dependent manner.

## 3.3 MATERIALS AND METHODS

### 3.3.1 Normal cell culture conditions

Cells were cultured as described in Chapter 2 Materials and Methods 2.3.9.

### 3.3.2 RNA oligos and transfections

miRNA and LNA oligos were prepared and transfected as described in Chapter 2 Materials and Methods 2.3.9. An additional Control siRNA oligo was used, Control siRNA 2, adapted from.

### 3.3.3 Cell counting assays

For miRNA overexpression experiments, fibroblasts were seeded at 10,000 cells per well in 6-well plates. Cells were cultured in DMEM supplemented with 10% FBS. Cells were allowed to grow 24 hours, and then cells were transiently transfected with miR-191 or siGFP duplexes (100 nM final concentration). 0, 24, 48, 72, and 96, hours after transfection, cells were trypsinized, and counted in a hemacytometer. 9 fields were averaged for each biological replicate. For miRNA inhibition experiments, fibroblasts were seeded at 10,000 cells per well in 6-well plates. Cells were cultured in DMEM supplemented with 10% FBS. Cells were allowed to grow 24 hours, and then media was replaced with low serum DMEM 0.1% FBS. 24 hours after replacement with DMEM 0.1% FBS, cells were transiently transfected with miR-191 miRCURY Locked Nucleic Acid (LNA) miRNA Inhibitor and Negative Control Inhibitor obtained from Exiqon (10 nM final concentration). 0, 24, and 48 hours after transfection, cells were trypsinized, and counted in a hemacytometer. 9 fields were averaged for each biological replicate.

### 3.3.4 Flow cytometry

Fibroblasts were seeded at 50,000 cells per well in 6 well plates. Cells were cultured in DMEM supplemented with 10% FBS. Cells were allowed to grow 24 hours, and then cells were transiently transfected with miR-191, control siRNA, or Control siRNA 2 duplexes (100 nM final concentration). 24 hours after transfection, cells were

trypsinized, washed with PBS, and fixed for 24 hours in 70% ethanol at -20°C. For Ki67 combined with PI staining, after ethanol fixation, cells were washed with Stain Buffer (BD Pharmingen), incubated 30 minutes with FITC Mouse Anti-Human Ki67 antibody (BD Pharmingen), washed, and resuspended in 500 μl Stain Buffer with Propidium Iodide Staining Solution (5 μg/ml) (BD Pharmingen). For PI staining alone, after ethanol fixation, cells were washed twice with PBS, then resuspended in PI staining solution (50ug/mL PI with 100ug/mL RNase in PBS). Flow cytometry analysis for Ki67 in primary human fibroblasts was done using a FACsCalibur flow cytometer and 10,000 events above threshold levels were counted for each sample (BD Biosciences). Data analysis was done using FlowJo. Flow cytometry analysis for Ki67 in cancer cell lines was done using a BD Accuri flow cytometer and 10,000 events above threshold levels were counted for each sample (BD Biosciences).

### 3.3.5 RISC immunoprecipitation

We adapted the protocol developed by Hendrickson *et. al.* (52) for immunoprecipitating Ago2-mRNA complexes. Ago2 is an essential component of RISC. Briefly, HeLa cells were grown in 10 $cm^2$ tissue culture plates and transfected with either miRNA mature duplexes or siGFP duplexes at a final concentration of 100 nM or mock transfected. After 24 hours, cells were washed twice with PBS, and 0.5 ml of lysis buffer was added onto the cell monolayer followed by incubation at 4°C for 30 minutes. Cell lysate was collected by scrapping and cleared by centrifugation at 14,000 rpm at 4°C. Cleared lysate was then incubated with 50 μl of protein-G beads (Roche) for 1 hour at 4°C (pre-clearing). Before pre-clearing, 50 μl of the cleared lysate was removed as input for total RNA profiling. Pre-cleared lysate was incubated with 15 μg of Ago2 antibody (ab57113, Abcam) and incubated at 4°C for 3 hours. After antibody incubation, 50 μl of protein-G beads were added to the lysate and incubated for 1 hour at 4°C. Beads were washed 8 times with lysis buffer and Ago2-RNA complexes were extracted by adding 1 ml TRIzol reagent (Invitrogen) directly to the beads. RNA extraction was carried out as per the manufacturers instructions.

### 3.3.6 RNA-seq library preparation

rRNA was removed using the Ribo-Zero rRNA Removal Kit (Epicentre), and the rRNA removal reaction was cleaned using the RNeasy MinElute Cleanup Kit (Qiagen). RNA was then fragmented using the NEBNext Magnesium RNA Fragmentation Module (New England BioLabs), and size selected using AMPure XP beads (Agencourt) at 1.8X volume. The ends of the fragmented RNA were then prepared for adaptor ligation using T4 Polynucleotide Kinase (New England BioLabs), and the reaction was cleaned up with the RNeasy MinElute Cleanup Kit (Qiagen). Libraries were then prepared from the now rRNA depleted, fragmented, size selected, and kinased RNAs using the NEBNext Small RNA Library Prep Set according to the manufacturers protocol (New England BioLabs). Libraries were cleaned and further size selected using 0.8X volume AMPure XP beads, and then additional size selections with 1.0X beads were performed as necessary. At least 20 million paired end 100bp reads were generated for each replicate using a HiSeq 2000 (Illumina) by the Genomic Sequencing and Analysis Facility at the University of Texas at Austin.

### 3.3.7 RNA-seq data processing

Barcodes were removed, adaptors were removed using Cutadapt, and reads mapping to rRNAs and tRNAs were filtered. Reads were mapped to the human genome (hg19) by TopHat2 software version 2.0.9 (89). We combined biological replicates and assigned an expression value (FPKM) for each RefSeq gene with Cuffdiff (89). Too avoid denominator inflation in subsequent ratio calculations, all FPKMs less then 1 were hard capped to 1.

### 3.3.8 RNA-seq gene expression repression

Repression of gene expression for each gene was calculated as the ratio of the FPKM in the miRNA transfection to the FPKM in the control transfection:

$$\text{Repression} = \frac{\text{FPKM for the control}}{\text{FPKM for the miRNA}}$$

### 3.3.9 RNA-seq RNA induced silencing complex immunoprecipitation enrichment

RNA-seq RNA induced silencing complex immunoprecipitations (RIP) enrichment was calculated as follows: RIP FPKMs were first normalized to gene expression FPKMs, and then enrichment was calculated as the ratio of the normalized miRNA transfection to the normalized control transfection:

$$\text{Enrichment} = \frac{\text{FPKM for the miRNA RIP / FPKM for the miRNA gene expression}}{\text{FPKM for the control RIP / FPKM for the control gene expression}}$$

### 3.3.10 Defining a miRNA target list using RIP enrichment and gene expression repression

mRNAs were ranked by averaging RIP enrichment values and gene expression repression values to make a target score. mRNAs with a score of 1.5 or greater were designated as the target set.

### 3.3.11 Gene Ontology analysis

Gene ontology analysis was performed with the GeneCodis online tool (90-92).

### 3.3.12 Luciferase reporter assays

Entire 3' UTRs or at least 0.5 kb up- and down-stream of the predicted miR-191 binding site (whichever was shorter) were produced by PCR from human genomic DNA and inserted into the psi-CHECK2 plasmid using XhoI and NotI restriction sites downstream from the Renilla luciferase gene (Promega). For each plasmid produced this way, a mutant plasmid was subsequently made via deletion of the 22 bp sequence corresponding to the full position of miR-191 at the putative binding site (QuikChange Lightning Mutagenesis Kit, Agilent).

HEK293 cells were plated in 24-well plates at $10^5$ cells/well in DMEM supplemented with 10% FBS and 1% Pen-Strep and grown overnight (Hyclone, Gibco). Each plasmid was co-transfected at 50 ng/well with either miR-191 or siGFP at a 100 nM in triplicate (Lipofectamine, Invitrogen). Cells were harvested 24 hours post-transfection and luciferase activity was measured using the Promega Dual Luciferase kit according to

manufacturer's instructions. Data was first normalized per-well by dividing Renilla luminescence by Firefly luminescence. Then, the mean of the three biological replicates for each miR-191 transfected group was divided by the mean of its corresponding siGFP transfected group, and the results were displayed in bar graphs grouped by plasmid.

### 3.3.13 Quantitative Reverse-Transcription PCR for interferon stimulated genes

RNA from quiescent and proliferating fibroblasts was extracted with the TRIzol reagent (Invitrogen) and reverse transcribed the High-Capacity cDNA Reverse Transcription Kit from ABI that uses random hexamers. PCR was performed using the SYBR GREEN PCR Master Mix from Applied Biosystems. The target gene mRNA expression was normalized to the expression of GAPDH and relative mRNA fold changes were calculated by the ΔΔCt method.

### 3.3.14 Western blotting

For western blots of putative miR-191 targets, primary human fibroblasts or HeLa cells were seeded in 6-well plates at 5 x $10^4$ cells/well in DMEM supplemented with 10% FBS (Hyclone, Gibco). 24 hours after plating, miR-191 or si-GFP was transfected at a 100 nM concentration (Lipofectamine, Invitrogen). Transfected cells were lysed at 24 hr, 48 hr, 72 hr, or 96 hr post-transfection.

Cell lysates were separated on 4-20% gradient SDS-PAGE gels (Biorad) and proteins were transferred onto PVDF membranes. Membranes were blocked with 5% milk or 5% BSA in TBST and probed overnight with primary antibody in blocking solution (AGO2: 1/1000, Abacam, ab57113; CDK9: 1/1000, Abcam, ab76320; NOTCH2: 1/500, ab8926; RPS6KA3: 1/1000, Abcam, ab75832; GAPDH: 1/1000, Abcam, ab9486). The membranes were washed, incubated with HRP-conjugated secondary antibody in blocking solution (1/5000, Santa Cruz Biotechnology, sc-2004), and washed again. HRP substrate solution was added to the membranes, and incubated for four minutes (Pierce). Blots were exposed to autoradiographic film and developed (Carestream Kodak Biomax). Images of the films were scanned and band intensities

quantified using a white-light transilluminator imaging system (FlourChem Q, ProteinSimple).

### 3.3.15 Cancer survival analysis

Survival probabilities of NSCLC patients were generated with MIRUMIR (http://www.bioprofiling.de/GEO/MIRUMIR/mirumir.html) (93).

### 3.3.16 Statistical analysis

Statistical significance was estimated using a one-sided, two sided, or paired Student's t-test as indicated, and assuming unequal variance.

## 3.4 RESULTS

### 3.4.1 miR-191 represses primary human cell proliferation

To investigate the role of miR-191 in primary human cell proliferation, we transiently overexpressed miR-191 by transfecting the mature duplex form of the miRNA into proliferating fibroblasts and assayed cell growth. miR-191 transfected cells showed significant reductions in cell growth rate compared to control (Figure 3.1). To confirm the effect of miR-191 on cell proliferation, we transfected miR-191 into proliferating fibroblasts and counted cells expressing the proliferation marker Ki67 protein using flow cytometry (53, 54). miR-34a, a well known tumor suppressor, served as a positive control (94). miR-191 transfection significantly decreased the percentage of Ki67 positive cells compared to multiple controls, indicating that miR-191 represses proliferation (Figure 3.2). In addition, transfection of miR-191 into proliferating fibroblasts significantly decreased the rate of progression through the cell cycle (Figure 3.3). To rule out indirect effects from flooding the cells and the RNA silencing machinery with large amounts of the mature miRNA duplexes, we transiently inhibited miR-191 in fibroblasts induced into quiescence by serum removal. Inhibition of miR-191 in quiescent fibroblasts significantly increased the rate of cell growth (Figure 3.4).

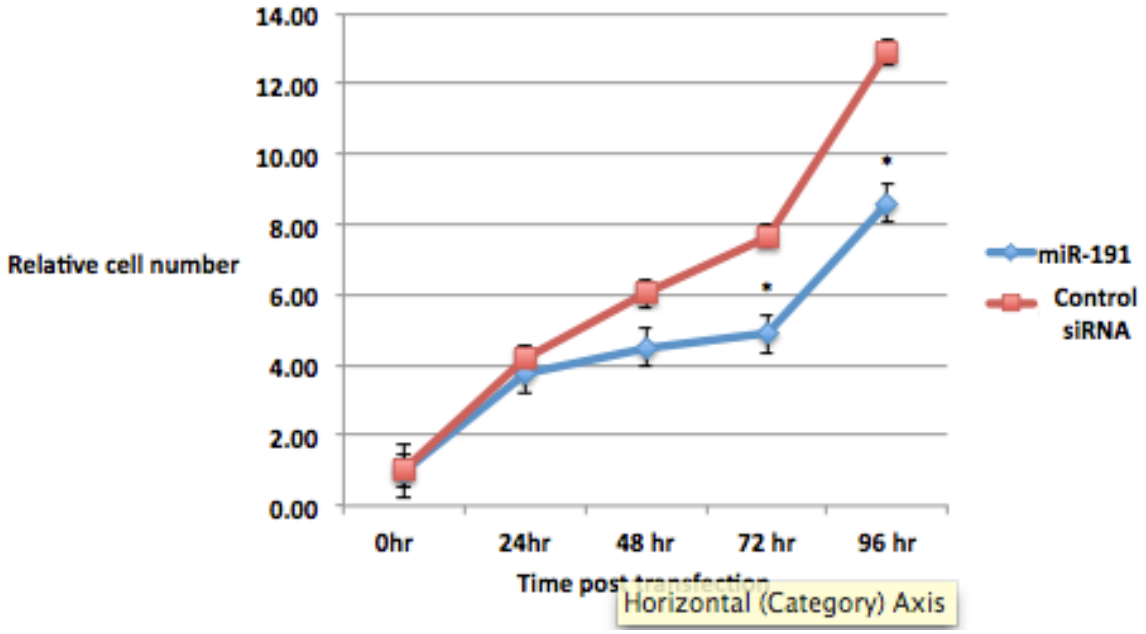


Figure 3.1 miR-191 transfection reduces cell growth.

Average cell number relative to 0hr following miR-191 or control siRNA transfection is shown for each time point indicated. Error bars denote ± SD, n = 4. P-values were estimated by Student's t-test. *P < 0.05.

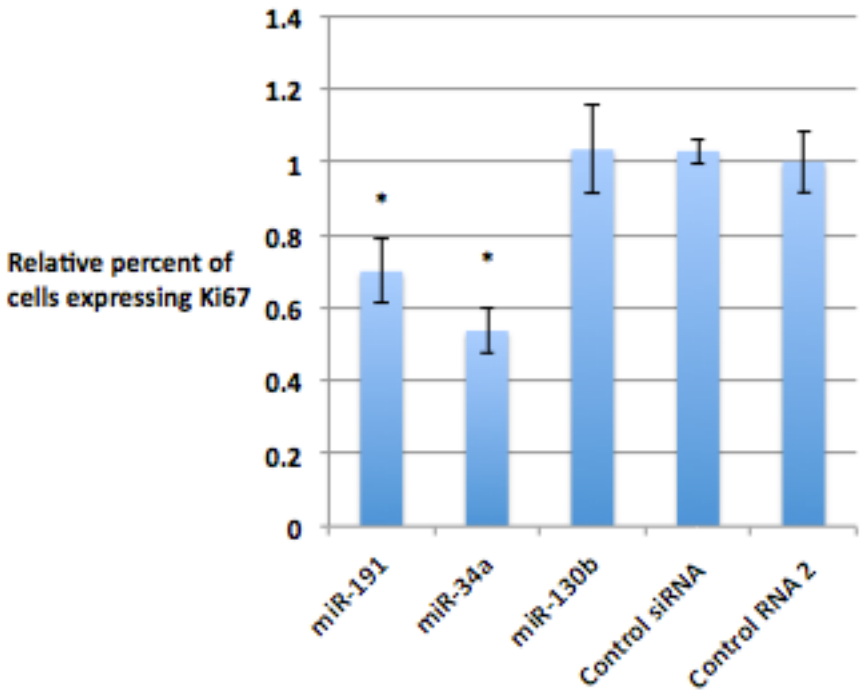


Figure 3.2 miR-191 transfection represses proliferation.

Shown by flow cytometry analysis for expression of proliferation marker Ki67 in miR-191 transfected fibroblasts. The Y-axis indicates the relative percentage of cells expressing Ki67. Bars are the mean percentage of cells expressing Ki67 relative to Control siRNA 2, and error bars denote ± SD, n = 3. P-values were estimated by Student's one tailed t-test. *$P < 0.05$.

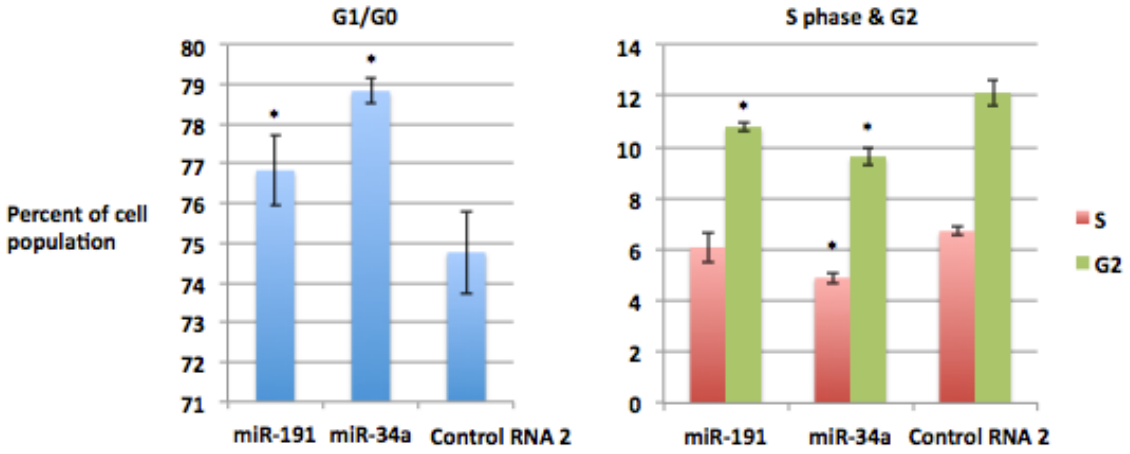


Figure 3.3 miR-191 transfection slows progression through the cell cycle.

Show by flow cytometry analysis of cell cycle progression using propidium iodide staining of miR-191 transfected fibroblasts. The Y-axis denotes the percentage of cells found in each stage of the cell cycle, and bars are the mean percentage the cell population found in each stage. Error bars indicate ± SD, n = 3. P-values were estimated by Student's paired t-test. *P < 0.05.

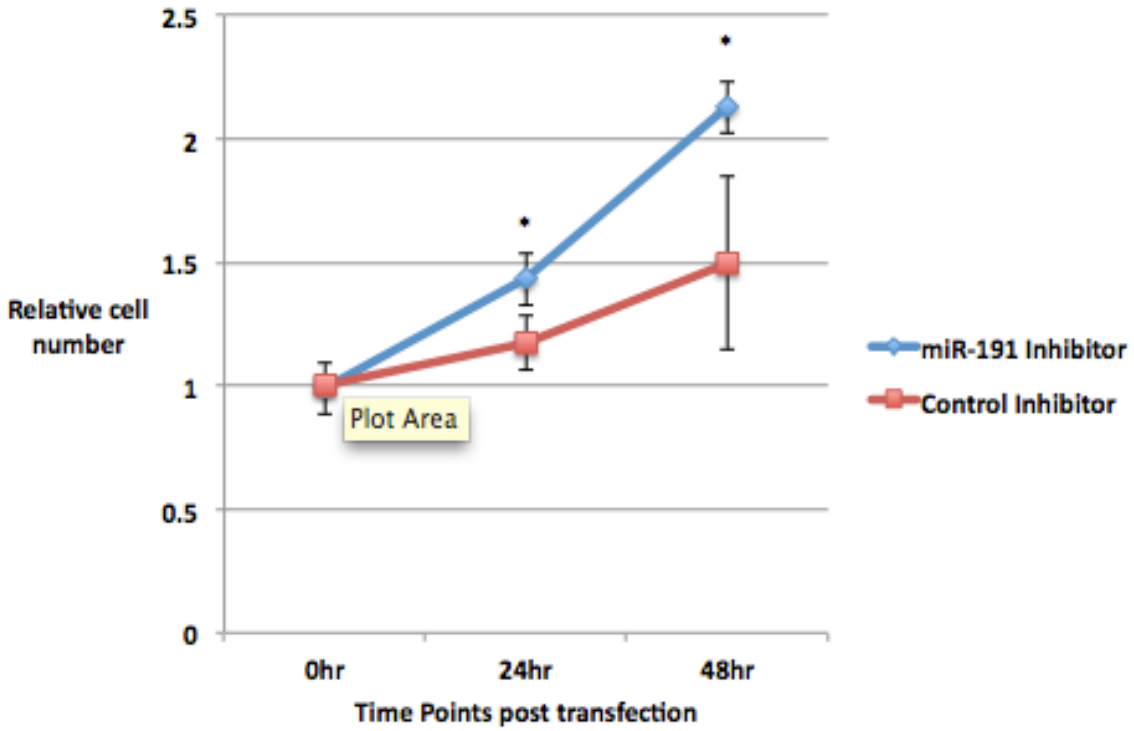


Figure 3.4 Inhibition of miR-191 increases cell growth in quiescent.

Fibroblasts were serum starved into quiescence. Average cell number relative to 0hr following transfection of an LNA targeting miR-191 or a LNA negative control is shown for each time point indicated. Error bars denote ± SD, n = 6. P-values were estimated by Student's one tailed t-test. *P < 0.05.

### 3.4.2 Transcriptome wide identification of miR-191 targets

To experimentally identify the targets of miR-191 we used two approaches: (1) Profiling of transcripts isolated from RNA-induced silencing complex (RISC) immunoprecipitations (RIPs) following transient overexpression of miR-191, and (2) profiling gene expression following transient overexpression of miR-191 (Figure 3.5). RISC is directed to target mRNAs by the mature miRNA guide strand, and mediates repression of gene expression (23). To immunoprecipitate RISC, we used a monoclonal antibody directed against Argonaute-2, an essential component of RISC (23). Increases in RISC occupancy on a given transcript following miRNA overexpression indicate direct targets of the overexpressed miRNA. We profiled RISC occupancy by quantifying

transcripts isolated from RIPs using both microarrays (RIP-ChIP) and RNA-seq (RIP-Seq). RIP Enrichment was defined as an increase in RISC occupancy on a given transcript following miRNA transfection compared to the control transfection. To obtain enough RNA for successful transcriptome wide profiling, all RIPs and gene expression experiments were conducted in HeLa cells, due to HeLa cells having a greater RNA content and being of a smaller size than human fibroblasts.

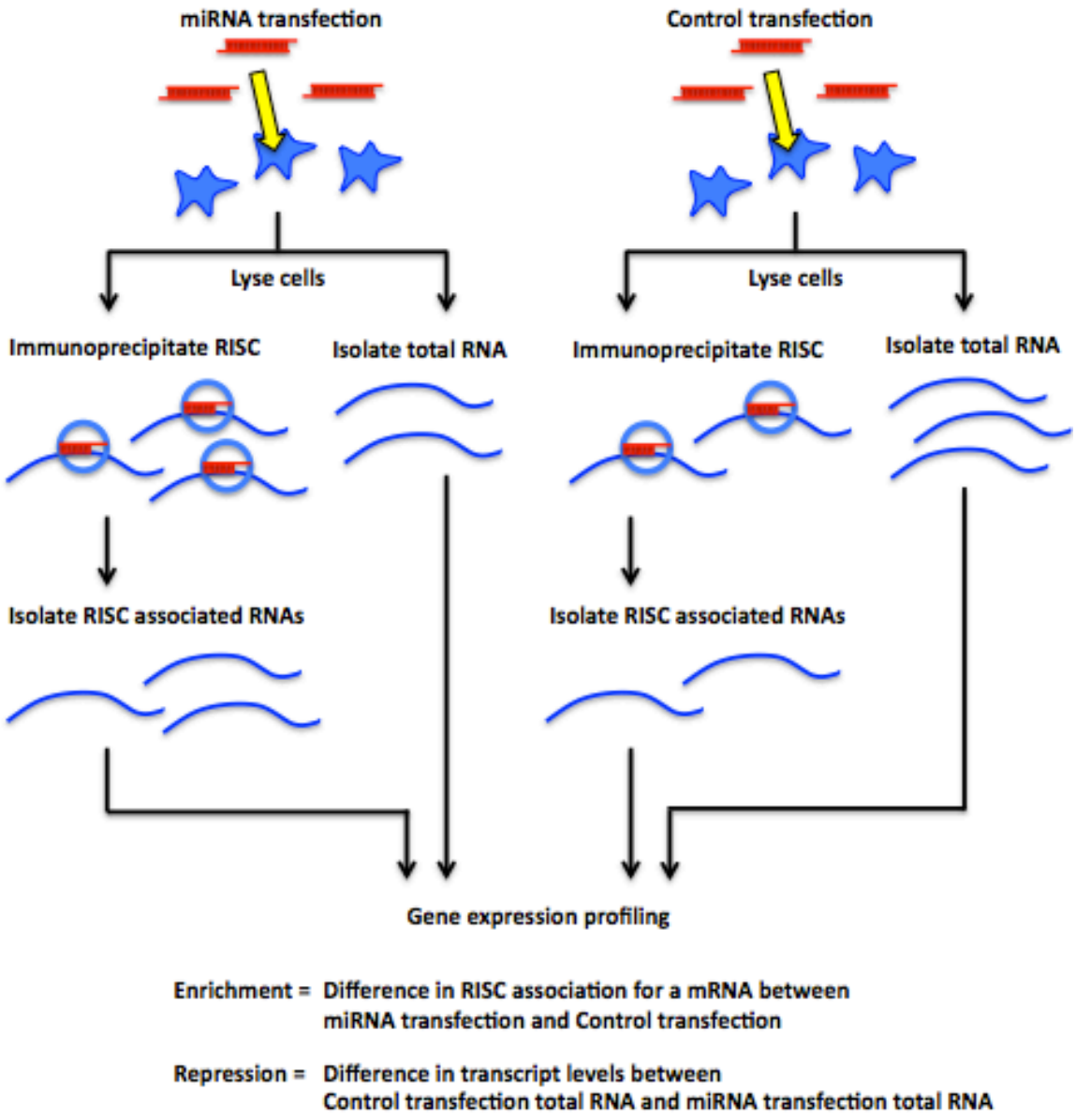


Figure 3.5 RISC associated RNA and total RNA samples from miRNA or Control siRNA transfected HeLas were isolated and profiled.

There was strong correlation between RIP-Seq transcript levels and RIP-ChIP transcript levels, a well as gene expression profiled by RNA-seq and microarray (Table 3.1 and Figure 3.6). No RIP Control siRNA comparison could be made because RIP-ChIP with a Control siRNA was not conducted. We also observed a small subset of genes in the Mock transfected (transfection reagent alone) RNA-seq samples that had

drastically different FPKMs those of miR-191 or Control siRNA transfected samples (Figure 3.7). For this reason, we used the Control siRNA as our control when possible.

| | Spearman Correlation | |
|---|---|---|
| | RIP | Gene expression |
| miR-191 RIP | 0.71 | 0.73 |
| Mock | 0.72 | 0.72 |
| Control siRNA | NA | 0.73 |

Table 3.1 RNA-seq and microarray Spearman rank correlation.

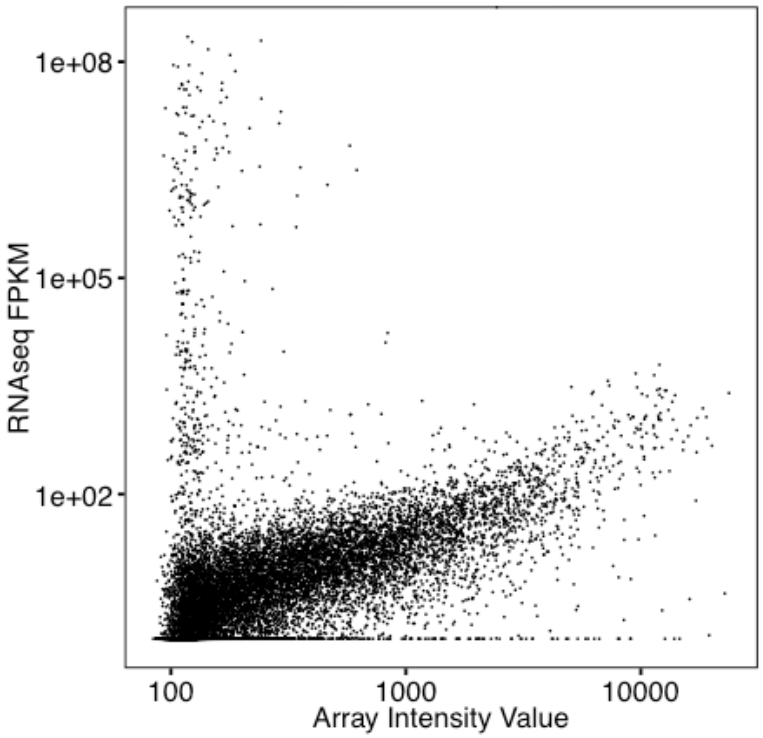


Figure 3.6 Example of RNA-seq and microarray correlation.

miR-191 gene expression RNA-seq FPKM values compared to miR-191 microarray intensity values. Average of n = 3 for the RNA-seq and n = 2 for the micro array.

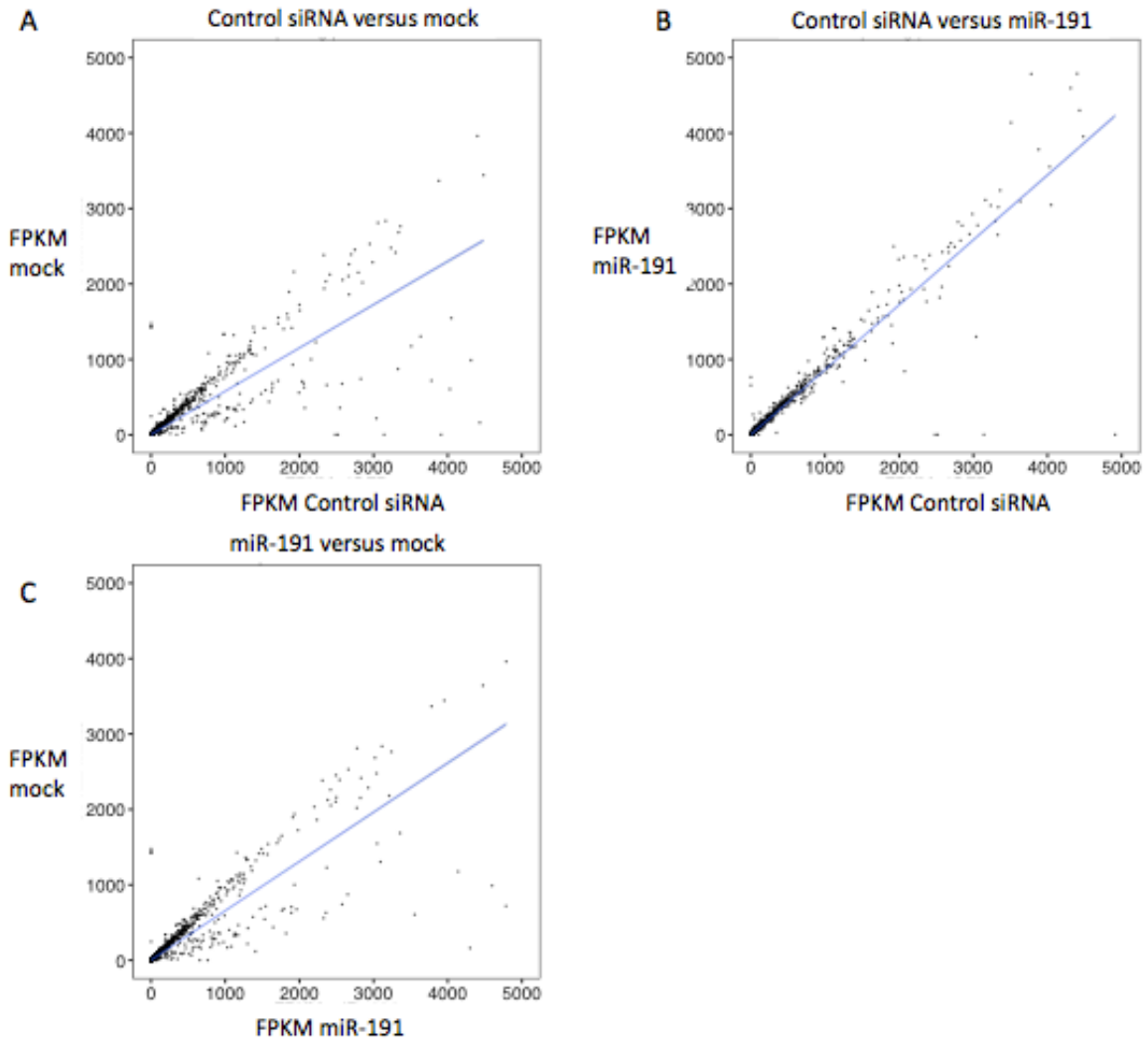


Figure 3.7 Comparing the Control siRNA to mock transfection in the gene expression experiments.

(A) Control siRNA FPKMs compared to mock. (B) Control siRNA compared to miR-191 FPKMs. (C) miR-191 compared to mock FPKMs. For A, B, and C, n = 3 for each condition, and FPKMs are the average of the 3 biological replicates.

To determine if the RIP-Seq effectively identified miR-191 targets, we first examined the enrichment of mRNAs in the RIP-Seq compared to their levels of repressions in the gene expression experiments. RIP enrichment correlated well with repression of gene expression, and RIP enriched mRNAs were significantly more repressed than all genes profiled (Figure 3.8). In addition, RIP enriched mRNAs were

significantly more repressed in the gene expression experiments than all genes that contain the miR-191 7mer miRNA seed match in their 3'UTR, indicating the RIP more successfully identifies genes repressed by miR-191 transfection than using presence of the seed match as the lone criteria (Figure 3.9). RIP enrichment in combination with presence of the seed further increased mRNA repression (Figure 3.9).

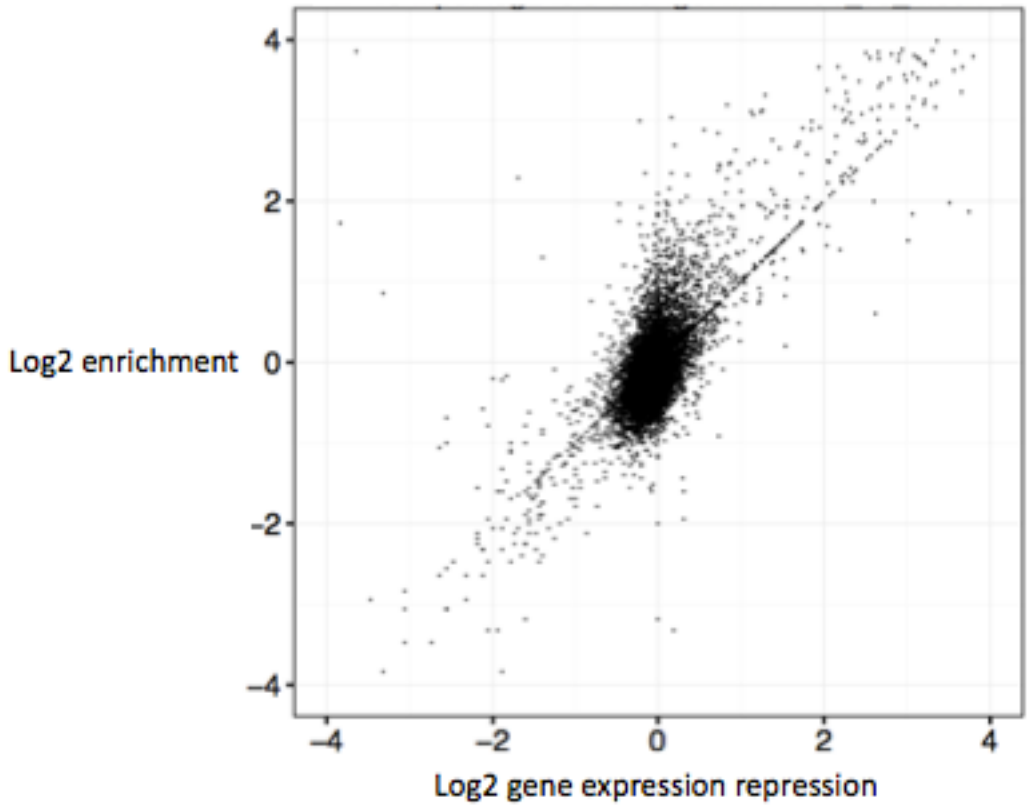


Figure 3.8 RIP enrichment correlates with repression of gene expression.

Enrichment in the RIP was compared to levels of repression in the gene expression experiments. The Y-axis indicates the log2 of the enrichment in the RIP-Seq, and the X-axis indicates the log2 of the gene expression repression value. Larger values indicate increased enrichment and increased repression. Pearson correlation= 0.78, n = 3.

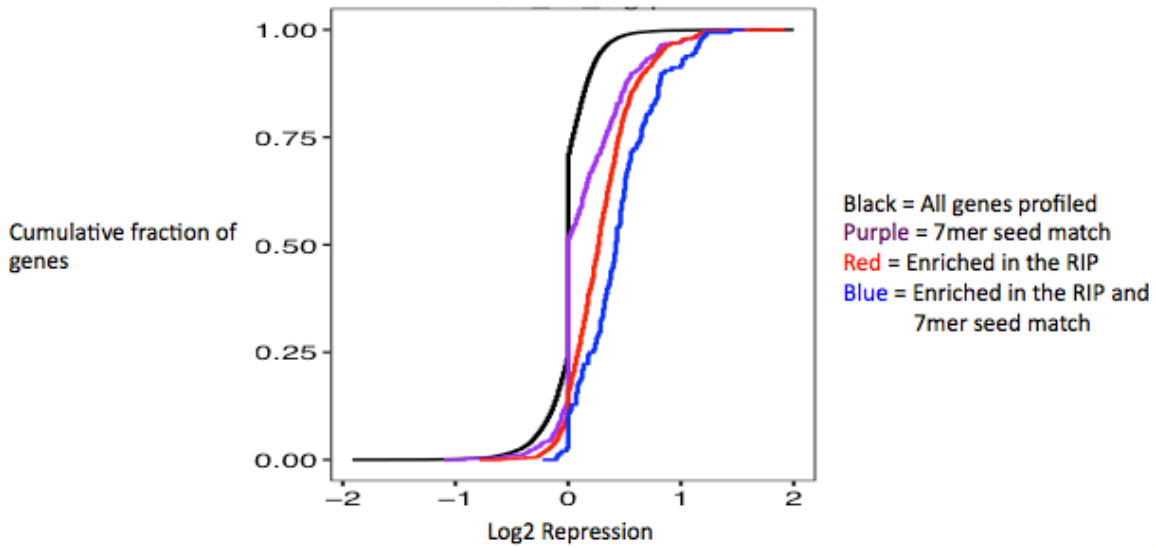


Figure 3.9 mRNAs enriched in the RIP-seq also show reduced expression following miR-191 transfection.

The Y-axis indicates the cumulative fraction of all mRNA transcripts profiled, and the X-axis shows the level of repression for each mRNA transcript profiled. Black: all mRNAs profiled; Purple: all mRNAs profiled with a miR-191 7-mer miRNA seed match in their 3'UTR; Red: all mRNAs 1.5 fold enriched in the RIP; Blue: all mRNAs 1.5 fold enriched in the RIP with a miR-191 7-mer miRNA seed match in their 3'UTR. mRNAs that contain a miR-191 miRNA 7mer seed match were significantly more repressed than all mRNAs profiled (p= 4.65e-24). mRNAs enriched in the RIP were significantly more repressed than mRNAs with a miR-191 7-mer seed match (p= 2.54e-12). mRNAs enriched in the RIP with a 7mer miR-191 seed match were significantly more repressed than mRNAs enriched in the RIP (p= 3.97e-17) Significance estimates were calculated with Student's t-test. n = 3.

As an additional means of determining RIP-seq effectiveness, we examined levels of enrichment for mRNAs that have a miR-191 seed match compared to all mRNAs profiled. mRNAs that contain a 7mer miR-191 seed match in their 3'UTR were significantly more enriched in the RIP than all mRNAs profiled (Figure 3.10).

Conversely, mRNAs most enriched in the RIP had a high frequency of miR-191 seed sites in their 3'UTRs (Figure 3.11). Extending that analysis to the gene expression data, mRNAs that were most repressed following miR-191 transfection had the highest frequency of miR-191 seed sites (Figure 3.12). Using a combination of both RIP

enrichment and repression of gene expression to identify miRNA targets produced the highest frequency of seed sites in the most highly ranked targets (Figure 3.13).

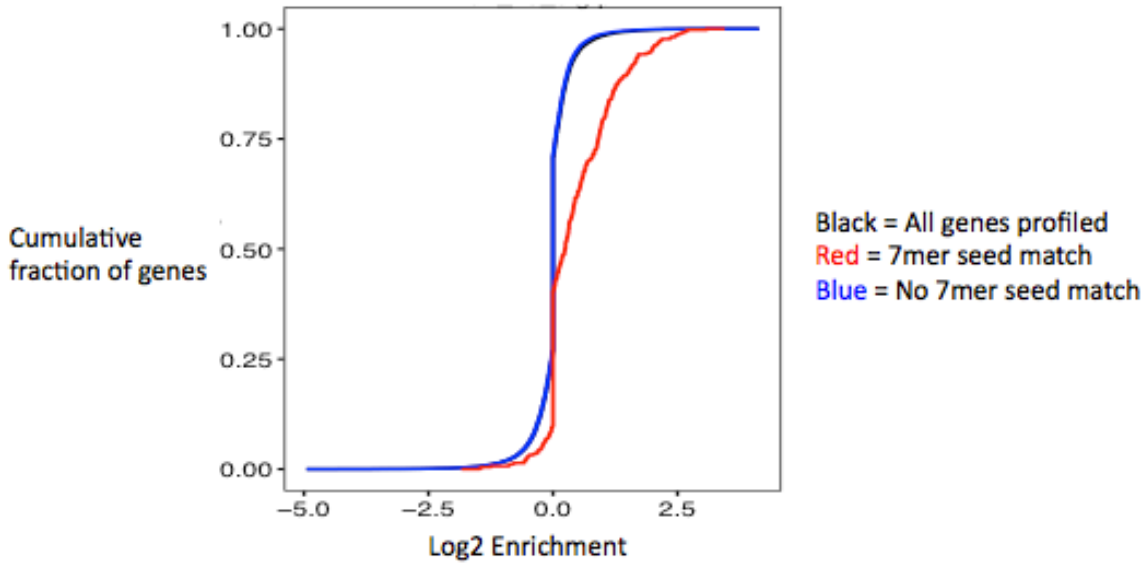


Figure 3.10 mRNAs with a miR-191 seed match were significantly enriched in the RIP-seq.

p= 4.65e-24, Student's t-test. The Y-axis shows the cumulative fraction of all mRNA transcripts profiled, and the X-axis indicates the amount of enrichment in the RIP. Black: all mRNAs profiled; Red: mRNAs containing a 7-mer miR-191 seed match in their 3'UTR; Blue: mRNAs with no 7-mer miR-191 seed match in their 3'UTR. n = 3

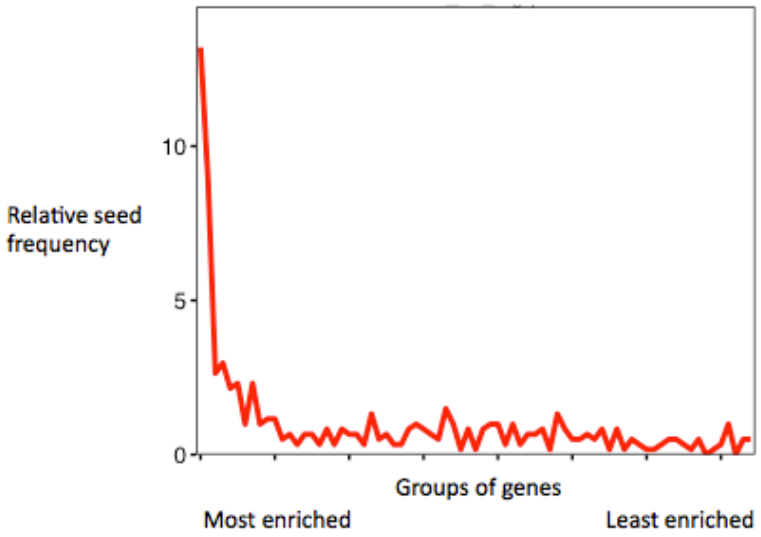


Figure 3.11 mRNAs enriched in the RIP-seq had the highest frequency of miR-191 seed matches.

The X-axis denotes consecutive groups of 250 genes, ranked from most to least enriched in the RIP-seq. The line is the frequency indicated on the Y-axis of the miR-191 7-mer seed match in the 3'UTRs of the gene group relative to the frequency of the seed match in all mRNAs profiled. n = 3.

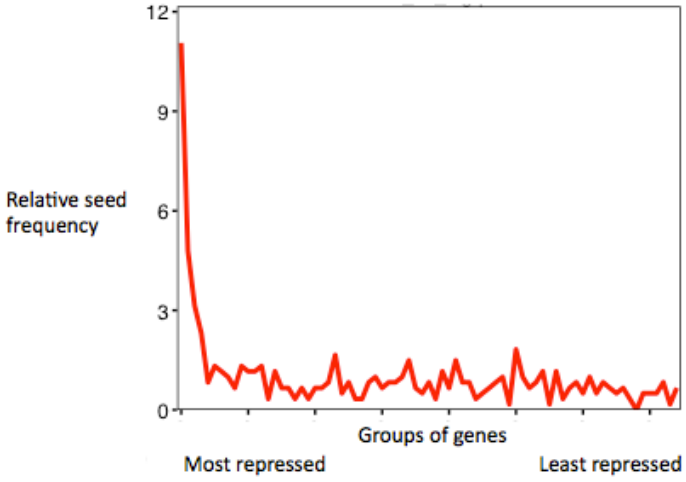


Figure 3.12 mRNAs repressed in the gene expression experiments had the highest frequency of miR-191 7-mer seed matches.

The X-axis indicates consecutive groups of 250 genes, ranked from most repressed to least repressed. The line is the frequency indicated on the Y-axis of miR-191 7-mer seed matches in the 3'UTRs of the gene group relative to the frequency of miR-191 seed matches in all mRNAs profiled. n = 3.

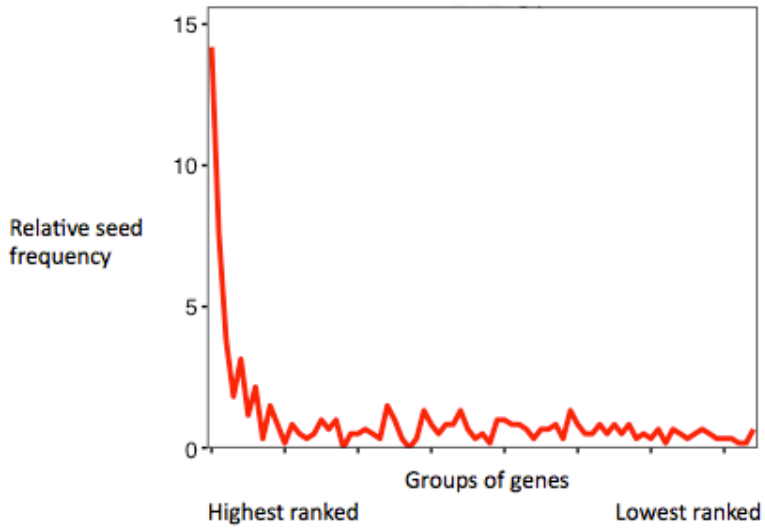


Figure 3.13 The highest ranked miR-191 targets had the highest frequency of miR-191 seed matches.

RIP-seq enrichment and gene expression repression data were combined to rank miR-191 targets. The X-axis denotes consecutive groups of 250 genes, from most highly ranked to least highly ranked. The line is the frequency indicated on the Y-axis of miR-191 7-mer seed matches in the 3'UTRs of the gene group relative to the frequency of seed matches in all mRNAs profiled. Combined gene expression RNA-seq data, n = 3, with RIP-seq data, n = 3.

### 3.4.3 mRNAs with miR-191 seed sites in the coding sequence display greater RISC occupancy and repression of gene expression than mRNAs with seed sites in the 3'UTR

miRNAs have traditionally been observed to post transcriptionally mediate gene expression by pairing to the 3'UTR of the target mRNA (24, 26). Extensive RISC binding to the CDS (coding sequence) region for a subset of miRNAs has been detected, but mediation of gene expression by CDS targeting was minor (27, 29, 30, 95, 96). This implies that although there is RISC occupancy of the CDS, functional targeting occurs through the 3'UTR. Due to a large fraction of miR-191 7mer seed matches being located in the CDS of protein coding genes, we hypothesized that miR-191 may mediate extensive RISC occupancy of the CDS, but exert a stronger influence on gene expression through 3'UTR pairing (Figure 3.14). In support of this hypothesis, we observed an

increase in the proportion of miR-191 target sites in the CDS of our experimentally identified miR-191 mRNA target set compared to all mRNAs profiled (64% compared to 42%) (Figure 3.14). Our data also showed that mRNAs with a miR-191 target site in the CDS were significantly more enriched in the RIP than mRNAs with a miR-191 target site in the 5'UTR or 3'UTR (Figure 3.15). The group of mRNAs most enriched in the RIP-seq do not show significant differences in enrichment between 5'UTR, CDS, or 3'UTR seed matches (Figure 3.15). Surprisingly, there is significantly stronger repression of gene expression when there is a CDS seed match present than one in the 3'UTR or 5'UTR for both the RNA-seq and microarray experiments (Figure 3.16 and data not shown). In the group of most repressed mRNAs, we also see significantly stronger repression of gene expression when there is a CDS seed match compared to a 3'UTR seed match for both the RNA-seq and microarray data (Figure 3.16 and data not shown). Taken together, these results suggest that miR-191 may utilize extensive target pairing in the CDS, and exert a greater effect on gene expression through pairing to the CDS than the UTRs.

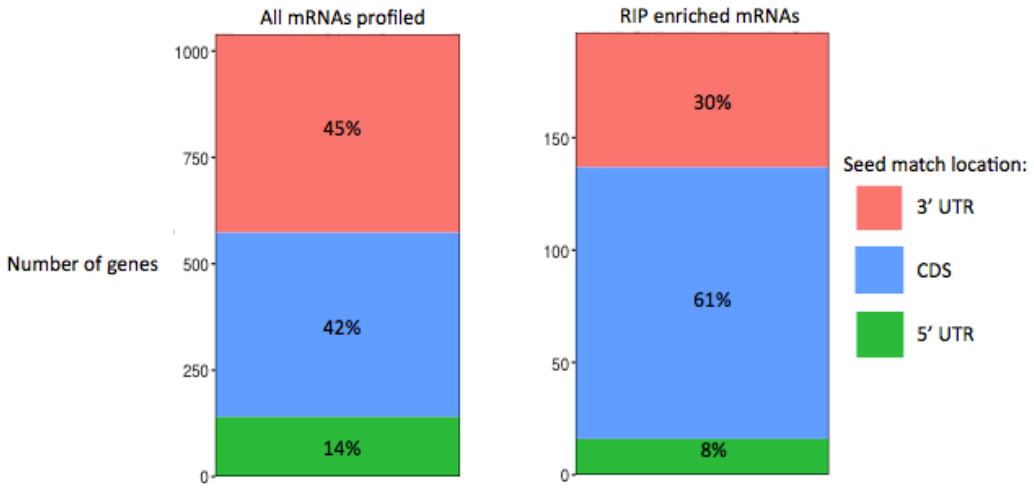


Figure 3.14 RIP-seq enriched mRNAs have a higher proportion of miR-191 seed matches in the CDS than all mRNAs profiled.

Left panel: All mRNAs profiled with a 7mer miR-191 seed match; Right panel: mRNAs 1.5 fold enriched in the RIP-seq with a 7mer miR-191 seed match. The Y-axis indicates the number of genes, and the colors denote the number of genes with a seed match in the given location. n = 3.

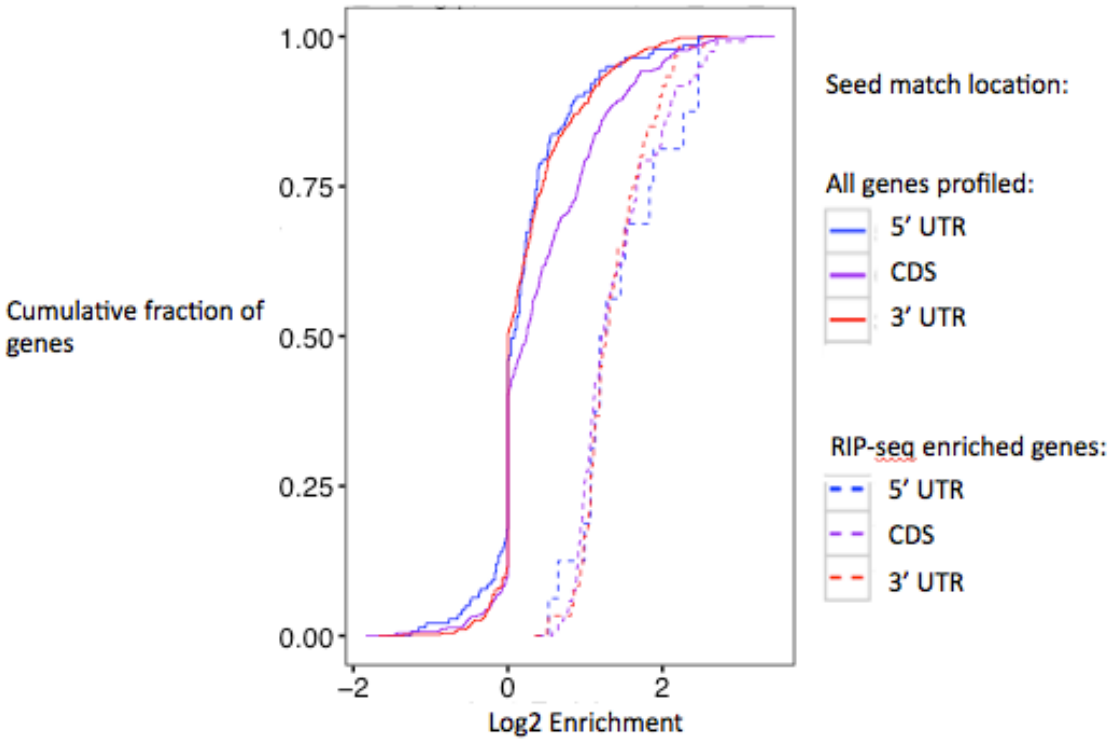


Figure 3.15 RIP-seq enrichment depending on seed match location.

mRNAs with a miR-191 seed match in the CDS were significantly more enriched in the RIP-seq than mRNAs with a miR-191 seed match in the 3'UTR or 5'UTR (p= 1.84e-06 and p= 6.50e-05 respectively). Colors denote the seed match location. The cumulative fraction of all mRNAs profiled with the indicated seed match location is shown on the Y-axis. The X-axis shows amount of enrichment in the RIP-seq. Solid lines are all mRNAs profiled with a miR-191 seed match, and dashed lines are the mRNAs 1.5 fold enriched in the RIP-seq with a seed match. P-values were estimated by Student's t-test. n = 3.

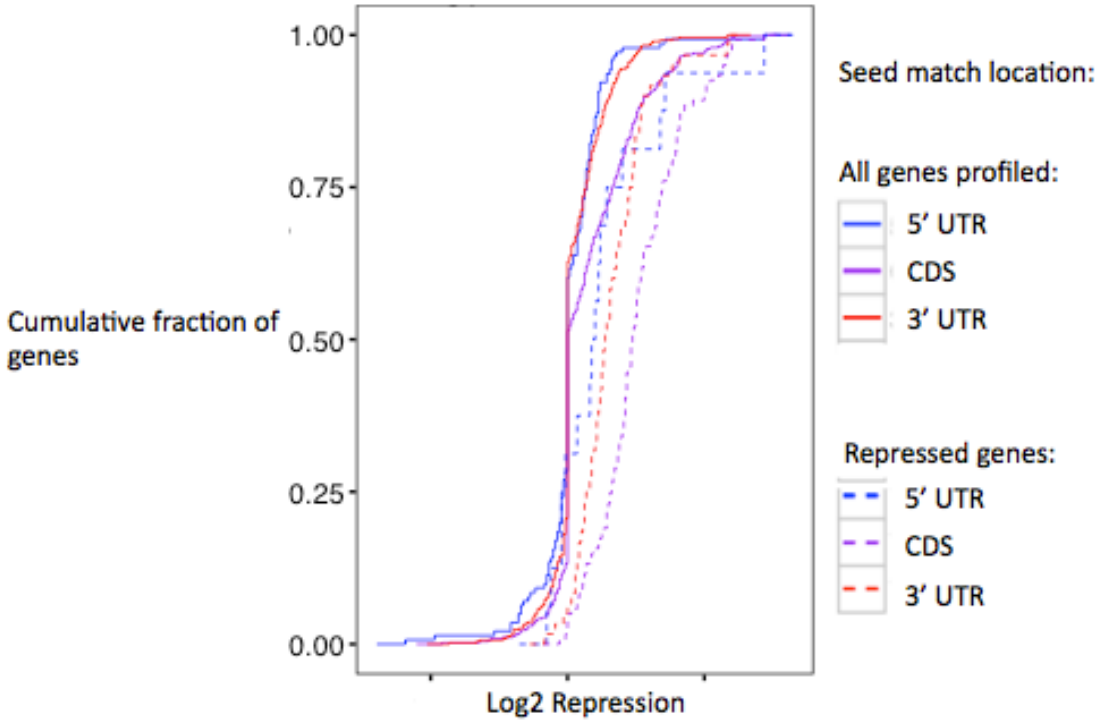


Figure 3.16 Gene expression repression depending on seed match location.

mRNAs with a miR-191 seed match in the CDS were significantly more repressed in the RNA-seq gene expression profiling than mRNAs with a seed match in the 3'UTR or 5'UTR (p= 6.35e-10 and p= 8.87e-08, respectively). mRNAs with a miR-191 seed match in the CDS were significantly more repressed in the RNA-seq gene expression profiling than mRNAs with a seed match in the 3' UTR (p= 1.17e-05). Colors denote the seed match location. The cumulative fraction of all mRNAs profiled with the indicated seed match location is shown on the Y-axis. The X-axis shows amount of repression measured by RNA-seq. Solid lines are all mRNAs profiled with a miR-191 seed match, and dashed lines are the mRNAs 1.5 fold repressed in the miR-191 RNA-seq with a seed match. P-values were estimated by Student's t-test. n = 3.

### 3.4.4 miR-191 directly targets multiple proto-oncogenes

In our experimentally identified set of miR-191 targets, there was strong enrichment for genes associated with cell proliferation, cell division, the MAPK signaling pathway, and cancer pathways (Figure 3.17 & Appendix 1). We selected multiple proto-oncogenes and regulators of proliferation to further investigate as miR-191 targets. To confirm direct miR-191 targeting of the genes, we cloned ~0.5 - 1kb sections of the 3'UTRs into luciferase reporter constructs. CDK6 was one of our putative targets and had previously been identified as a direct target of miR-191 by multiple groups (87, 88, 97). The luciferase reporter assays confirmed 7 of the 8 putative targets as direct targets of

miR-191, and deletions of the miR-191 seed matches showed that the miR-191 mediated repression of the 3'UTRs in the assay was dependent on the miR-191 seed matches in the 3'UTRs (Figure 3.18). To further confirm these genes as direct targets and examine the effect of miR-191 on the expression of these genes in primary human fibroblasts, we transfected mature miR-191 duplexes into primary fibroblasts and assayed transcript and protein levels. miR-191 transfection in fibroblasts significantly repressed the transcript levels of AGO2, BCL2, CDK6, CDK9, NOTCH2, and RPS6KA3, but not PRMT or SLC7A1 ($p= 0.11$ and $p= 0.08$) (Figure 3.19). Western blotting for a subset of the genes following miR-191 transfection in fibroblasts and HeLas confirmed miR-191 repression of CDK9, NOTCH2, and RPS6KA3, Ago2 only showed repression in HeLas (Figure 3.20 and data not shown). This discrepancy may be due to differences in protein stability in combination with the transient nature of the transfections.

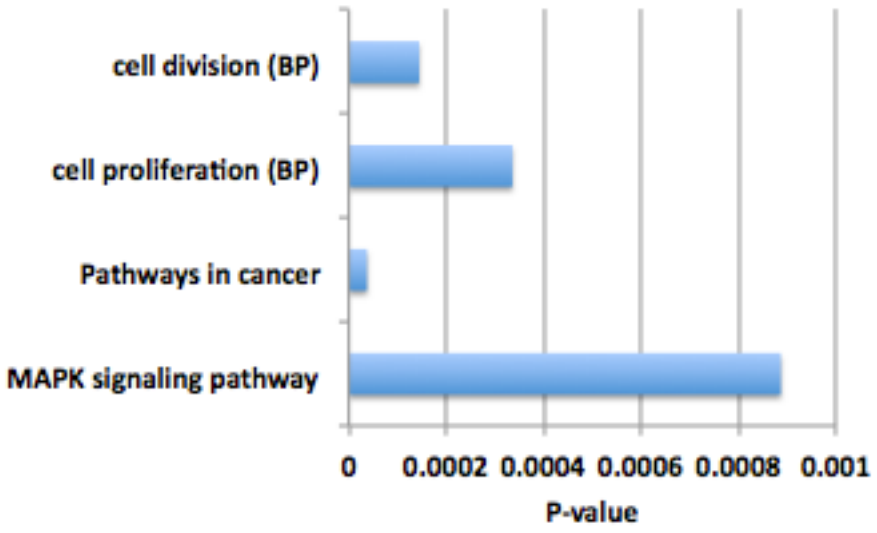


Figure 3.17 Enriched Gene Ontology terms and KEGG Pathways for the experimentally identified set of miR-191 targets.

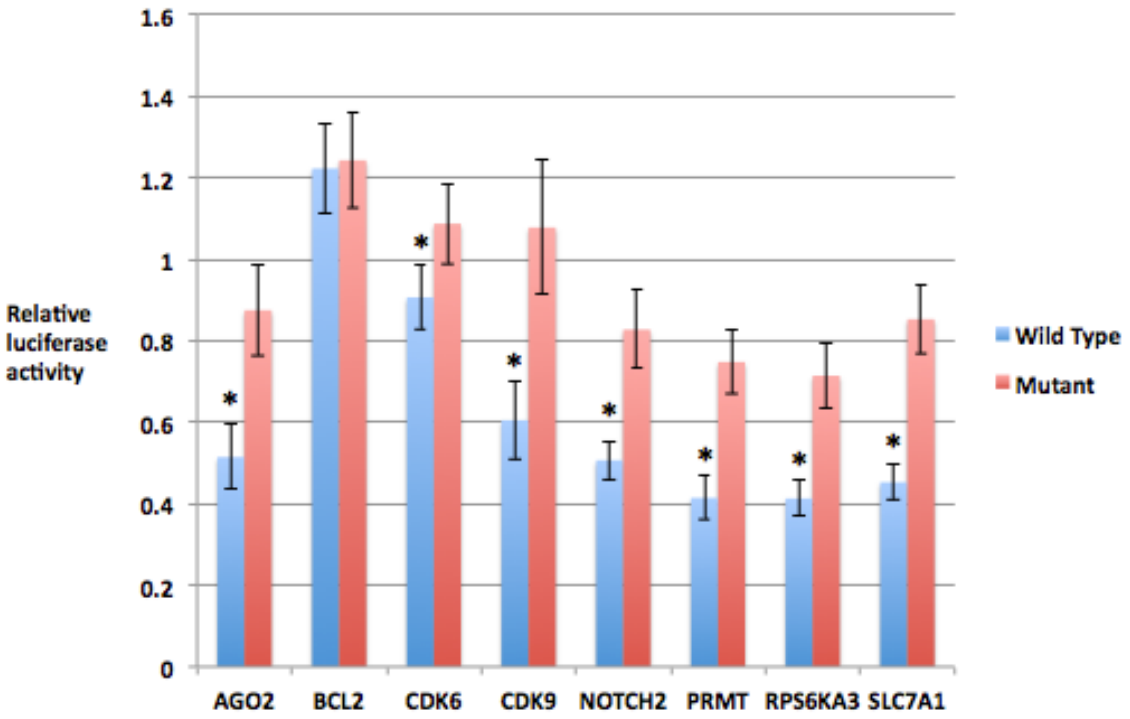


Figure 3.18 Direct targets of miR-191.

Luciferase reporter assays show miR-191 directly targets the 3'UTRs of the genes indicated on the X-axis. The Y-axis denotes relative luciferase units from miR-191 transfected HEK293 cells normalized to Control siRNA transfected cells. Red bars: 3'UTRs with the putative miR-191 target site entirely deleted. Blue bars: Intact 3'UTRs. Error bars denote ± SD, n = 6. Bars indicate the mean. P-values were estimated by Students one tailed paired t-test comparing intact 3'UTR samples to mutant 3'UTR samples. *$P < 0.05$.

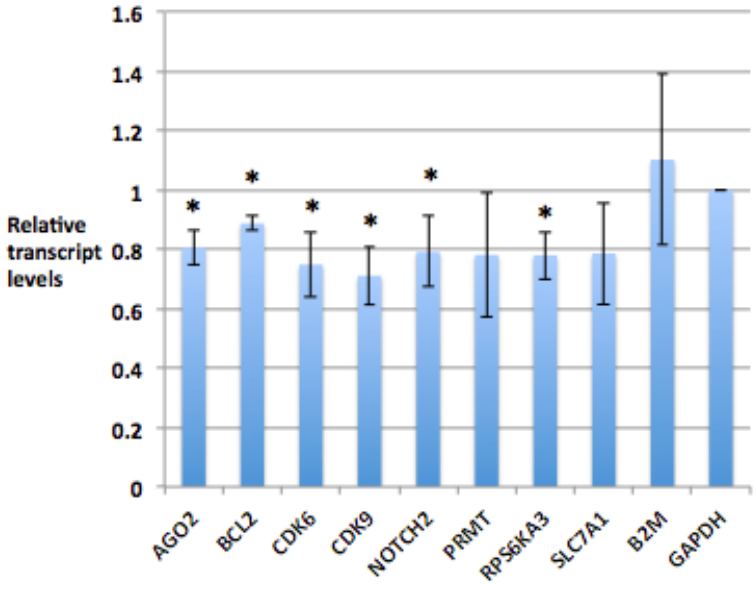


Figure 3.19 miR-191 transfection significantly decreased AGO2, BCL2, CDK6, CDK9, NOTCH2, and RPS6KA3 transcript levels in fibroblasts.

Fold changes are indicated on the Y-axis relative to the Control siRNA transfection. GAPDH was used to normalize input RNA levels. Bars indicate the mean, and error bars denote ± SD, n = 3. P-values were estimated by Student's one tailed t-test. *P < 0.05.

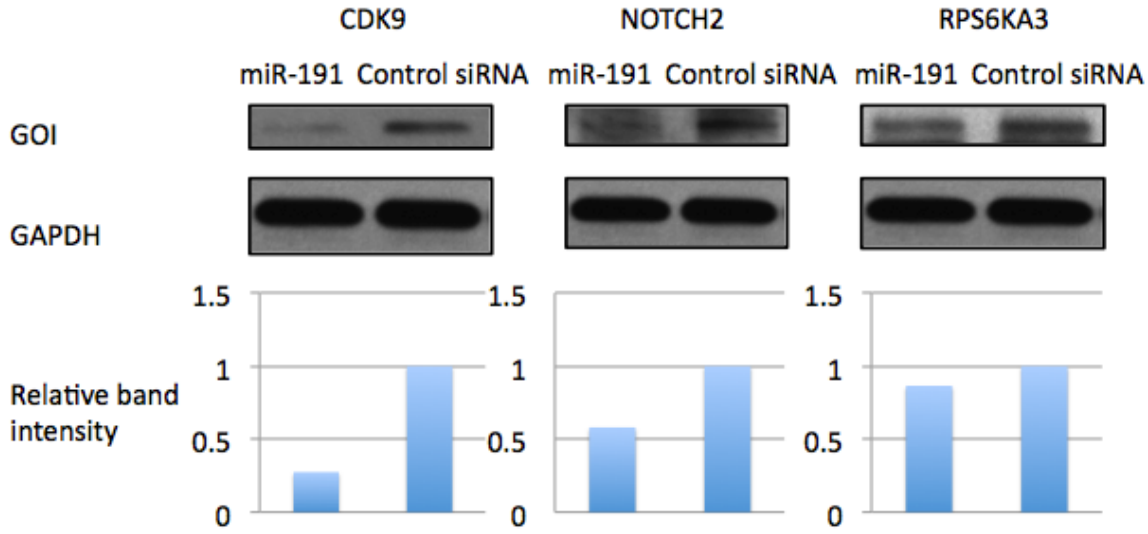


Figure 3.20 miR-191 transfection in fibroblasts decreased protein expression of CDK9, NOTCH2, and RPS6KA3.

Compared to Control siRNA transfection. Band intensities were quantified, normalized to GAPDH, and shown relative to the Control siRNA.

### 3.4.5 The involvement of miR-191 in NSCLC

miR-191 has previously been shown to repress or enhance proliferation in a cancer type and cancer subtype dependent manner (83, 84, 87). Despite the involvement of miR-191 in a plethora of different cancer types, miR-191 was shown to have to no effect on proliferation in lung cancer in the small cell lung cancer (SCLC) cell line A549 (98). We used the MIRUMIR tool to query the prognostic value of miR-191 in multiple cancer types, and observed the highest correlation between NSCLC and miR-191 expression (93). Patients with high miR-191 expression have a significantly lower survival probability than patients with low miR-191 expression (Figure 3.21). Transient overexpression of miR-191 in multiple NSCLC derived cell lines showed a cell type dependent effect on proliferation (Figure 3.22A). The effect on cell cycle progression following miR-191 transfection correlated with the effect of miR-191 on proliferation marker Ki67 in H2444 NSCLC cells, but not H460 cells or H2122 cells (Figure 3.22A & B). Although proliferation in H460 cells was significantly repressed, there was no change in cell cycle progression suggesting miR-191 has little effect on proliferation in H460s. There was a consistent and significant increase in cell cycle progression in H2122 cells following miR-191 transfection, but no change in the fraction of the cell population expressing Ki67. This may be due to a large fraction of the cancer cell population already existing in a proliferative state and expressing high levels of Ki67. In total, this data shows miR-191 has no overall consistent effect on NSCLC proliferation and suggests miR-191 may effect NSCLC progression in a cancer subtype dependent manner.

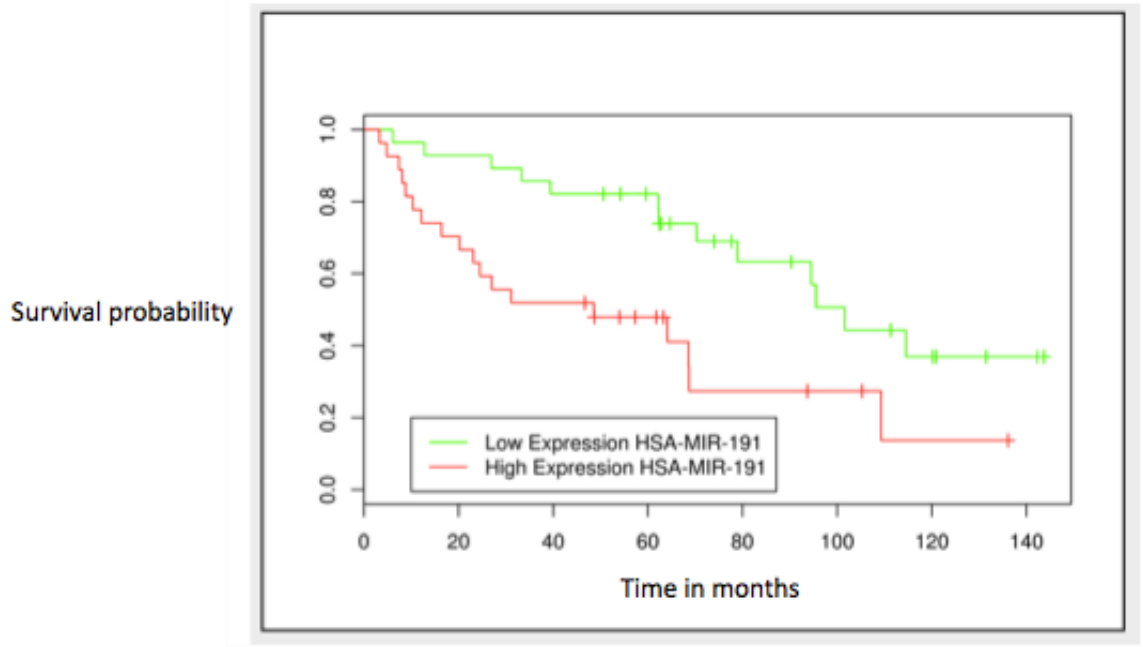


Figure 3.21 High miR-191 expression correlates with a lower survival probability in NSCLC cancer patients.

p= 4.27e-03. Kaplan-Meier survival curves for patients with NSCLC cancer with different levels of miR-191 expression were calculated using the MIRUMIR tool.

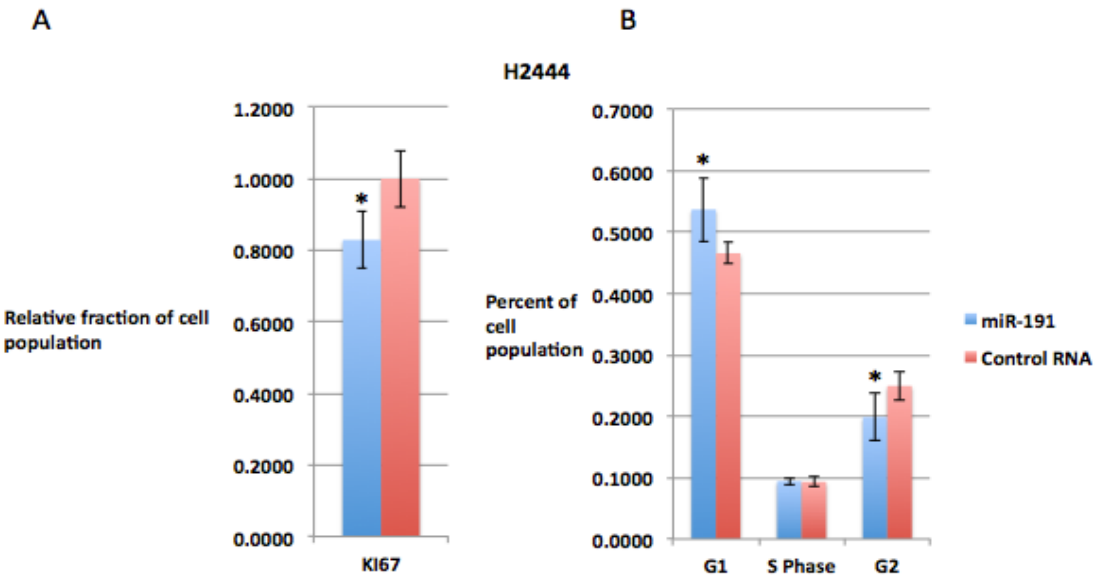


Figure 3.22 miR-191 transfection regulates NSCLC cell proliferation in a cell type specific manner.

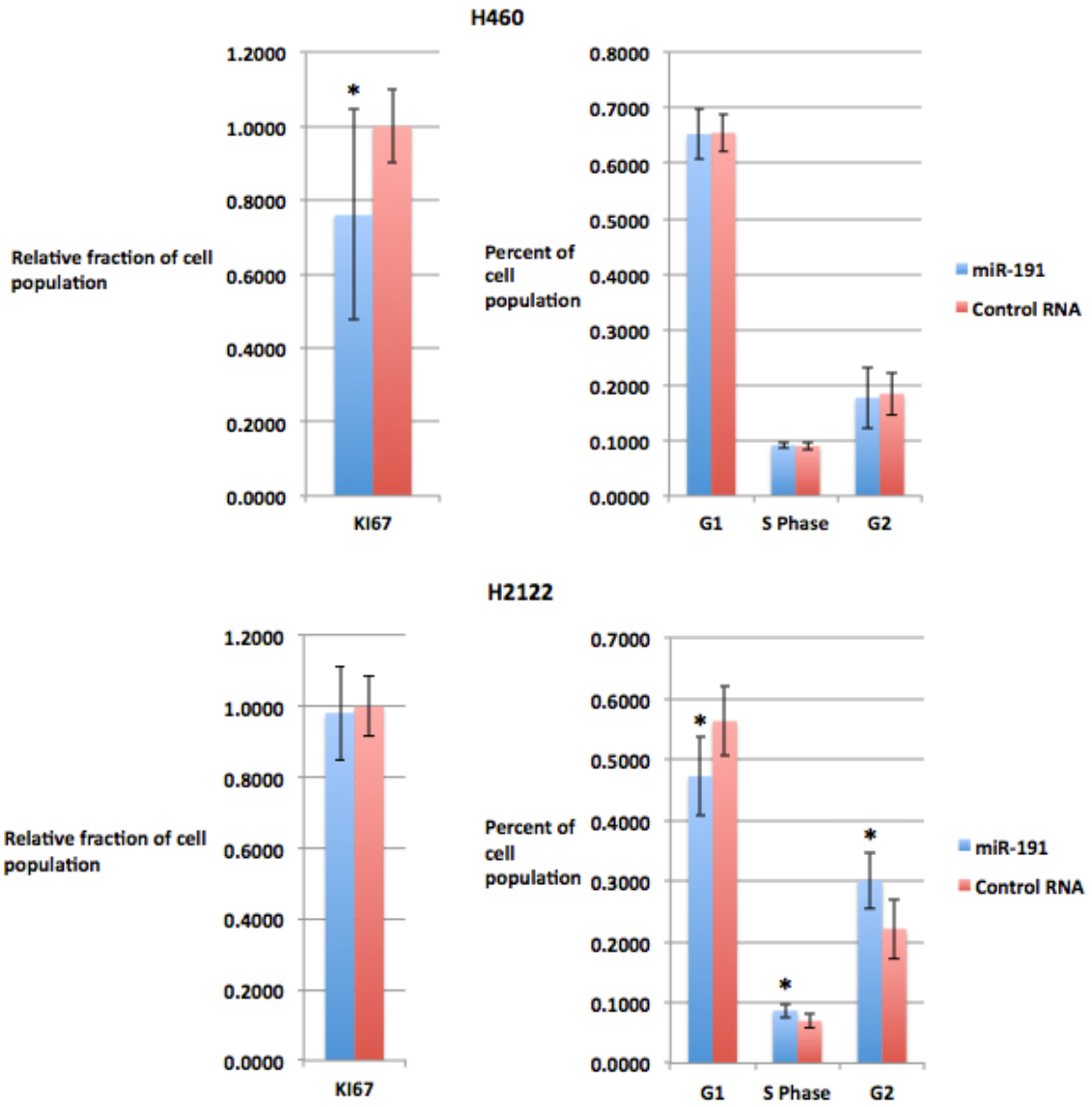


Figure 3.22 miR-191 transfection regulates NSCLC cell proliferation in a cell type specific manner.

(A) Shown by flow cytometry analysis for expression of proliferation marker Ki67 in miR-191 transfected NSCLC cell lines. The Y-axis indicates the relative percentage of cells expressing Ki67. Bars are the mean percentage of cells expressing Ki67 relative to the Control siRNA. (B) miR-191 transfection alters cell cycle progression of NSCLC cell lines in a cell line dependent manner. Shown by flow cytometry analysis of cell cycle progression using propidium iodide staining of miR-191 transfected NSCLC cell lines. The Y-axis denotes the percentage of cells found in each stage of the cell cycle, and bars are the mean percentage the cell population found in each stage. For A and B, error bars indicate ± SD, n = 6. P-values were estimated by Student's t-test. *$P < 0.05$.

## 3.5 DISCUSSION

In this study, we showed that miR-191 regulates proliferation in multiple cell types and targets a number of proto-oncogenes. By constructing a transcriptome wide miR-191 target set, we were able to identify and confirm the regulators of proliferation CDK9, NOTCH2, and RPS6KA3 as direct targets of miR-191. We demonstrated that miR-191 represses proliferation and cell cycle progression in primary human fibroblasts. In addition, our results suggested that miR-191 mediates gene expression of a large proportion of its target genes by binding to the CDS. Finally, we explored the role of miR-191 in NSCLC proliferation, and observed cell line specific regulation by miR-191.

CDK9 regulates RNA polymerase II controlled gene expression to mediate cell growth, proliferation, apoptosis and differentiation (99). CDK9 activity is deregulated in numerous malignancies and human pathologies, and is a target for pharmacological inhibition for cancer therapies (99). NOTCH2 is overexpressed in multiple cancer types and has been shown to have oncogenic effects, including on proliferation (100, 101). RPKS6KA3 is part of the MAPK3 pathway, and promotes proliferation in multiple cancer types (102, 103). Although the effect of miR-191 on the protein levels of CDK9, NOTCH2, and RPS6KA3 was modest, moderate repression of multiple key proliferation associated genes may have large phenotypic effects in concert.

miR-191 expression is frequently altered in tumors, and may be up or down regulated depending on cancer type (97). miR-191 has predominately been shown to act as an oncogene, promoting tumorigenesis in gastric, colorectal, breast, thyroid, and hepatocellular carcinoma, but has also been shown to inhibit tumorigenesis in thyroid carcinoma and breast cancer (83, 85, 87, 97). In multiple cases, miR-191 influences tumor progression by regulating proliferation; miR-191 promotes proliferation in hepatocellular carcinoma, and in gastric carcinoma by targeting NDST1, but inhibits proliferation in thyroid carcinoma by targeting CDK6 (83, 84). The duality of miR-191 is illustrated in breast cancer: miR-191 impairs or promotes breast cancer tumorigenesis depending on ER-alpha receptor status (87, 104). We examined the effect of miR-191 on proliferation of multiple NSCLC cell lines, and observed a cell line dependent effect on proliferation despite the significant correlation of high miR-191 expression with low

survival probability in NSCLC. Interestingly, in a different lung cancer subtype, SCLC, miR-191 had no effect on proliferation (98). Taken as a whole, the cancer, cancer subtype, and cell line specific effects of miR-191 on proliferation suggest miR-191 regulates proliferation in a manner dependent upon cancer subtype and genetic context.

Transcriptome wide gene expression analysis following miRNA perturbation has shown that miRNA seed matches in the CDS have little effect on transcript levels (24, 26). Transcriptome wide profiling of miRNA targets using more recently developed biochemical techniques has revealed extensive RISC occupancy of the CDS, but the effect on transcript levels by CDS targeting was generally negligible (27, 29, 30, 95, 96). At most, target sites in the CDS exert about half as strong of an effect on transcript levels as targets in the 3'UTR (27). We observed a large fraction of miR-191 seed matches in the CDS, and in agreement with previous studies extensive miR-191 dependent RISC occupancy of the CDS. However, we also showed extensive miR-191 dependent regulation of transcript levels for mRNAs with a miR-191 seed match in the CDS, and the mRNAs with a seed match in their CDS showed a significantly stronger response than those with a 3'UTR seed match. The regulatory effect exerted by miR-191 through CDS binding may be an isolated case, but it raises the intriguing possibility that other miRNAs may employ CDS binding to regulate gene expression.

In summary, we demonstrated that miR-191 represses proliferation of primary human cells, and exerts a cell type dependent effect on NSCLC proliferation. We also showed that miR-191 targets and represses expression through binding to the CDS. Finally, we constructed a transcriptome wide profile of miR-191 targets and confirmed multiple novel proto-oncogene targets of miR-191.

# Chapter 4 miR-503 represses human cell proliferation and directly targets the oncogene DDHD2 by non-canonical target pairing.

## 4.1 ABSTRACT

The pathways regulating the transition of mammalian cells from quiescence to proliferation are mediated by multiple miRNAs. Our understanding of miRNA targeting has significantly improved, but the majority of miRNA regulatory networks are still largely unknown and require experimental validation. Here we show that miR-503, miR-103, and miR-494 promote proliferation in primary human cells. We experimentally identified their targets using RNA-induced silencing complex immunoprecipitations (RIPs) and gene expression profiling. Through analysis of the transcriptome wide target profiles, we observed evidence of non-canonical target pairing by the miRNAs. We identified the oncogene DDHD2 as a target of miR-503 that requires pairing outside of the canonical 5' seed region of miR-503. Further bioinformatics analysis implicated miR-503 and DDHD2 in breast cancer tumorigenesis. Our results provide an extensive transcriptome wide set of targets for miR-503, miR-103, and miR-494, and suggest the involvement of miR-503 in breast cancer by its direct non-canonical targeting of DDHD2.

## 4.2 INTRODUCTION

miRNAs were initially observed to predominantly target and direct the RNA-induced silencing complex (RISC) to mRNAs through perfect pairing of the seed region located at the 5' end of the miRNA (23, 24, 26). There are known examples of miRNAs that utilize further pairing to either complement pairing at the 5' seed, or compensate for mismatches in pairing at the 5' seed, but until recently, miRNAs were thought to rarely employ non-canonical targeting (105). Recent improvements in methodologies to globally identify miRNA targets revealed more widespread use of alternative targeting by miRNAs (27-30). In one case, Loeb *et al*. noted approximately 40% of miR-155 dependent binding of RISC occurred at sites without perfect seed pairing (29). Most

recently, Helwark *et al*. observed 60% of all miRNA target pairs displayed bulges or mismatches in the seed region (27).

miR-503, miR-103, and miR-494 have previously been shown to act as either oncogenes or tumor suppressors in different cellular contexts (106-110). miR-503 acts as a tumor suppressor in non-small cell lung cancer, glioblastoma, and hepatocellular carcinoma (110-114). Despite the broad involvement of miR-503 in repressing tumorigenesis in various cancers, the function of miR-503 has not been explored in either primary cells or breast cancer.

In this study, we investigated the regulation of cell proliferation in primary human cells by miR-503, miR-103, and miR-494. We identified a transcriptome wide set of the targets of miR-503, -103, and -494 by conducting extensive profiling of RISC associated transcripts and gene expression profiling. Computational analysis of the globally identified targets indicated utilization of non-canonical target pairing for miR-503 and -103. We further explored the targeting mechanisms of miR-503 experimentally, and confirmed that miR-503 targets the oncogene DDHD2 through non-canonical target pairing. Additional bioinformatic analysis showed a link between miR-503, DDHD2, and breast cancer.

## 4.3 MATERIALS AND METHODS

Methods used were the same as those in described in Chapter 3 unless otherwise noted.

### 4.3.1 Defining a miRNA target list using RIP enrichment and gene expression repression

Target scores to rank each mRNA were generated by averaging RIP enrichment values and gene expression repression values. mRNAs with a score of 1.75 or greater were designated as the target set.

### 4.3.2 Searching for non-canonical target pairing

For miR-503, the criteria used to search for compensatory sites (5' mismatch + additional 3' pairing) were: (1) a 6-mer matching position 1-6 with 1 mismatch, and (2)

an 8-mer matching position 11-18 with 0 – 3 mismatches, (3) a 1 base pair wobble allowed in the length of the sequence separating the 6-mer and 8-mer. To search for complementary sites (5' mismatch + additional 3' pairing) the criteria used were: (1) a 6-mer perfectly matching position 1-6, and (2) an 8-mer matching position 11-18 with 0 – 3 mismatches, (3) a 1 base pair wobble allowed in the length of the sequence separating the 6-mer and 8-mer.

For miR-103, the criteria used to search for compensatory sites (5' mismatch + additional 3' pairing) were: (1) a 6-mer matching position 2-7 with 1 mismatch, and (2) an 8-mer matching position 11-18 with 0 – 3 mismatches, (3) a 1 base pair wobble allowed in the length of the sequence separating the 6-mer and 8-mer. To search for complementary sites (5' mismatch + additional 3' pairing) the criteria used were: (1) a 6-mer perfectly matching position 2-7, and (2) an 8-mer matching position 13-20 with 0 – 3 mismatches, (3) a 1 base pair wobble allowed in the length of the sequence separating the 6-mer and 8-mer.

### 4.3.3 Luciferase reporter assays

We cloned 0.9 kb of the 3'UTR of DDHD2 centered around the putative miR-503 binding site into the psi-CHECK2 plasmid (Promega) downstream from the Renilla luciferase gene using XhoI and NotI restriction sites. This plasmid was used to produce three mutant variants. In the whole-site deletion variant, the entire 22 bp sequencing corresponding to the length of miR-503 at its binding site was deleted. In the 3' deletion variant, the 6 bp sequence corresponding to positions 7-12 of the putative binding site (Figure 4.16) (and positions 11-16 of the miRNA in a putative duplex) was deleted. In the 5' deletion variant, the 6 bp sequence corresponding to positions 17-22 of the putative binding site (Figure 4.16) (and positions 2-7 of the miRNA in a putative duplex) was deleted.

HEK293 cells were plated in 24-well plates at $10^5$ cells/well in DMEM supplemented with 10% FBS and 1% Pen-Strep and grown overnight (Hyclone, Gibco). Each plasmid was co-transfected at 50 ng/well with either miRNA or siGFP duplex at a 100 nM in triplicate (Lipofectamine, Invitrogen). Cells were harvested 24 hours post-

transfection and luciferase activity was measured using the Promega Dual Luciferase kit according to manufacturer's instructions. Data was first normalized per-well by dividing Renilla luminescence by Firefly luminescence. Then, the mean of the three biological replicates for each miRNA transfected group was divided by the mean of its corresponding siGFP transfected group to determine the relative luciferase activity value.

### 4.3.4 Western blotting

Primary human fibroblasts or HeLa cells were seeded in 6-well plates at 5 x $10^4$ cells/well in DMEM supplemented with 10% FBS (Hyclone, Invitrogen). 24 hours after plating, miR-503 or siGFP duplexes were transfected at a 100 nM concentration (Lipofectamine, Invitrogen). Transfected cells were lysed at 24 hr, 48 hr, 72 hr, or 96 hr post-transfection.

Cell lysates were separated on 4-20% gradient SDS-PAGE gels (Biorad) and proteins were transferred onto PVDF membranes. Membranes were blocked with 5% milk or 5% BSA in TBST and probed overnight with primary antibody in blocking solution (DDHD2: 1/500, Abacam, ab103965 ; GAPDH: 1/1000, Abcam, ab9486). The membranes were washed, incubated with HRP-conjugated secondary antibody in blocking solution (1/5000, Santa Cruz Biotechnology, sc-2004), and washed again. HRP substrate solution was added to the membranes, and incubated for four minutes (Pierce). Blots were exposed to autoradiographic film and developed (Carestream Kodak Biomax). Images of the films were scanned and band intensities quantified using a white-light transilluminator imaging system (FlourChem Q, ProteinSimple).

### 4.3.5 Cancer survival and copy number alteration analysis

Survival probabilities of ER+ breast cancer patients were generated with MIRUMIR (http://www.bioprofiling.de/GEO/MIRUMIR/mirumir.html) (93). Data on DDHD2 copy number alteration frequency and patient survival in patients with different cancer types was generated using cBio portal (http://www.cbioportal.org/public-portal/)(115). For each cancer type the percentage of patients with DDHD2 amplifications, and patient survival probabilities, were calculated as an average of all data

sets available for this cancer type. P-values were calculated with a hypergeometric distribution.

## 4.4 RESULTS

### 4.4.1 miR-503, miR-103, and miR-494 repress proliferation

miRNAs that regulate proliferation are differentially expressed in quiescent and proliferating primary human fibroblasts (116). Using previously published data as well as additional miRNA expression profiling of primary human fibroblasts transitioning from quiescence to proliferation, we identified numerous miRNAs induced in fibroblasts transitioning from quiescence to proliferation (116). Multiple miRNAs were selected for further study based on two criteria: (1) Consistent induction by serum stimulation, and (2) bioinformatic analysis indicating that the miRNA targets proliferation and or cell cycle related genes (data not shown).

As a preliminary screen to identify miRNAs that regulate proliferation, we transiently overexpressed each miRNA by transfecting the mature duplex form of the miRNA into proliferating fibroblasts and assayed cell proliferation by expression of the proliferation marker Ki67 (53, 54). Surprisingly, multiple miRNAs appeared to decrease Ki67 levels, although this decrease was not statistically significant (Figure 4.1). miRNAs induced by serum stimulation were expected to increase proliferation, but there are numerous examples of miRNAs that participate in negative feedback loops (116-118). Of the miRNAs assayed, miR-503, miR-103, and miR-494 displayed the greatest reduction in Ki67 levels and were selected for further study (Figure 4.1).

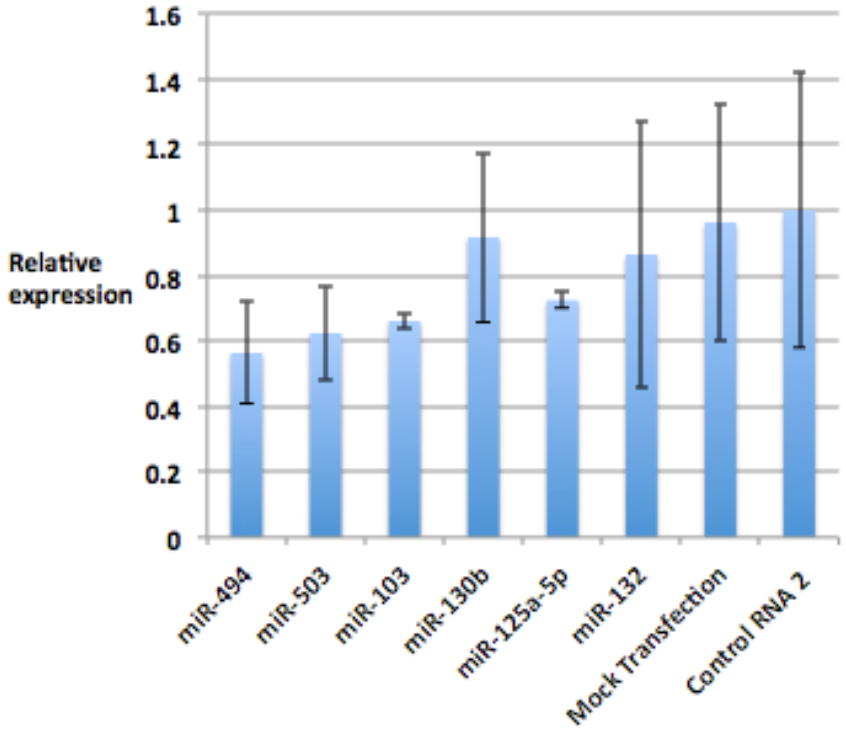


Figure 4.1 Screening for miRNA regulation of proliferation.

Proliferation of primary fibroblasts as measured by Ki67 expression levels. miRNA or Control siRNA duplexes were transfected into normally growing fibroblasts, and Ki67 levels of the cell population were measured by qRT-PCR. The column graph shows Ki67 expression levels relative to the control, which was set to a value of 1.0. Bars indicate the mean, and error bars denote ± s.d., n=3. *P*-values were estimated by Student's paired t-test. *, P<0.05.

To more thoroughly investigate the effect of miR-503, miR-103, and miR-494 on cell proliferation, we transiently overexpressed each of these miRNAs in proliferating fibroblasts and assayed the rate of cell growth. miR-503, -103, and -494 transfected cells showed significant reductions in the rate of cell growth (Figure 4.2). To confirm their effect on cell growth, we transfected miR-503, -103, -494, and miR-34a, a well known tumor suppressor (94), into proliferating fibroblasts and counted cells expressing Ki67 protein using flow cytometry. miR-503, -103, and -494 transfection significantly decreased the percentage of Ki67 positive cells compared to multiple controls, indicating that these three miRNAs repress proliferation, although not to the extent of miR-34a

(Figure 4.3). In addition, transient overexpression of miR-503, -103, and -494 in proliferating fibroblasts significantly decreased the rate of progression through the cell cycle (Figure 4.4). To rule out indirect effects from flooding the cells and the RNA silencing machinery with large amounts of the mature miRNA duplexes, we transiently inhibited miR-503, -103, and -494 in fibroblasts induced into quiescence by serum removal. Inhibition of miR-503, -103, and -494 in quiescent fibroblasts significantly increased the rate of cell growth (Figure 4.5).

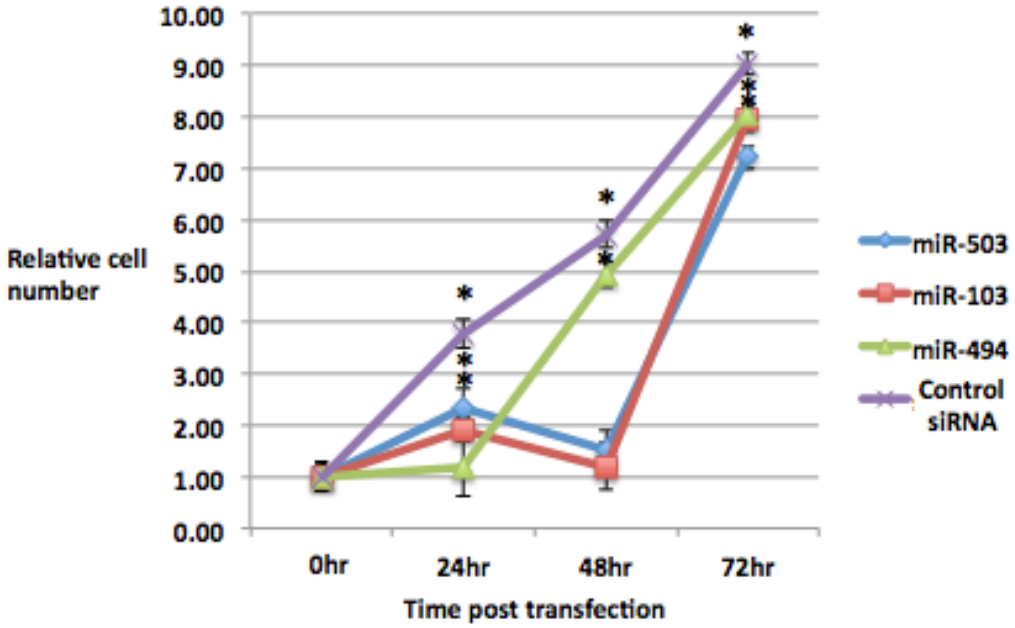


Figure 4.2 miR-503, -103, and -494 transfection reduces cell growth.

Average cell number relative to 0hr following miRNA or Control siRNA transfection is shown for each time point indicated in primary human fibroblasts. Error bars denote ± SD, n = 6. P-values were estimated by Student's t-test.

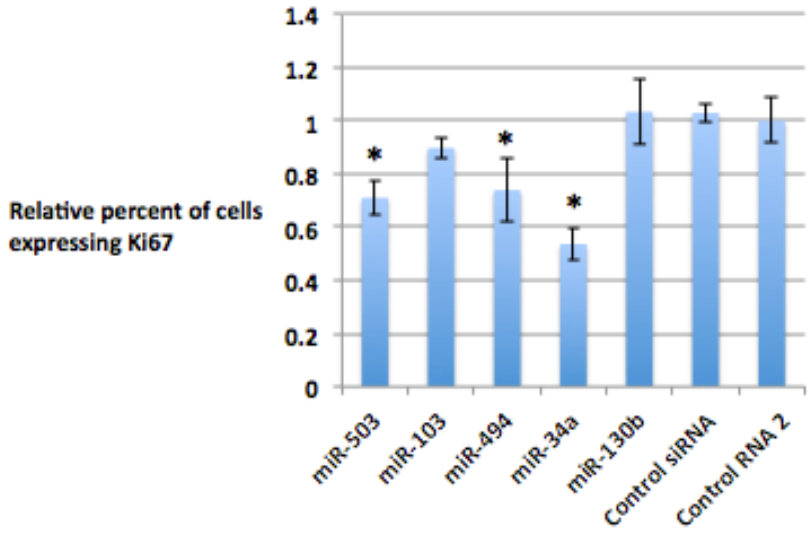


Figure 4.3 miR-503 and -494 transfection represses proliferation.

Shown by flow cytometry analysis for proliferation marker Ki67 of miR-503, -103, or -494 transfected fibroblasts. The Y-axis indicates the relative percentage of cells expressing Ki67. Bars are the mean percentage of cells expressing Ki67 relative to Control RNA 2, and error bars denote ± SD, n = 3. P-values were estimated by Student's t-test.

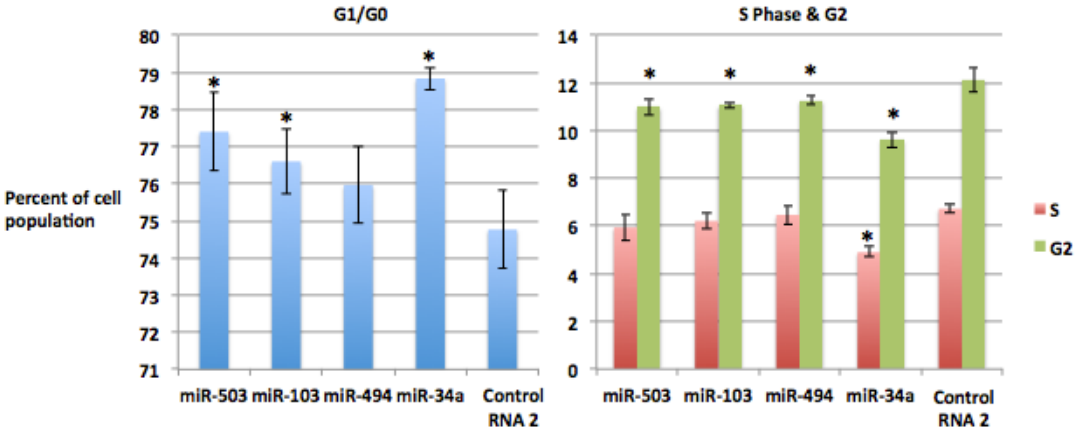


Figure 4.4 miR-503, -103, and -494 transfection inhibits progression through the cell cycle.

Shown by flow cytometry analysis of cell cycle progression using propidium iodide staining of miR-503, -103, or -494 transfected fibroblasts. The Y-axis indicates the percentage of cells found in each stage of the cell cycle, and bars are the mean percentage the cell population found in each stage. Error bars denote ± SD, n = 3. P-values were estimated by Student's paired t-test. *P < 0.05.

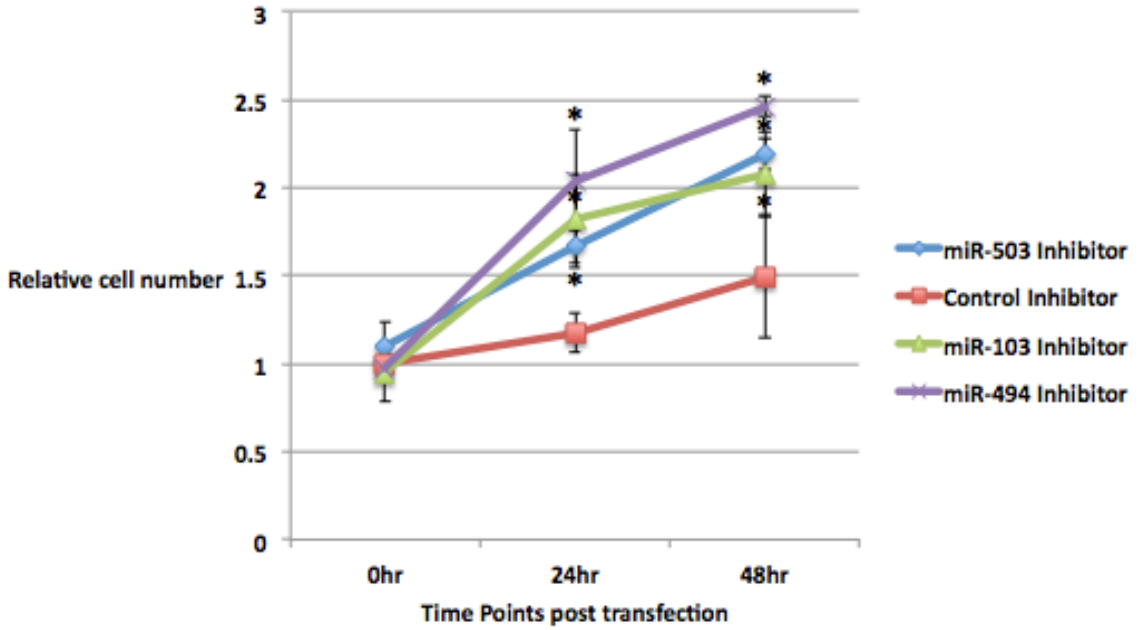


Figure 4.5 Inhibition of miR-503, -103, and -494 increases cell growth in fibroblasts serum starved into quiescence.

Average cell number relative to 0hr following transfection of an LNA targeting miR-503, -103, or -494 or a LNA negative control is shown for each time point indicated. Error bars denote ± SD, n = 6. P-values were estimated by Student's t-test. *P < 0.05.

### 4.4.2 Transcriptome wide identification of miR-503, -103, and -494 targets

To experimentally identify the targets of miR-503, -103, and -494 we used two approaches: (1) profiling of transcripts isolated from RIPs after transient overexpression of miR-503, -103, and -494, and (2) profiling gene expression after transient overexpression of the miRNAs (Figure 3.5). To immunoprecipitate RISC, we used a monoclonal antibody directed against Argonaute-2, an essential component of RISC (23). RISC is directed to target mRNAs by the mature miRNA guide strand (23). Increases in RISC occupancy on a given transcript following miRNA overexpression indicate direct targets of the overexpressed miRNA. We globally profiled RISC occupancy by quantifying transcripts isolated from RIPs using both microarrays (RIP-ChIP) and RNA-seq (RIP-Seq). As described for miR-191, enrichment was defined as an increase in RISC occupancy on a given transcript following miRNA transfection compared to the control

transfection. To obtain enough RNA for successful global profiling, all RIPs and gene expression experiments were conducted in HeLa cells, due to HeLa cells having a greater RNA content and being of a smaller size than human fibroblasts. As with miR-191, we observed strong correlation between the RNA-Seq and microarray experiments (Table 4.1). As previously stated, No RIP Control siRNA comparison could be made because RIP-ChIP with a Control siRNA was not conducted.

| | Spearman Correlation | |
|---|---|---|
| | RIP | Gene expression |
| miR-503 | 0.74 | 0.72 |
| miR-103 | 0.72 | 0.72 |
| miR-494 | 0.74 | 0.72 |
| siGFP | NA | 0.73 |
| Mock | 0.72 | 0.72 |

Table 4.1 RNA-seq and microarray Spearman rank correlation.

To determine if the RIP-Seq effectively identified miRNA targets, we first examined the enrichment of mRNAs in the RIP-Seq compared to their levels of repression in the gene expression experiments. Enrichment in the RIP-Seq correlated well with repression of gene expression (Table 4.2). mRNAs enriched in the RIPs for miR-503, -103, and -494 were significantly more repressed than all mRNAs profiled (Figure 4.6). In addition, mRNAs enriched in the RIPs for miR-503, -103, and -494 were significantly more repressed than all genes that contain the respective 7mer miRNA seed match in their 3'UTR, indicating the RIPs more successfully identified genes repressed by the miRNAs than using presence of the seed match as the lone criteria to identify miRNA targets (Figure 4.6).

| | Pearson Correlation |
|---|---|
| miR-503 | 0.65 |
| miR-103 | 0.58 |
| miR-494 | 0.63 |

Table 4.2 RIP enrichment correlates with repression of gene expression.

Enrichment in the RIP was compared to levels of repression in the gene expression experiments. Pearson correlation, n = 3.

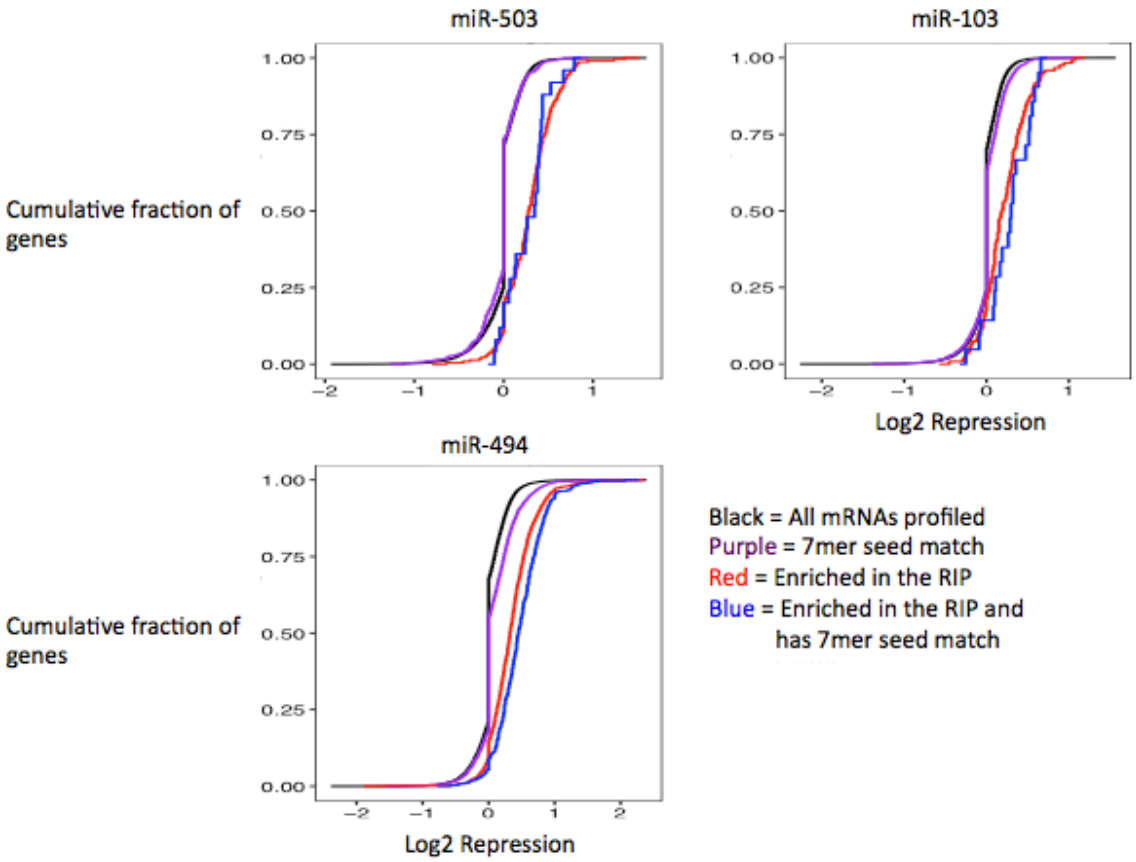


Figure 4.6 mRNAs enriched in the RIP-seq also showed reduced expression following miR-503, miR-103, or -494 transfection.

The Y-axis denotes the cumulative fraction of all mRNA transcripts profiled, and the X-axis indicates the level of repression for each mRNA transcript profiled. Black: all mRNAs profiled; Red: all mRNAs profiled that contain the respective 7-mer miRNA seed site in their 3'UTR; Purple: all mRNAs 1.75 fold enriched in the RIP; Blue: all mRNAs 1.75 enriched in the RIP that contain the respective 7-mer miRNA seed site in their 3'UTR. mRNAs that contain the respective miRNA 7-mer seed were significantly more repressed than all mRNAs profiled for miR-103, and -494, but not -503 (p= 1.16e-4, 3.17e-36, and 0.09, respectively). mRNAs enriched in the RIPs were significantly more repressed than mRNAs containing the respective miRNA seed for miR-503, -103, and -494 (p= 2.95e-40, 4.69e-13, and 1.82e-81, respectively). mRNAs enriched in the RIP and containing the 7-mer miRNA seed were significantly more repressed than mRNAs enriched in the RIP for miR-494, but not miR-503 or -103 (p= 2.77e-08, 0.79, and 0.31, respectively) Significance estimates were calculated with Student's t-test. n = 3.

As a second measure of RIP-seq effectiveness, we examined miRNA seed site frequency in RIP enriched mRNAs. mRNAs most enriched in the miR-503, -103, and -

494 RIPs had a high frequency of their corresponding miRNA seed sites (Figure 4.7). Conversely in the gene expression data, mRNAs that were most repressed following miRNA transient over expression showed the greatest enrichment for miR-503, -103, and -494 seed sites (Figure 4.8). Using a combination of both RIP enrichment data and repression of gene expression data to identify miRNA targets produced the highest frequency of seed sites in the most highly ranked targets (Figure 4.9). In addition, there was enrichment for proliferation related genes in the targets identified for miR-503 and miR-494, but there were not enough target genes identified for miR-103 to produce meaningful results (Appendix 1) (90-92).

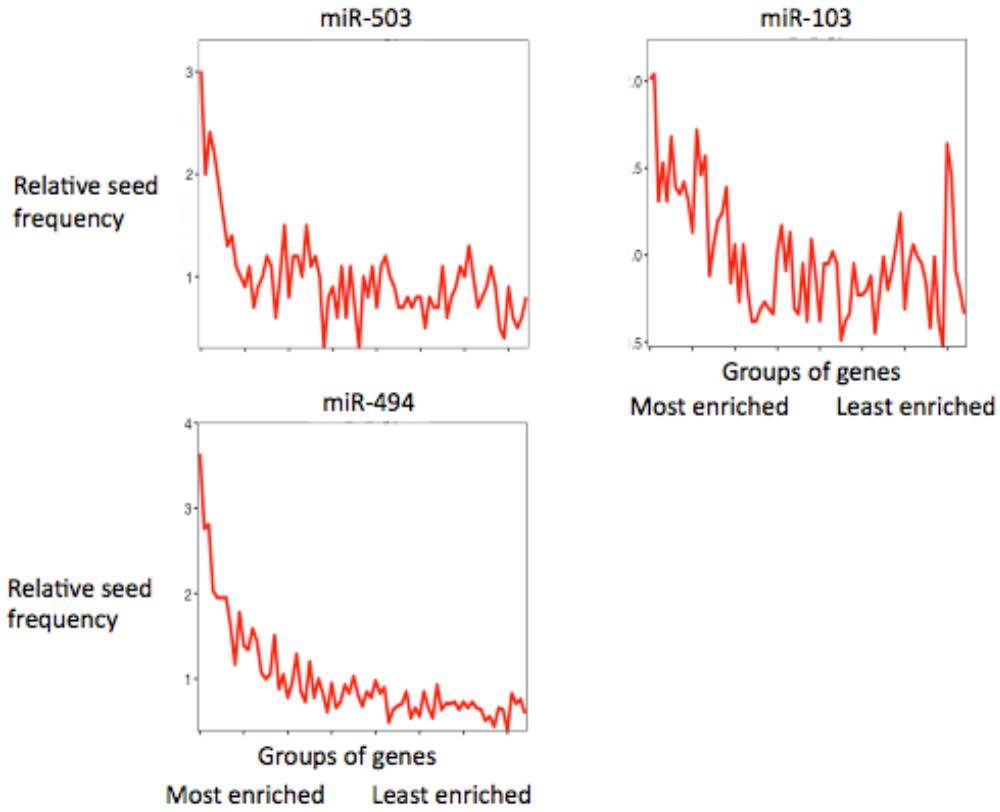


Figure 4.7 mRNAs enriched in the RIPs had the highest frequency of the respective miRNA seed site.

The X-axis denotes consecutive groups of 250 genes, ranked from most enriched to least enriched in the RIP-seq. The line is the frequency indicated on the Y-axis of the respective 7-mer miRNA seed in the gene group relative to the frequency of the seed in all genes profiled. n = 3.

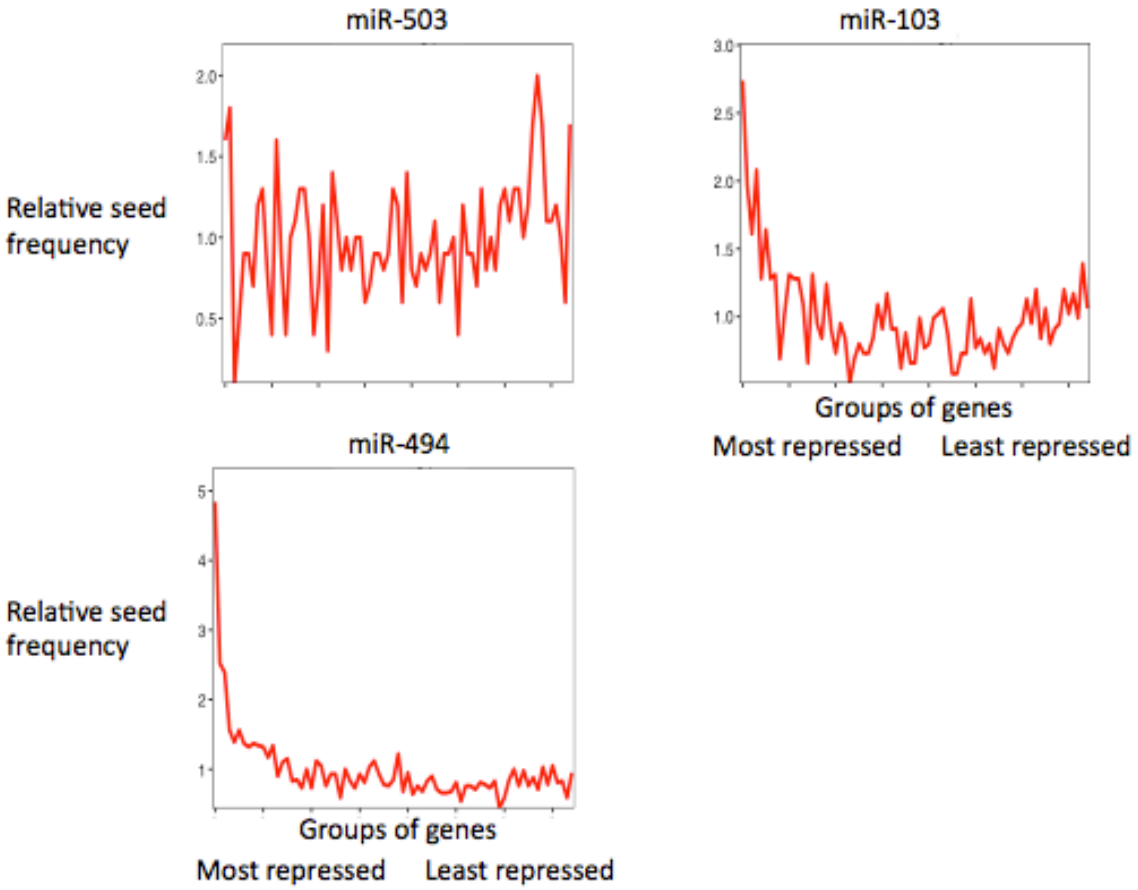


Figure 4.8 miR-103, and -494, mRNAs repressed in the gene expression experiments had the highest frequency of the respective miRNA seed.

The X-axis indicates consecutive groups of 250 genes, ranked from most repressed to least repressed. The line is the frequency indicated on the Y-axis of the respective 7-mer miRNA seed in the gene group relative to the frequency of the seed in all genes profiled. n = 3.

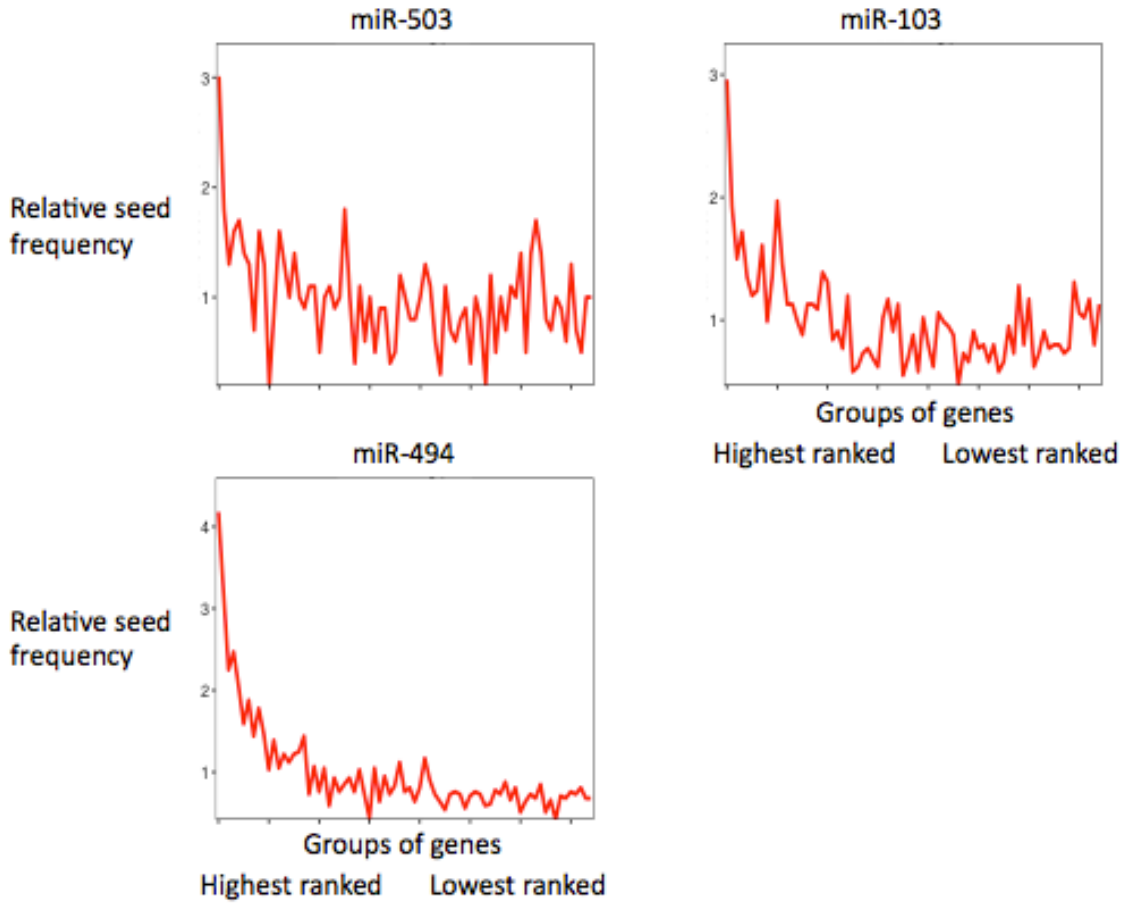


Figure 4.9 The highest ranked miRNA targets had the highest frequency of the respective miRNA seed sites.

RIP enrichment and gene expression repression data were combined to rank miRNA targets. The X-axis denotes consecutive groups of 250 genes, from most highly ranked to least highly ranked. The line is the frequency indicated on the Y-axis of the respective 7-mer miRNA seed in the gene group compared to the frequency of the seed in all genes profiled. Combines gene expression data, n = 3, with RIP-seq data, n = 3.

### 4.4.3 Enrichment of sequences pairing to the 3' end of the miRNAs in the experimentally profiled miRNA targetome

To determine the sub-sequences of miR-503, -103, and -494 that are used for targeting, we examined enrichment of 6-mer sequences that pair different areas of the mature miRNAs in the 3'UTRs of the experimentally identified target gene sets (Figure

4.10). As expected, there was a high frequency of 6-mer sequences that pair to the seed region, positions 2-7, of the mature miRNAs (Figure 4.10). Surprisingly, there was also a high frequency of sequences that pair the 3' end of the mature miRNAs. We observed the same phenomenon in targets identified by the separately conducted RIP-Chip and microarray gene expression profiling experiments (data not shown). Nelson *et al*. had previously reported this same finding when conducting global target identification for miR-103, and concluded that miR-103 utilized 3' pairing for targeting, although they did not further explore this observation experimentally (119). Based on the enrichment for the 5' seed site and a distinct 3' site for miR-503 and miR-103, as well as the observed miR-103 3' enrichment by Nelson *et al*., we hypothesized that miR-503 and -103 were using complementary or compensatory pairing to target mRNAs. Complementary pairing employs a perfect 5' seed match with additional 3' pairing, and compensatory pairing uses additional 3' pairing to compensate for mismatches or bulges in the 5' seed site (Figure 4.11)(23). Although miR-494 targets also displayed extensive enrichment for 6-mers pairing outside of the 5' seed region, the areas of enrichment were more diffuse, making them more difficult to investigate experimentally (Figure 4.10).

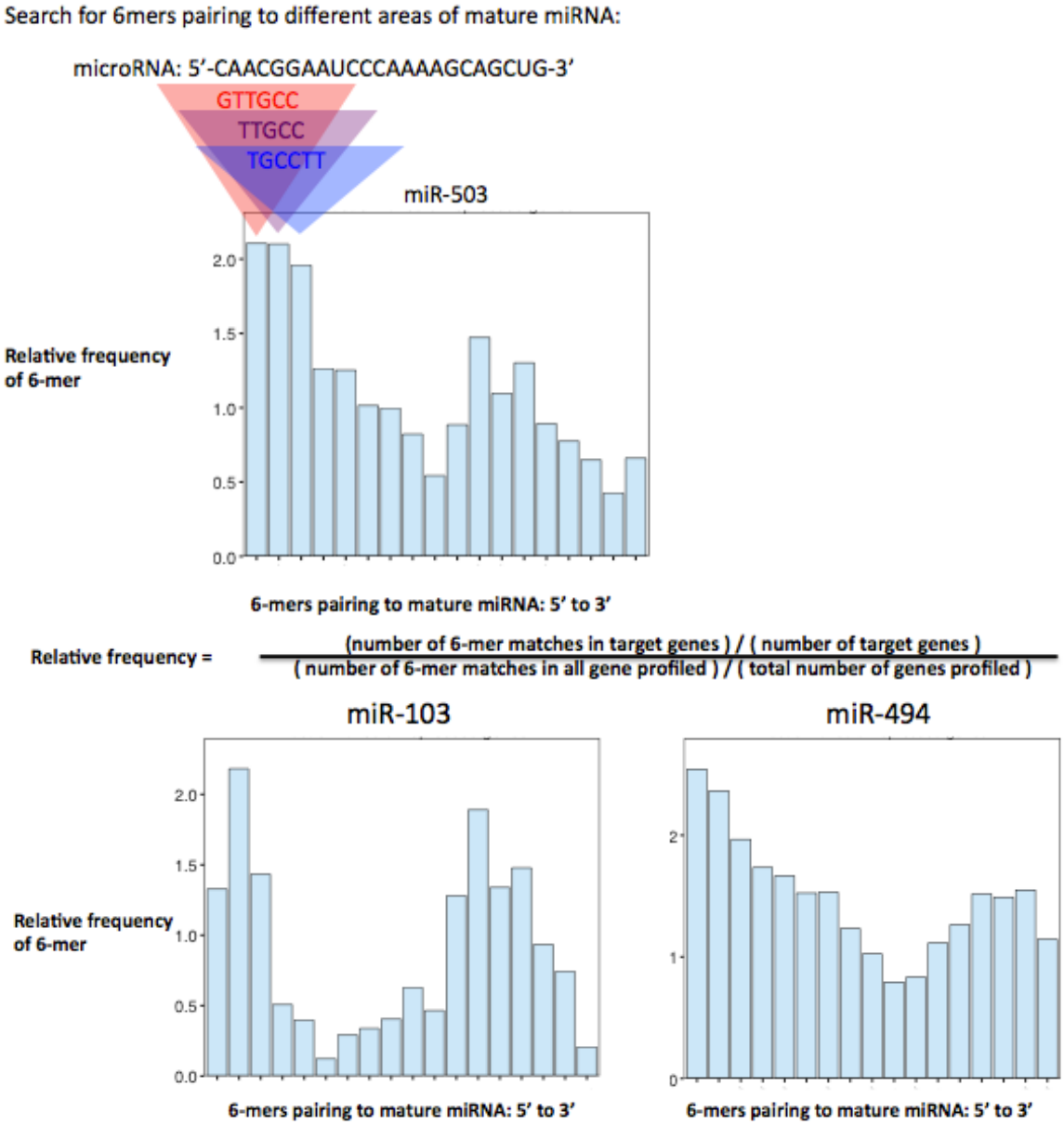


Figure 4.10 Enrichment of sequences pairing to the 3' end of the miRNAs in the experimentally determined miRNA targetomes.

Shown by the frequency of 6-mer sequences pairing to each 6-mer sequence in the mature miRNAs. Bars are the frequency indicated on the Y-axis of a 6-mer in the globally identified targets relative to all mRNAs profiled. 6-mers are organized along the X-axis from 5' end to 3' end of the mature miRNA.

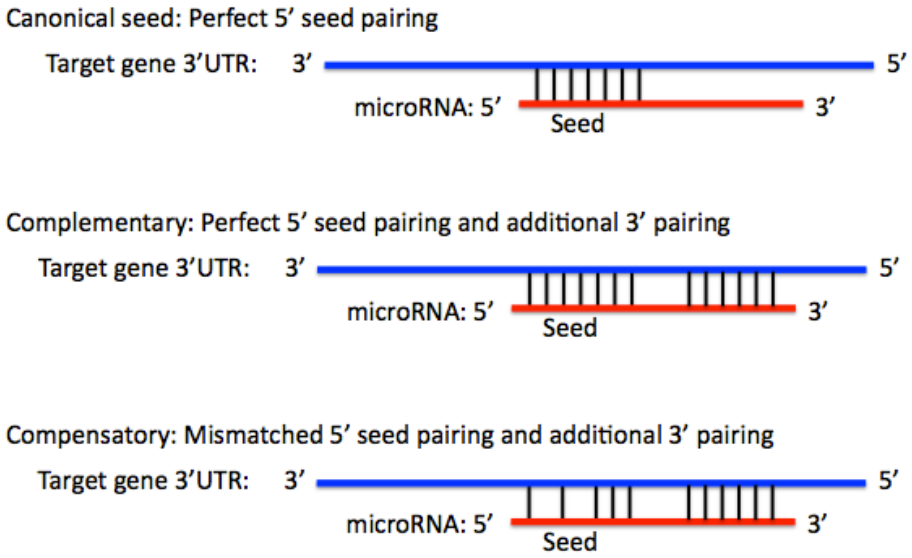


Figure 4.11 Different types of miRNA-target pairing.

To investigate the type of target pairing used by miR-503 and -103, we began by further analyzing our RIP-seq data and RNA-seq gene expression data. We first examined the frequency of compensatory and complementary pairing sites in highly ranked targets. Due to the most enriched 5' 6-mer for miR-503 being from position 1-6 (Figure 4.10), for miR-503 we used both a canonical 5' position 2-7 seed site, as well as a 5' position 1-6 seed site. The frequency of compensatory pairing sites in the target gene set for either miR-503 or miR-103 was not higher than the frequency of 5' seed sites (Figure 4.12). However, complementary pairing sites were much more frequent than the 5' seed sites and compensatory pairing sites (Figure 4.12).

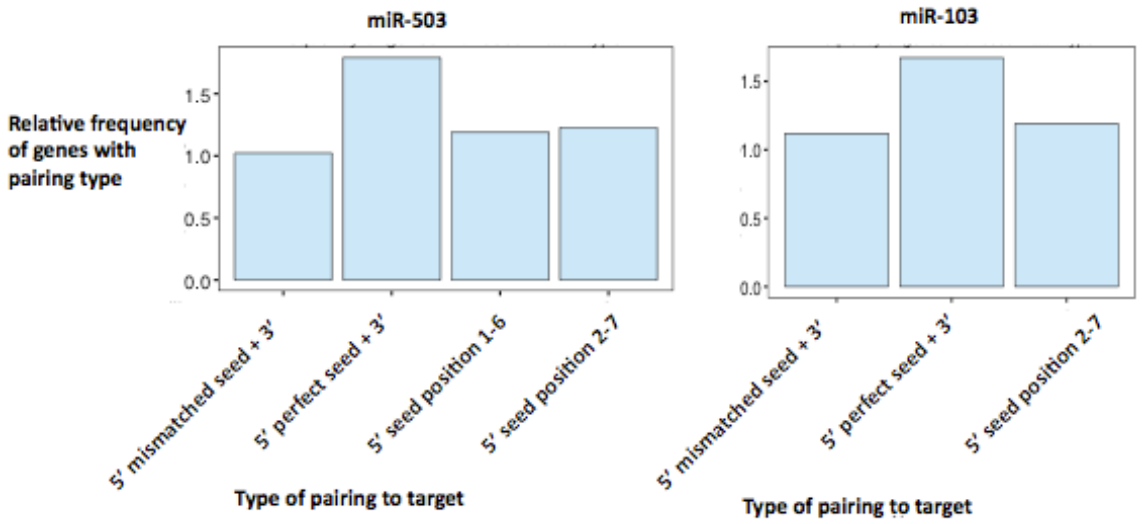


Figure 4.12 Frequency of different types of miRNA pairing sites in RIP-Seq enriched mRNAs.

Bars are the frequency of mRNAs with the indicated type of miRNA pairing site in the RIP enriched mRNAs, relative to the frequency of mRNAs with the indicated type of miRNA pairing site in all mRNAs profiled.

Next we examined RIP-seq enrichment and repression of mRNA targets with compensatory or complementary pairing sites. mRNAs that were enriched in the RIP for miR-503 and contained complementary pairing sites were significantly more repressed than all mRNAs that were enriched in the RIP (Figure 4.13A). In agreement with the RIP-Seq, the RIP-ChIP showed a significant but minor increase in repression for complementary pairing sites (data not shown). There were no significant differences in repression for miR-103 or in enrichment for either miR-503 or miR-103 depending on pairing type (Figure 4.13B and data not shown). When we expanded our analysis to include all genes profiled, we observed no significant differences in enrichment or repression between genes with a 5' seed site, a compensatory pairing site, or a complementary pairing site (data not shown). Taken together, this data strongly suggests miR-503 may utilize complementary target pairing. There were no differences between compensatory target pairing sites and the intact 5' seed alone for both miR-503 and miR-

103, making it difficult to draw conclusions as to utilization of compensatory target pairing.

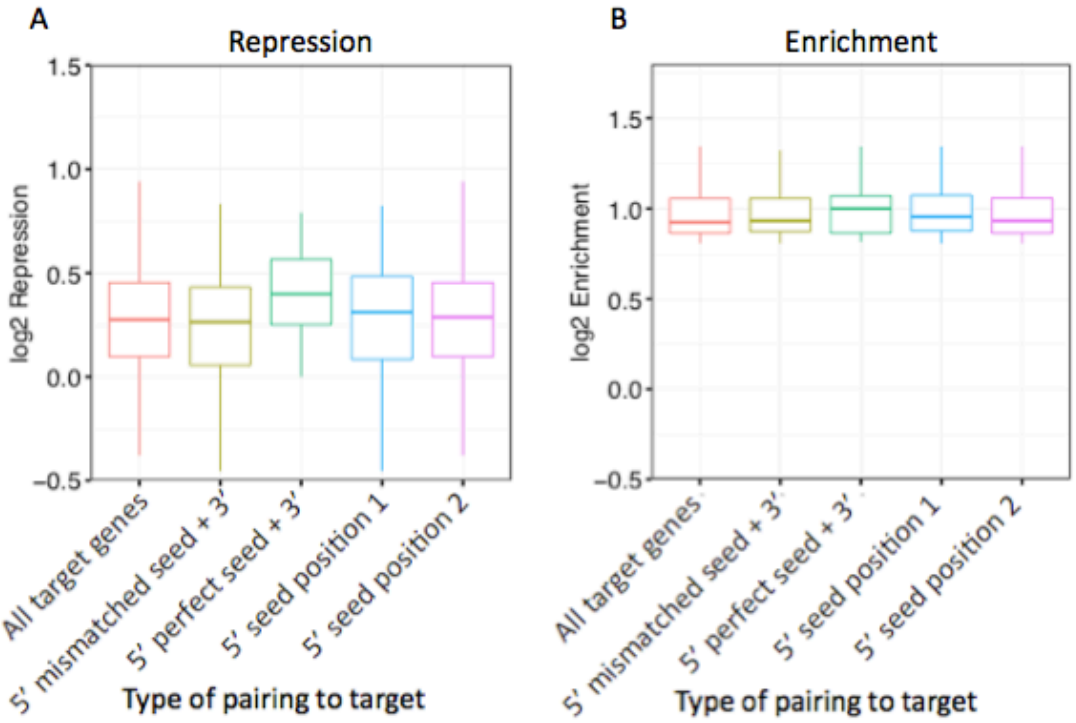


Figure 4.13 Repression of mRNAs with a complementary pairing site.

(A) RIP-seq enriched mRNAs containing a complementary pairing site in their 3'UTR are significantly more repressed than all RIP-seq enriched mRNAs, but not all RIP-seq enriched mRNAs that contain a perfect 5' seed in their 3'UTR (p= 0.04 and 0.06, respectively, Student's t-test). Shown by comparing repression of gene expression in miR-503 RIP enriched mRNAs with different types of miRNA-target pairing site. Each box and whiskers indicates gene expression repression for genes that contain the type of miRNA-target pairing site specified on the X-axis. Boxes extend from the 1$^{st}$ to 3$^{rd}$ quartile of gene expression repression, the band is the median, and whiskers denote the min and max excluding outliers. (B) There were no significant differences in miR-503 RIP enrichment of gene expression in RIP enriched mRNAs with different types of miRNA-target pairing site. Each box and whiskers indicates RIP enrichment for mRNAs that contain the type of miRNA pairing site specified on the X-axis. Boxes extend from the 1$^{st}$ to 3$^{rd}$ quartile of RIP enrichment, the band is the median, and whiskers denote the min and max excluding outliers.

### 4.4.4 Pairing of the 3' and 5' end of miR-503 is necessary for direct targeting by miR-503 of the cell growth promoting gene DDHD2

To experimentally determine the target pairing mechanisms used by miR-503 we cloned the 3'UTRs of multiple genes with pairing to the 5' and 3' end of miR-503 into luciferase reporter constructs. The genes were selected based on three criteria: (1) combined RIP-seq and RNA-seq gene expression repression rank, (2) sequences in their 3' UTR that paired the 5' and 3' end of miR-503, and (3) their involvement in promoting cell proliferation (Figure 4.14). For controls, we deleted the putative miR-503 target pairing sites in the 3'UTRs of the selected genes. Surprisingly, miR-503 repressed none of the reporters compared to controls with 3' UTRs from genes with sites with a mismatch in the 5' seed region and additional 3' pairing (Figure 4.15). miR-503 did repress expression of the reporter with the 3'UTR of DDHD2 that has a perfect miR-503 5' seed match and additional 3' pairing (Figure 4.15), indicating that miR-503 utilizes complementary but not compensatory target pairing. To determine the involvement of miR-503 5' and 3' pairing in targeting DDHD2, we constructed additional reporter constructs of the 3'UTR of DDHD2 with the sequence matching the 5' end of miR-503 deleted or the sequence matching the 3' end of miR-503 deleted (Figure 4.16). Unexpectedly, leaving 5' pairing intact and deleting only the sequence pairing the 3' end of miR-503 significantly relieved repression by miR-503, indicating miR-503 requires 3' pairing to target DDHD2 in addition to the 5' perfect seed match (Figure 4.16). As expected, deleting the sequence matching the 5' seed of miR-503 also significantly relieved repression (Figure 4.16). Interestingly, the difference was not significant in luciferase reporter activity between the 3' and 5' deletion constructs. To further confirm functional targeting of DDHD2 by miR-503, we transfected miR-503 into proliferating fibroblasts and HeLas. Transient overexpression of miR-503 did not repress the transcript levels of DDHD2 in proliferating primary human fibroblasts (data not shown) but did decrease protein levels in both fibroblasts and HeLas, indicating miR-503 more strongly represses DDHD2 expression through inhibition of translation than mRNA destabilization (Figure 4.17).

```
BRCA1

MIR-503 (23)    3'- GACGUCUUGACAAGGGCGACGAU -5' (1)
                    | ||| ||||||        |
3' UTR  (6964) 5'- ATCCAGGACTGTTTATAGCTGTT -3' (6986)


CBLL1

MIR-503 (23)    3'- GACGUCUUGACAAGGGCGACGAU -5' (1)
                    |   |  ||||||   | | ||
3' UTR  (2300) 5'- CAAAATTACTGTTAGTGTTTCTT -3' (2322)


CCNT2

MIR-503 (23)    3'- GACGUCUUGACAAGGGCGACGAU -5' (1)
                       || ||||||   |     |
3' UTR  (2772) 5'- GCAAAGTACTGTTAAGGTGATAA -3' (2794)


PAPPA

MIR-503 (23)    3'- GACGUCUUGACAAGGGCGACGAU -5' (1)
                    | |   ||||||  | ||| |
3' UTR  (5565) 5'- TTCCCATACTGTTTTCTCTGATC -3' (5587)


STAMBP

MIR-503 (23)    3'- GACGUCUUGACAAGGGCGACGAU -5' (1)
                    |   |  ||||||   |
3' UTR  (2856) 5'- CCTTTTGACTGTTGATGGCTTCT -3' (2878)


ZNF268

MIR-503 (23)    3'- GACGUCUUGACAAGGGCGACGAU -5' (1)
                    |||  |||||||
3' UTR  (4547) 5'- ATGCCTAACTGTTGTATTCTGCT -3' (4569)


DDHD2

MIR-503 (23)    3'- GACGUCUUGACAAGGGCGACGAU -5' (1)
                    |    |||||||   ||||||
3' UTR  (651)   5'- TTTTGCAACTGTTTGAGCTGCTG -3' (673)
```

Figure 4.14 Diagram of miR-503 non-canonical target pairing sites in the 3' UTRs of putative targets.

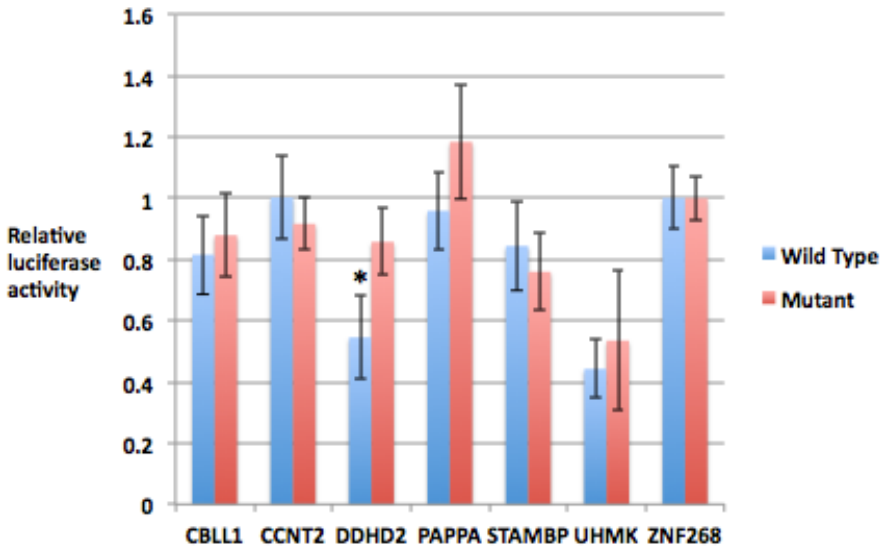


Figure 4.15 Luciferase reporter assays investigating non-canonical miR-503 target pairing.

The 3'UTRs of mRNAs being investigated are indicated on the X-axis. The Y-axis denotes relative luciferase units from miR-503 transfected cells normalized to Control siRNA transfected cells. Red bars: 3'UTRs with the putative miR-503 target site entirely deleted. Blue bars: Intact 3'UTRs. Error bars denote ± SD, n = 3. P-values were estimated by 1 tailed Student's t-test. *$P < 0.05$.

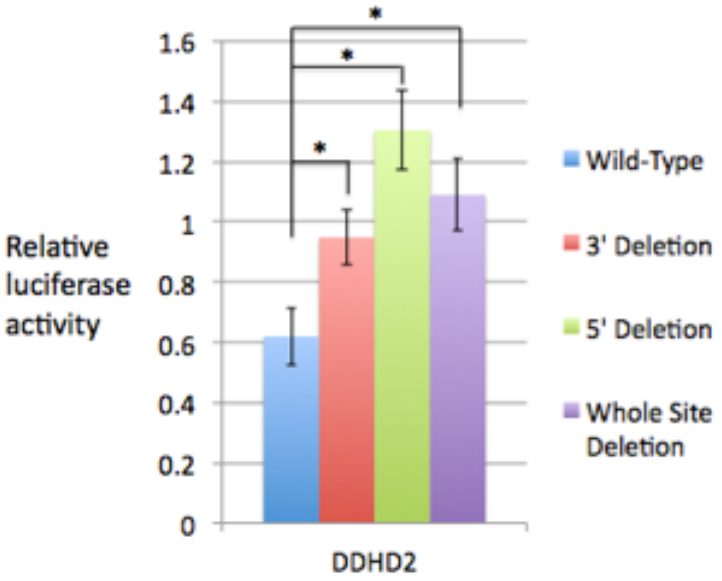


```
DDHD2 (Wild Type)

MIR-503 (23)   3'- GACGUCUUGACAAGGGCGACGAU -5' (1)
                   |    |||||||   ||||||
3' UTR  (651)  5'- TTTTGCAACTGTTTGAGCTGCTG -3' (673)


DDHD2 (3' Deletion)

MIR-503 (23)   3'- GACGUCUUGACAAGGGCGACGAU -5' (1)
                   |               ||||||
3' UTR  (651)  5'- TTTTGC-------TGAGCTGCTG -3' (673)


DDHD2 (5' Deletion)

MIR-503 (23)   3'- GACGUCUUGACAAGGGCGACGAU -5' (1)
                   |    |||||||
3' UTR  (651)  5'- TTTTGCAACTGTTTGA------G -3' (673)
```

Figure 4.16 Pairing by the 3' and 5' end of miR-503 to the 3'UTR of DDHD2 is necessary to repress expression.

Shown by luciferase reporter assay activity with different sections of the miR-503 target site in the 3'UTR of DDHD2 deleted. The Y-axis denotes relative luciferase units from miR-503 transfected cells normalized to Control siRNA transfected cells. Blue bar: Intact 3'UTRs. Red: 3'UTR with deletion of pairing to 3' end of miR-503. Yellow: 3'UTR with deletion of pairing to 5' end of miR-503. Red bars: 3'UTR with the putative miR-503 target site entirely deleted. Error bars denote ± SD, n = 3. P-values were estimated by 1 tailed Student's t-test. *P < 0.05.

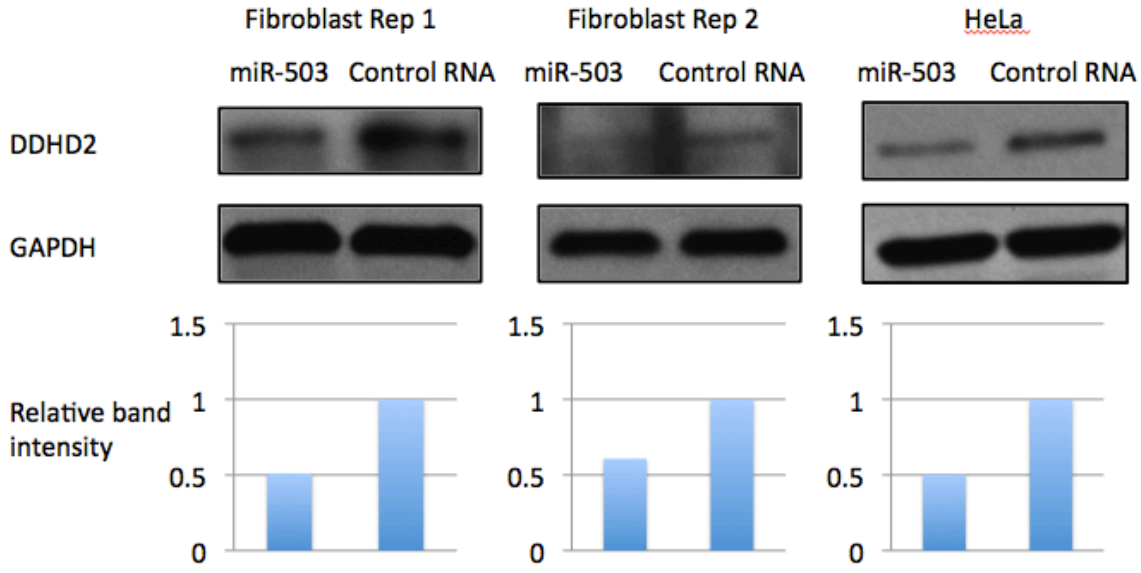


Figure 4.17 miR-503 transfection decreased protein expression of DDHD2.

DDHD2 protein expression following miR-503 transfection in fibroblasts and HeLas compared to Control siRNA transfection. Band intensities were quantified, normalized to GAPDH, and shown relative to the Control siRNA.

### 4.4.5 The involvement of miR-503 in ER+ breast cancer

DDHD2 has previously been shown to be tumor promoting in breast cancer by cooperating functionally with Myc to stimulate breast cancer cell growth (120). In addition, DDHD2 was observed to be located in an area of high level copy number aberrations in breast tumors (120). Amplification of this area most frequently occurs in estrogen receptor positive (ER+) breast tumors (120).

We used the MIRUMIR tool to query the prognostic value of miR-503 expression levels in a published data set of patients with high-risk ER+ breast cancers (93). Patients with high miR-503 expression had a significantly higher survival probability than patients with low miR-503 expression (Figure 4.18). Analysis of DDHD2 alterations using the cBio portal revealed that DDHD2 tends to be amplified in a variety of cancers, and most predominantly in breast invasive carcinoma (~12% of cases) (Figure 4.19). In addition, patients with copy number alterations of DDHD2 had a significantly lower survival probability than patients without copy number alterations of DDHD2 (Figure

4.20). This data suggests miR-503 plays a role in breast cancer tumorigenesis at least in part by targeting DDHD2.

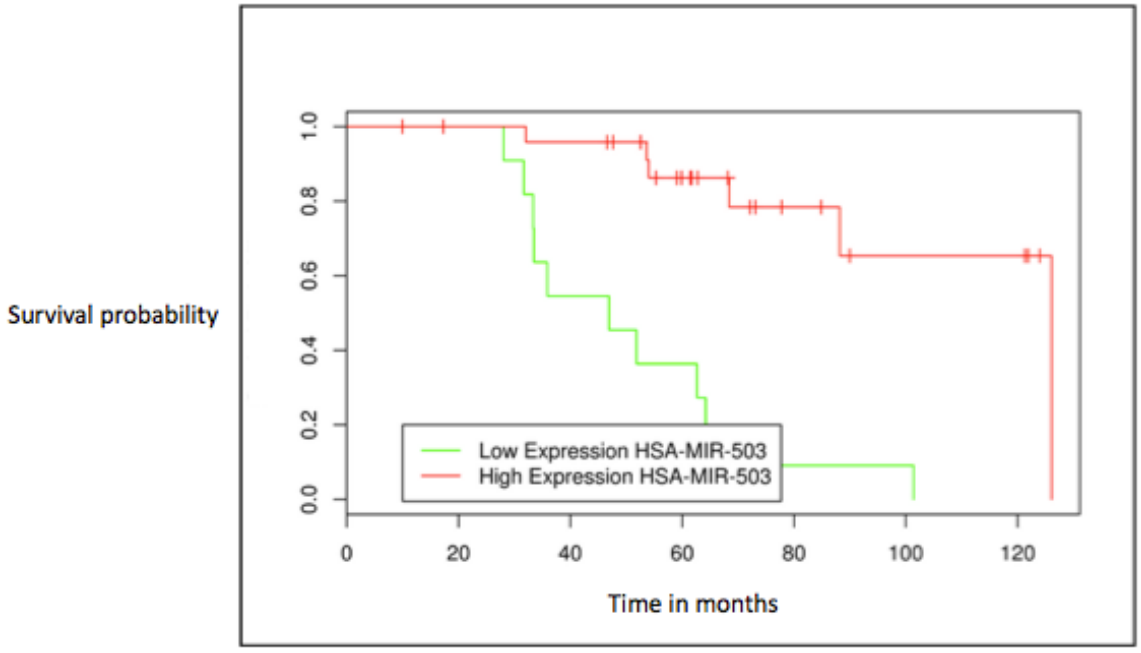


Figure 4.18 Low miR-503 expression correlates with a lower survival probability in ER+ breast cancer patients.

p= 8.56e-06. Kaplan-Meier survival curves for patients with ER+ breast cancer expressing different levels of miR-503 were calculated using the MIRUMIR tool.

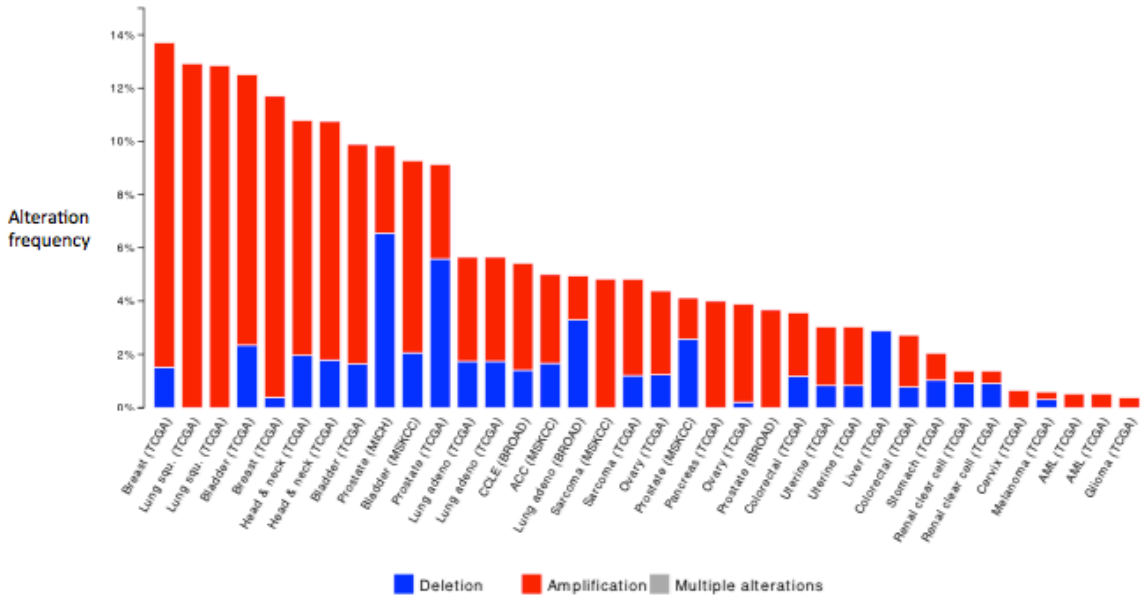


Figure 4.19 DDHD2 is frequently amplified in breast cancer.

The bars are the frequency of DDHD2 copy number alterations in the different types of cancer indicated on the X-axis. The frequency of patients with DDHD2 amplification was calculated using the cBio portal. Blue: Deletion; Red: Amplification.

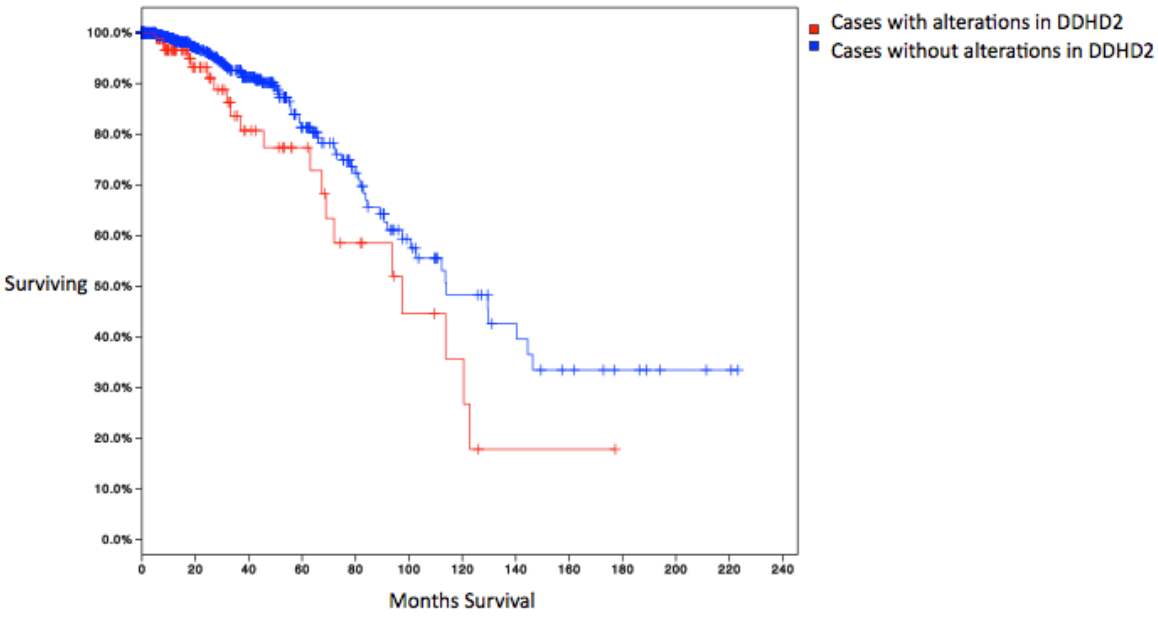


Figure 4.20 DDHD2 copy number alterations correlate with survival probability.

Patients with copy number alterations in DDHD2 (red line) have a lower survival probably than those without amplifications in DDHD2 (blue line) (Logrank test p= 0.027795). Kaplan-Meier survival curves were was calculated using the cBio portal.

## 4.5 DISCUSSION

In this study, we experimentally determined the targetome of multiple miRNAs that repress cell proliferation, and showed that miR-503 regulates the expression of the proto-oncogene DDHD2 by non-canonical targeting. We began by screening for miRNA involvement in primary cell proliferation, and identified miR-503, -103, and -494 as regulators of primary cell proliferation. We then constructed transcriptome wide target sets for miR-503, -103, and -494 using RIP and global gene expression profiling methodologies. Our analysis of the target sets revealed potentially widespread use of non-canonical targeting for each of the miRNAs. We went on to show that miR-503 targets the oncogene DDHD2 non-canonically, requiring 3' pairing of miR-503; and further analysis linked miR-503 to ER+ breast cancer through DDHD2.

Recent advances in methodologies to profile the entire miRNA targetome have uncovered extensive mediation of RISC binding by non-canonical targeting (27-30).

However, the effects of non-canonical targeting on gene expression ranged from moderate at most, to statistically insignificant depending on the study (27, 29, 121). This discrepancy may be due to differences in the reliance on miRNA seed interactions to identify targets. In our experiments, we found evidence of extensive non-canonical targeting by miR-503, -103, and -494 mediating both RISC occupancy and gene expression. We went on to experimentally confirm that 3' target pairing was necessary for miR-503 to repress DDHD2. miR-503 targeting of DDHD2 may represent an isolated case, but analysis of our experimentally identified transcriptome wide target set suggests miR-503 uses 3' target pairing to mediate gene expression throughout its targetome.

In addition, we showed that miR-503 acts like a tumor suppressor by non-canonically targeting the putative oncogene DDHD2. Relatively little is known about DDHD2. DDHD2 was previously shown to promote tumorigenesis in breast cancer by cooperating functionally with Myc to enhance breast cancer cell growth (120). DDHD2 is located in an area that is frequently amplified in breast tumors, and most frequently in ER+ breast tumors (120). Our analysis showed that decreased miR-503 expression correlated with low patient survivability, and that DDHD2 copy number alterations were most frequent in invasive breast carcinoma and correlate significantly with low patient survivability. Taken together, these data suggest that miR-503 may function as a previously unknown tumor suppressor in ER+ breast cancer.

miR-503 has been shown to act as a tumor suppressor in several cancers, and decreases in miR-503 expression have been reported in multiple cancer types (110, 111, 113, 122). In addition, miR-503 has been shown to target multiple oncogenes and regulators of proliferation (111, 114, 122, 123). miR-503 inhibits hepatocellular carcinoma, glioblastoma multiforme, and non small cell lung cancer (NSCLC) tumorigenesis by repressing proliferation, inducing cell cycle arrest, and reducing metastasis (110, 111, 113, 124). Additionally, miR-503 also represses hepatocullelar carcinoma tumor angiogenesis by targeting the potent angiogenic factors FGF2 and VEGFA (113). miR-503 has also been shown to play a role in repressing endometrial cancer (122). Considered as a whole, these studies suggest that miR-503 operates as a potent tumor suppressor that regulates multiple pathways that are frequently deregulated

in tumorigenesis. Moderate repression of multiple key regulatory genes can have large phenotypic effects in concert, and miR-503 may conceivably inhibit breast cancer tumorigenesis by repressing multiple previously known targets in addition to DDHD2.

In summary, we demonstrated that miR-503 represses cell proliferation, and may function as a tumor suppressor in ER+ cancer by utilizing non-canonical 3' pairing to target the proto-oncogene DDHD2. In addition, we provide experimentally determined transcriptome wide target profiles of the proliferation related miRNAs miR-503, -103, and -494.

# Chapter 5 Summary and Future Directions

In this work we: (1) Explored the function of multiple miRNAs in regulating proliferation; (2) Used RIP methodologies to construct transcriptome wide profiles of the targets of miR-191, -503, -103, and -494; (3) Discovered a miR-22 Myc regulatory network that links the gene networks controlling the cell cycle and interferon response (4) Identified multiple proto-oncogenes targeted by miR-191; and (5) Characterized the non-canonical targeting of the proto-oncogene DDHD2 by miR-503.

## 5.1 CELL TYPE SPECIFIC REGULATION

We comprehensively demonstrated that miR-22 promotes proliferation in primary human fibroblasts by targeting cell cycle arrest pathways that are mediated by the tumor suppressor p53, and identified multiple specific inhibitors of cell cycle progression that are targeted by miR-22. Other groups have also observed that miR-22 acts like a proto-oncogene, promoting proliferation and invasion of cancer cells by inhibiting the tumor suppressor PTEN (39-41). However, multiple groups have also reported that miR-22 inhibits proliferation of several cancer cell lines (42-44). We also showed that miR-22 up regulates Myc expression levels by repressing MXD4, a transcriptional repressor of Myc, but other groups have shown that miR-22 inhibits Myc activity by repressing Myc's binding partners (42, 44).

In addition, we demonstrated that miR-191 represses primary cell proliferation and targets multiple proto-oncogenes and promoters of proliferation. miR-191 expression significantly correlates with NSCLC survival; however, we observed varying and cell line specific effects on proliferation by miR-191 in NSCLC cell lines. miR-191 has been shown to act as an oncogene in multiple cancer types, but also has been shown to frequently function as a tumor suppressor in several other cancer types (83, 85, 87, 97). In breast cancer, Di Leva *et al*. elegantly demonstrated that miR-191 promotes or impairs tumorigenesis depending on ER-alpha receptor status (104).

As illustrated by these examples, an individual miRNA is frequently found to have opposing functions depending on context. Generally, these differences in function

are hypothesized to depend on cell type or genetic background, and are not further explored. With current advances in miRNA target identification methodologies allowing for significantly higher quality profiling of miRNA targets, as well as the exponential increases in sequencing throughput and datasets available, these cell type specific differences can more feasibly and should be explored.

## 5.2 miRNA TARGETING LOCATION

Using our experimentally determined miR-191 targetome, we showed that seed matches in the CDS had increased RISC occupancy and a greater effect on transcript levels than seed matches in the 3' UTR. Multiple groups have observed extensive RISC occupancy of the CDS; however, seed matches in the CDS having greater efficacy has not been previously reported (24, 26, 27, 29, 30, 95, 96). In general seed matches in the CDS have been observed to have no significant effect on gene expression, but it should be noted that most studies examining miRNA targeting of the CDS region profiled all targets of the miRNAome rather than focus on a single miRNA, suggesting the signal may be more diffuse. Our experiments were comprised of multiple replicates and isolated to one cell type and one miRNA, but this makes it difficult to draw broader conclusions as to the efficacy of seed matches in the CDS. In addition, it is possible that the effect on gene expression is an artifact derived from highly overexpressing the miRNA. As an initial step to further explore CDS targeting, CDS targeting by miR-191 should be confirmed by luciferase reporter, and effects on protein levels examined. More generally, it would be interesting to utilize cross linking methodologies, allowing for more robust identification of miRNA binding sites, in combination with transcriptome wide profiling of gene expression, to explore CDS targeting for additional miRNAs and in additional cell types.

## 5.3 ALTERNATIVE TARGETING MECHANISMS

We showed that miR-503 requires pairing of its 3' end to the 3' UTR of DDHD2 to effectively repress gene expression despite the presence of a 7-mer seed match. Complementary miRNA-target pairing with a perfect 5' seed match and additional

pairing at the 3' end has been previously reported; however, while the 3' pairing enhanced target repression, it was not necessary for miRNA function. Multiple studies have reported extensive non-canonical miRNA-target pairing with mismatches in the seed, but the effect on gene expression by non-canonical targeting was minor (24, 27, 29, 30). miR-503 pairing to DDHD2 differs from this type of non-canonical pairing by utilizing a perfect seed match, but it also differs from standard compensatory pairing because the 3' pairing is necessary. Taken together, this data raises multiple questions: (1) Is miR-503 DDHD2 pairing an isolated case or is miRNA-target pairing that requires 3' pairing in addition to a perfect seed match more widespread? (2) Do a subset of miRNAs utilize non-canonical targeting to regulate gene expression? Most studies exploring miRNA targeting examined either the entire miRNA targetome or a single miRNA-target interaction, and if a minority subset of miRNAs utilize extensive non-canonical targeting this signal may be lost when the whole targetome is considered. (3) Can miR-503 be confirmed to require 3' target pairing to regulate expression of other genes? And if so, what fraction of its total targets?

### 5.4 miR-503 IN BREAST CANCER

Our identification of DDHD2 as a direct target of miR-503 and our analysis of available clinical data strongly suggested that miR-503 functions as a tumor suppressor in ER+ breast cancer. We showed that high miR-503 expression correlated with increased patient survival. DDHD2 has been reported to function as an oncogene in ER+ breast cancer, and we observed that DDHD2 frequently exhibits copy number alterations in ER+ breast cancer and the copy number alterations correlated with decreased patient survival (120). Taken together these data suggest multiple avenues of further exploration: (1) Exploring miR-503 regulation of proliferation in ER+ breast cancer cell lines; (2) Examining miR-503 point mutation and copy number alterations in ER+ breast cancer cohorts; (3) Identifying other miR-503 oncogenic targets in ER+ breast cancer; (4) Determining if miR-503 suppresses ER+ breast cancer tumorigenesis through a single linear pathway or if it operates through a broader network of pathways; and (5)

Investigating if there is a more specific genetic background in which miR-503 functions as a tumor suppressor.

## 5.5 EXPLORING ALTERNATIVE FUNCTIONS

Transcriptome wide target identification for this group of miRNAs was used as a tool to understand the regulation of proliferation by these miRNAs. We explored the pathways associated with proliferation that were regulated by miR-22, and partially for miR-191 and miR-503; however, we did not pursue any of the interesting proliferation associated targets identified for miR-494 or miR-103. In addition, we limited our focus to proliferation associated genes because we were exploring a specific phenotype, but there may be other interesting functions that are regulated by these miRNAs. miRNAs frequently regulate multiple functions and pathways, and it is likely that this group of miRNAs is significantly involved in mediating other important biological processes (19). There remains a great deal of biology available to explore through this large dataset we have produced of multiple miRNA targetomes.

# Appendix

GO Term Enrichment analysis for experimentally determined miRNA target sets.

miR-191

| GO Term Biological Process | Hyp | Hyp Corrected |
|---|---|---|
| toll-like receptor signaling pathway (BP) | 6.54E-07 | 0.000725541 |
| toll-like receptor 1 signaling pathway (BP) | 3.98E-06 | 0.000881722 |
| toll-like receptor 2 signaling pathway (BP) | 3.98E-06 | 0.000881722 |
| toll-like receptor 4 signaling pathway (BP) | 7.48E-06 | 0.00103675 |
| regulation of transcription, DNA-dependent (BP) | 6.85E-06 | 0.00108474 |
| Toll signaling pathway (BP) | 9.11E-06 | 0.0011229 |
| MyD88-dependent toll-like receptor signaling pathway (BP) | 6.10E-06 | 0.00112737 |
| MyD88-independent toll-like receptor signaling pathway (BP) | 2.51E-06 | 0.00139424 |
| protein transport (BP) | 3.84E-06 | 0.00142073 |
| toll-like receptor 3 signaling pathway (BP) | 2.14E-05 | 0.00236779 |
| stress-activated MAPK cascade (BP) | 7.51E-05 | 0.00757622 |
| anti-apoptosis (BP) | 8.87E-05 | 0.00819412 |
| gene expression (BP) | 0.000144769 | 0.0114678 |
| cell division (BP) | 0.000144454 | 0.0123231 |
| regulation of translation in response to stress (BP) | 0.000178871 | 0.0132245 |
| mitotic cell cycle (BP) | 0.000261759 | 0.0170759 |
| vesicle-mediated transport (BP) | 0.000285185 | 0.0175705 |
| canonical Wnt receptor signaling pathway (BP) | 0.000256932 | 0.0178086 |
| innate immune response (BP) | 0.000306104 | 0.0178668 |
| cell proliferation (BP) | 0.000335669 | 0.0186129 |
| gonad development (BP) | 0.000375344 | 0.0198217 |
| transcription from RNA polymerase II promoter (BP) | 0.000673591 | 0.0339551 |
| positive regulation of macrophage derived foam cell differentiation (BP) | 0.000777607 | 0.0374942 |
| chromatin modification (BP) | 0.000946698 | 0.0437453 |
| multicellular organismal development (BP) | 0.00108807 | 0.0446914 |
| JUN phosphorylation (BP) | 0.00105424 | 0.0449675 |
| regulation of DNA-dependent transcription in response to stress (BP) | 0.00105424 | 0.0449675 |
| lipid storage (BP) | 0.00117275 | 0.0464491 |
| apoptotic process (BP) | 0.00123455 | 0.047211 |
| spermatogenesis (BP) | 0.001287 | 0.0475761 |

| KEGG Pathway Enrichment | Hyp | Hyp Corrected |
|---|---|---|
| Toll-like receptor signaling pathway | 0.00242287 | 0.0329106 |
| Adipocytokine signaling pathway | 0.0020567 | 0.0304765 |
| Focal adhesion | 0.00143282 | 0.023355 |
| Prostate cancer | 0.00119769 | 0.0216915 |
| MAPK signaling pathway | 0.000886753 | 0.0180676 |
| Hepatitis C | 0.00044294 | 0.0120332 |
| Ribosome biogenesis in eukaryotes | 0.000445001 | 0.0103622 |
| Phosphatidylinositol signaling system | 7.27E-05 | 0.00236896 |
| Pathways in cancer | 3.70E-05 | 0.00200889 |
| Neurotrophin signaling pathway | 4.66E-05 | 0.00189977 |
| Inositol phosphate metabolism | 1.09E-05 | 0.00089092 |
| Small cell lung cancer | 1.94E-06 | 0.000315659 |

miR-503

| GO Term Biological Process | Hyp | Hyp Corrected |
|---|---|---|
| translational elongation (BP) | 8.36E-05 | 0.0172273 |
| translation (BP) | 0.000326803 | 0.0336607 |
| septin ring assembly (BP) | 0.00245557 | 0.0337231 |
| oncosis (BP) | 0.00245557 | 0.0337231 |
| sialic acid transport (BP) | 0.00245557 | 0.0337231 |
| glycine decarboxylation via glycine cleavage system (BP) | 0.00245557 | 0.0337231 |
| ER-associated misfolded protein catabolic process (BP) | 0.00245557 | 0.0337231 |
| protein K48-linked ubiquitination (BP) | 0.00264529 | 0.0340582 |
| gene expression (BP) | 0.000515233 | 0.0353793 |
| posttranscriptional regulation of gene expression (BP) | 0.00490517 | 0.0360881 |
| regulation of microtubule polymerization (BP) | 0.00490517 | 0.0360881 |
| acetylcholine transport (BP) | 0.00490517 | 0.0360881 |
| eosinophil degranulation (BP) | 0.00490517 | 0.0360881 |

| | | |
|---|---|---|
| cellular response to potassium ion starvation (BP) | 0.00490517 | 0.0360881 |
| rRNA export from nucleus (BP) | 0.00490517 | 0.0360881 |
| regulation of translation in response to stress (BP) | 0.00490517 | 0.0360881 |
| endonucleolytic cleavage to generate mature 3'-end of SSU-rRNA from (SSU-rRNA, 5.8S rRNA, LSU-rRNA) (BP) | 0.00490517 | 0.0360881 |
| negative regulation of gene silencing by miRNA (BP) | 0.00490517 | 0.0360881 |
| cellular protein metabolic process (BP) | 0.00533524 | 0.0378986 |
| mitotic cell cycle DNA replication checkpoint (BP) | 0.00734884 | 0.0398384 |
| cellular response to erythropoietin (BP) | 0.00734884 | 0.0398384 |
| peptidyl-cysteine methylation (BP) | 0.00734884 | 0.0398384 |
| negative regulation of GTPase activity (BP) | 0.00734884 | 0.0398384 |
| minus-end-directed organelle transport along microtubule (BP) | 0.00734884 | 0.0398384 |
| mitotic cell cycle spindle checkpoint (BP) | 0.00734884 | 0.0398384 |
| arginyl-tRNA aminoacylation (BP) | 0.00734884 | 0.0398384 |
| chaperone-mediated protein folding (BP) | 0.00734884 | 0.0398384 |
| negative regulation of cysteine-type endopeptidase activity involved in apoptotic process (BP) | 0.00757002 | 0.0399852 |
| endocrine pancreas development (BP) | 0.00333896 | 0.0404603 |
| positive regulation of cell differentiation (BP) | 0.00158771 | 0.0408835 |
| regulation of cyclin-dependent protein kinase activity (BP) | 0.00813201 | 0.0418799 |
| endonucleolytic cleavage in ITS1 to separate SSU-rRNA from 5.8S rRNA and LSU-rRNA from tricistronic rRNA transcript (SSU-rRNA, 5.8S rRNA, LSU-rRNA) (BP) | 0.00978657 | 0.0428943 |
| response to purine-containing compound (BP) | 0.00978657 | 0.0428943 |
| positive regulation of vesicle fusion (BP) | 0.00978657 | 0.0428943 |
| antral ovarian follicle growth (BP) | 0.00978657 | 0.0428943 |
| regulation of DNA-dependent transcription in response to stress (BP) | 0.00978657 | 0.0428943 |
| cellular response to nutrient (BP) | 0.00978657 | 0.0428943 |
| RNA metabolic process (BP) | 0.00375194 | 0.0429389 |
| viral infectious cycle (BP) | 0.0014849 | 0.0436986 |
| viral reproduction (BP) | 0.00887137 | 0.0445732 |
| protein K63-linked ubiquitination (BP) | 0.00133308 | 0.0457692 |
| regulation of catalytic activity (BP) | 0.0067616 | 0.0464296 |
| mRNA metabolic process (BP) | 0.0022566 | 0.046486 |
| cell cycle (BP) | 0.00440884 | 0.0478011 |
| neutrophil degranulation (BP) | 0.0122184 | 0.0484036 |

| | | |
|---|---|---|
| tubulin complex assembly (BP) | 0.0122184 | 0.0484036 |
| ubiquitin-dependent SMAD protein catabolic process (BP) | 0.0122184 | 0.0484036 |
| cellular response to acid (BP) | 0.0122184 | 0.0484036 |
| germ cell development (BP) | 0.00216066 | 0.0494551 |

miR-103

| GO Term Biological Process | Hyp | Hyp Corrected |
|---|---|---|
| interleukin-4-mediated signaling pathway (BP) | 0.00420517 | 0.0455841 |
| production of molecular mediator involved in inflammatory response (BP) | 0.00420517 | 0.0455841 |
| nuclear envelope disassembly (BP) | 0.00420517 | 0.0455841 |
| polar body extrusion after meiotic divisions (BP) | 0.00420517 | 0.0455841 |
| methionyl-tRNA aminoacylation (BP) | 0.00420517 | 0.0455841 |
| mitotic prophase (BP) | 0.00420517 | 0.0455841 |
| cellular amino acid catabolic process (BP) | 0.00420517 | 0.0455841 |
| D-serine transport (BP) | 0.00420517 | 0.0455841 |
| mannose biosynthetic process (BP) | 0.00420517 | 0.0455841 |
| positive regulation of odontogenesis of dentin-containing tooth (BP) | 0.00420517 | 0.0455841 |
| regulation of mitotic anaphase (BP) | 0.00420517 | 0.0455841 |
| activation of mitotic anaphase-promoting complex activity (BP) | 0.00420517 | 0.0455841 |
| positive regulation of DNA metabolic process (BP) | 0.00630122 | 0.0461521 |
| termination of signal transduction (BP) | 0.00630122 | 0.0461521 |
| negative regulation of T-helper 1 cell differentiation (BP) | 0.00630122 | 0.0461521 |
| central nervous system neuron axonogenesis (BP) | 0.00630122 | 0.0461521 |
| positive regulation of axon regeneration (BP) | 0.00630122 | 0.0461521 |
| activation of Cdc42 GTPase activity (BP) | 0.00630122 | 0.0461521 |
| embryonic skeletal limb joint morphogenesis (BP) | 0.00630122 | 0.0461521 |
| heart valve morphogenesis (BP) | 0.00630122 | 0.0461521 |
| spermidine biosynthetic process (BP) | 0.00630122 | 0.0461521 |
| protein localization to chromatin (BP) | 0.00630122 | 0.0461521 |
| ER to Golgi vesicle-mediated transport (BP) | 0.00444203 | 0.0462996 |

miR-494

| GO Term Biological Process | Hyp | Hyp Corrected |
|---|---|---|
| transcription from RNA polymerase II promoter (BP) | 5.76E-07 | 0.00077091 |
| transcription, DNA-dependent (BP) | 1.56E-06 | 0.00104253 |
| S phase of mitotic cell cycle (BP) | 2.81E-06 | 0.00125464 |
| protein transport (BP) | 3.84E-06 | 0.00128557 |
| response to DNA damage stimulus (BP) | 9.99E-06 | 0.00222775 |
| cell death (BP) | 8.98E-06 | 0.00240313 |
| regulation of transcription, DNA-dependent (BP) | 1.52E-05 | 0.00290808 |
| positive regulation of I-kappaB kinase/NF-kappaB cascade (BP) | 2.05E-05 | 0.00342125 |
| histone H4-R3 methylation (BP) | 2.34E-05 | 0.00347463 |
| positive regulation of apoptotic process (BP) | 3.09E-05 | 0.00412906 |
| DNA repair (BP) | 3.52E-05 | 0.00428337 |
| signal transduction (BP) | 6.14E-05 | 0.00632049 |
| liver development (BP) | 6.67E-05 | 0.00637801 |
| neural tube closure (BP) | 6.03E-05 | 0.00672292 |
| negative regulation of sequence-specific DNA binding transcription factor activity (BP) | 8.36E-05 | 0.00745652 |
| multicellular organismal development (BP) | 9.00E-05 | 0.00752423 |
| regulation of apoptotic process (BP) | 0.000110389 | 0.00868828 |
| G1/S transition of mitotic cell cycle (BP) | 0.000155688 | 0.0115728 |
| negative regulation of transcription from RNA polymerase II promoter (BP) | 0.000180342 | 0.0120649 |
| apoptotic process (BP) | 0.000177874 | 0.0125261 |
| RNA metabolic process (BP) | 0.000201523 | 0.0128399 |
| amino acid transport (BP) | 0.000212041 | 0.0128959 |
| cell migration involved in sprouting angiogenesis (BP) | 0.000266785 | 0.0148732 |
| DNA damage response, signal transduction by p53 class mediator resulting in cell cycle arrest (BP) | 0.000256932 | 0.0149467 |
| RNA splicing (BP) | 0.000285622 | 0.0152865 |
| intracellular protein transport (BP) | 0.00033602 | 0.0166516 |
| angiogenesis (BP) | 0.000324596 | 0.0167042 |
| cell cycle arrest (BP) | 0.000360897 | 0.0172457 |
| cellular nitrogen compound metabolic process (BP) | 0.0003942 | 0.0181876 |
| actin polymerization or depolymerization (BP) | 0.000479442 | 0.0213831 |
| regulation of smooth muscle cell migration (BP) | 0.000531843 | 0.0215638 |
| negative regulation of monocyte differentiation (BP) | 0.000531843 | 0.0215638 |
| negative regulation of cell division (BP) | 0.000531843 | 0.0215638 |

| | | |
|---|---|---|
| JNK cascade (BP) | 0.000595673 | 0.0227717 |
| transport (BP) | 0.000587736 | 0.0231291 |
| response to hypoxia (BP) | 0.000622661 | 0.0231422 |
| negative regulation of cysteine-type endopeptidase activity involved in apoptotic process (BP) | 0.000711948 | 0.0257456 |
| protein homooligomerization (BP) | 0.00106255 | 0.0330625 |
| peptidyl-arginine methylation (BP) | 0.00105424 | 0.0335852 |
| entrainment of circadian clock by photoperiod (BP) | 0.00105424 | 0.0335852 |
| regulation of proteasomal ubiquitin-dependent protein catabolic process (BP) | 0.00105424 | 0.0335852 |
| negative regulation of transcription, DNA-dependent (BP) | 0.00114499 | 0.0340443 |
| small GTPase mediated signal transduction (BP) | 0.00112461 | 0.0341984 |
| vesicle-mediated transport (BP) | 0.001199 | 0.0348754 |
| response to calcium ion (BP) | 0.000994371 | 0.0350123 |
| innate immune response (BP) | 0.00103562 | 0.0355296 |
| transforming growth factor beta receptor signaling pathway (BP) | 0.00179774 | 0.0421996 |
| cellular membrane organization (BP) | 0.00177641 | 0.0424435 |
| viral reproduction (BP) | 0.00175717 | 0.0427472 |
| positive regulation of NF-kappaB transcription factor activity (BP) | 0.00150707 | 0.0429035 |
| positive regulation of T-helper 1 cell differentiation (BP) | 0.00174149 | 0.0431502 |
| negative regulation of leukocyte migration (BP) | 0.00174149 | 0.0431502 |
| anti-apoptosis (BP) | 0.00158985 | 0.0434126 |
| response to estrogen stimulus (BP) | 0.0015635 | 0.0435825 |
| interspecies interaction between organisms (BP) | 0.00171326 | 0.0440835 |
| mRNA processing (BP) | 0.00170199 | 0.0446523 |
| 2-oxoglutarate metabolic process (BP) | 0.00167523 | 0.0448292 |
| neuron projection development (BP) | 0.0020567 | 0.0466417 |
| nucleotide-excision repair (BP) | 0.0020567 | 0.0466417 |
| positive regulation of sequence-specific DNA binding transcription factor activity (BP) | 0.00219591 | 0.0489687 |

## References


1. Coller, H.A., Sang, L. and Roberts, J.M. (2006) A new description of cellular quiescence. *PLoS Biol*., **4**, e83.

2. Matsumoto, A., Takeishi, S., Kanie, T., Susaki, E., Onoyama, I., Tateishi, Y., Nakayama, K. and Nakayama, K.I. (2011) p57 is required for quiescence and maintenance of adult hematopoietic stem cells. *Cell Stem Cell*, **9**, 262–271.

3. White, P., Brestelli, J.E., Kaestner, K.H. and Greenbaum, L.E. (2005) Identification of transcriptional networks during liver regeneration. *J. Biol. Chem*., **280**, 3715–3722.

4. Yusuf, I. and Fruman, D.A. (2003) Regulation of quiescence in lymphocytes. *Trends Immunol*., **24**, 380–386.

5. Tzachanis, D., Lafuente, E.M., Li, L. and Boussiotis, V.A. (2004) Intrinsic and extrinsic regulation of T lymphocyte quiescence. *Leuk. Lymphoma*, **45**, 1959–1967.

6. Martin, P. (1997) Wound healing--aiming for perfect skin regeneration. *Science*, **276**, 75–81.

7. Hanahan, D. and Weinberg, R.A. (2011) Hallmarks of cancer: the next generation. *Cell*, **144**, 646–674.

8. Vogelstein, B., Papadopoulos, N., Velculescu, V.E., Zhou, S., Diaz, L.A. and Kinzler, K.W. (2013) Cancer genome landscapes. *Science*, **339**, 1546–1558.

9. Chang, H.Y., Sneddon, J.B., Alizadeh, A.A., Sood, R., West, R.B., Montgomery, K., Chi, J.-T., van de Rijn, M., Botstein, D. and Brown, P.O. (2004) Gene expression signature of fibroblast serum response predicts human cancer progression: similarities between tumors and wounds. *PLoS Biol*., **2**, E7.

10. Chang, H.Y., Nuyten, D.S.A., Sneddon, J.B., Hastie, T., Tibshirani, R., Sørlie, T., Dai, H., He, Y.D., van't Veer, L.J., Bartelink, H., et al. (2005) Robustness, scalability, and integration of a wound-response gene expression signature in predicting breast cancer survival. *Proc. Natl. Acad. Sci. U.S.A*., **102**, 3738–3743.

11. Iyer, V.R., Eisen, M.B., Ross, D.T., Schuler, G., Moore, T., Lee, J.C., Trent, J.M., Staudt, L.M., Hudson, J.J., Boguski, M.S., et al. (1999) The transcriptional program in the response of human fibroblasts to serum. *Science*, **283**, 83–87.

12. Croce, C.M. and Calin, G.A. (2005) miRNAs, cancer, and stem cell division. *Cell*, **122**, 6–7.

13. Davis, B.N. and Hata, A. (2009) Regulation of MicroRNA Biogenesis: A miRiad of

mechanisms. *Cell Commun. Signal*, **7**, 18.

14. Friedman, R.C., Farh, K.K.-H., Burge, C.B. and Bartel, D.P. (2009) Most mammalian mRNAs are conserved targets of microRNAs. *Genome Res.*, **19**, 92–105.

15. Lim, L.P., Lau, N.C., Garrett-Engele, P., Grimson, A., Schelter, J.M., Castle, J., Bartel, D.P., Linsley, P.S. and Johnson, J.M. (2005) Microarray analysis shows that some microRNAs downregulate large numbers of target mRNAs. *Nature*, **433**, 769–773.

16. Sun, X., Jiao, X., Pestell, T.G., Fan, C., Qin, S., Mirabelli, E., Ren, H. and Pestell, R.G. (2013) MicroRNAs and cancer stem cells: the sword and the shield. *Oncogene*.

17. Li, Y. and Kowdley, K.V. (2012) MicroRNAs in Common Human Diseases. *Genomics Proteomics Bioinformatics*, **10**, 246–253.

18. Griffiths-Jones, S., Saini, H.K., van Dongen, S. and Enright, A.J. (2008) miRBase: tools for microRNA genomics. *Nucleic Acids Res.*, **36**, D154–8.

19. Mendell, J.T. and Olson, E.N. (2012) MicroRNAs in stress signaling and human disease. *Cell*, **148**, 1172–1187.

20. Ameres, S.L. and Zamore, P.D. (2013) Diversifying microRNA sequence and function. *Nat. Rev. Mol. Cell Biol.*, **14**, 475–488.

21. Yang, J.-S. and Lai, E.C. (2011) Alternative miRNA biogenesis pathways and the interpretation of core miRNA pathway mutants. *Mol. Cell*, **43**, 892–903.

22. Czech, B. and Hannon, G.J. (2011) Small RNA sorting: matchmaking for Argonautes. *Nat. Rev. Genet.*, **12**, 19–31.

23. Bartel, D.P. (2009) MicroRNAs: target recognition and regulatory functions. *Cell*, **136**, 215–233.

24. Grimson, A., Farh, K.K.-H., Johnston, W.K., Garrett-Engele, P., Lim, L.P. and Bartel, D.P. (2007) MicroRNA targeting specificity in mammals: determinants beyond seed pairing. *Mol. Cell*, **27**, 91–105.

25. Guo, H., Ingolia, N.T., Weissman, J.S. and Bartel, D.P. (2010) Mammalian microRNAs predominantly act to decrease target mRNA levels. *Nature*, **466**, 835–840.

26. Lim, L. P., Lau, N.C., Garrett-Engele, P., Grimson, A., Schelter, J.M., Castle, J., Bartel, D.P., Linsley, P.S. and Johnson, J.M. (2005) Microarray analysis shows that some microRNAs downregulate large numbers of target mRNAs. *Nature*, **433**, 769–773.

27. Helwak, A., Kudla, G., Dudnakova, T. and Tollervey, D. (2013) Mapping the human miRNA interactome by CLASH reveals frequent noncanonical binding. *Cell*, **153**, 654–665.

28. Chi, S.W., Hannon, G.J. and Darnell, R.B. (2012) An alternative mode of microRNA target recognition. *Nat. Struct. Mol. Biol.*, **19**, 321–327.

29. Loeb, G.B., Khan, A.A., Canner, D., Hiatt, J.B., Shendure, J., Darnell, R.B., Leslie, C.S. and Rudensky, A.Y. (2012) Transcriptome-wide miR-155 Binding Map Reveals Widespread Noncanonical MicroRNA Targeting. *Mol. Cell*, **48**, 760–770.

30. Hafner, M., Landthaler, M., Burger, L., Khorshid, M., Hausser, J., Berninger, P., Rothballer, A., Ascano, M., Jungkamp, A.-C., Munschauer, M., et al. (2010) Transcriptome-wide identification of RNA-binding protein and microRNA target sites by PAR-CLIP. *Cell*, **141**, 129–141.

31. Calin, G.A., Sevignani, C., Dumitru, C.D., Hyslop, T., Noch, E., Yendamuri, S., Shimizu, M., Rattan, S., Bullrich, F., Negrini, M., et al. (2004) Human microRNA genes are frequently located at fragile sites and genomic regions involved in cancers. *Proc. Natl. Acad. Sci. U.S.A.*, **101**, 2999–3004.

32. Volinia, S., Calin, G.A., Liu, C.-G., Ambs, S., Cimmino, A., Petrocca, F., Visone, R., Iorio, M., Roldo, C., Ferracin, M., et al. (2006) A microRNA expression signature of human solid tumors defines cancer gene targets. *Proc. Natl. Acad. Sci. U.S.A.*, **103**, 2257–2261.

33. Calin, G.A., Dumitru, C.D., Shimizu, M., Bichi, R., Zupo, S., Noch, E., Aldler, H., Rattan, S., Keating, M., Rai, K., et al. (2002) Frequent deletions and down-regulation of micro- RNA genes miR15 and miR16 at 13q14 in chronic lymphocytic leukemia. *Proc. Natl. Acad. Sci. U.S.A.*, **99**, 15524–15529.

34. Samantarrai, D., Dash, S., Chhetri, B. and Mallick, B. (2013) Genomic and epigenomic cross-talks in the regulatory landscape of miRNAs in breast cancer. *Mol. Cancer Res.*, **11**, 315–328.

35. Papagiannakopoulos, T., Shapiro, A. and Kosik, K.S. (2008) MicroRNA-21 targets a network of key tumor-suppressive pathways in glioblastoma cells. *Cancer Res.*, **68**, 8164–8172.

36. Schramedei, K., Mörbt, N., Pfeifer, G., Läuter, J., Rosolowski, M., Tomm, J.M., Bergen, von, M., Horn, F. and Brocke-Heidrich, K. (2011) MicroRNA-21 targets tumor suppressor genes ANP32A and SMARCA4. *Oncogene*, **30**, 2975–2985.

37. Deng, S., Calin, G.A., Croce, C.M., Coukos, G. and Zhang, L. (2008) Mechanisms of microRNA deregulation in human cancer. *Cell Cycle*, **7**, 2643–2646.

38. Kumar, M.S., Lu, J., Mercer, K.L., Golub, T.R. and Jacks, T. (2007) Impaired microRNA processing enhances cellular transformation and tumorigenesis. *Nat. Genet.*, **39**, 673–677.

39. Bar, N. and Dikstein, R. (2010) miR-22 forms a regulatory loop in PTEN/AKT pathway and modulates signaling kinetics. *PLoS ONE*, **5**, e10859.

40. Liu, L., Jiang, Y., Zhang, H., Greenlee, A.R., Yu, R. and Yang, Q. (2010) miR-22 functions as a micro-oncogene in transformed human bronchial epithelial cells induced by anti-benzo[a]pyrene-7,8-diol-9,10-epoxide. *Toxicol In Vitro*, **24**, 1168–1175.

41. Poliseno, L., Salmena, L., Riccardi, L., Fornari, A., Song, M.S., Hobbs, R.M., Sportoletti, P., Varmeh, S., Egia, A., Fedele, G., et al. (2010) Identification of the miR-106b~25 microRNA cluster as a proto-oncogenic PTEN-targeting intron that cooperates with its host gene MCM7 in transformation. *Sci Signal*, **3**, 29.

42. Ting, Y., Medina, D.J., Strair, R.K. and Schaar, D.G. (2010) Differentiation-associated miR-22 represses Max expression and inhibits cell cycle progression. *Biochem. Biophys. Res. Commun.*, **394**, 606–611.

43. Tsuchiya, N., Izumiya, M., Ogata-Kawata, H., Okamoto, K., Fujiwara, Y., Nakai, M., Okabe, A., Schetter, A.J., Bowman, E.D., Midorikawa, Y., et al. (2011) Tumor suppressor miR-22 determines p53-dependent cellular fate through post-transcriptional regulation of p21. *Cancer Res.*, **71**, 4628–4639.

44. Xiong, J., Du, Q. and Liang, Z. (2010) Tumor-suppressive microRNA-22 inhibits the transcription of E-box-containing c-Myc target genes by silencing c-Myc binding protein. *Oncogene*, **29**, 4980–4988.

45. Xu, D., Takeshita, F., Hino, Y., Fukunaga, S., Kudo, Y., Tamaki, A., Matsunaga, J., Takahashi, R.-U., Takata, T., Shimamoto, A., et al. (2011) miR-22 represses cancer progression by inducing cellular senescence. *J. Cell Biol.*, **193**, 409–424.

46. Li, J., Liang, S., Yu, H., Zhang, J., Ma, D. and Lu, X. (2010) An inhibitory effect of miR-22 on cell migration and invasion in ovarian cancer. *Gynecol. Oncol.*, **119**, 543–548.

47. Kim, J., Lee, J.H. and Iyer, V.R. (2008) Global identification of Myc target genes reveals its direct role in mitochondrial biogenesis and its E-box usage in vivo. *PLoS ONE*, **3**, e1798.

48. Katome, T., Obata, T., Matsushima, R., Masuyama, N., Cantley, L.C., Gotoh, Y., Kishi, K., Shiota, H. and Ebina, Y. (2003) Use of RNA interference-mediated gene silencing and adenoviral overexpression to elucidate the roles of AKT/protein kinase B isoforms in insulin actions. *J. Biol. Chem.*, **278**, 28312–28323.

49. Gu, J. and Iyer, V.R. (2006) PI3K signaling and miRNA expression during the response of quiescent human fibroblasts to distinct proliferative stimuli. *Genome Biol.*, **7**, R42.

50. Dennis, G.J., Sherman, B.T., Hosack, D.A., Yang, J., Gao, W., Lane, H.C. and Lempicki, R.A. (2003) DAVID: Database for Annotation, Visualization, and Integrated Discovery. *Genome Biol.*, **4**, P3.

51. Lee, B.-K., Bhinge, A.A. and Iyer, V.R. (2011) Wide-ranging functions of E2F4 in transcriptional activation and repression revealed by genome-wide analysis. *Nucleic Acids Res.*, **39**, 3558–3573.

52. Hendrickson, D.G., Hogan, D.J., McCullough, H.L., Myers, J.W., Herschlag, D., Ferrell, J.E. and Brown, P.O. (2009) Concordant regulation of translation and mRNA abundance for hundreds of targets of a human microRNA. *PLoS Biol.*, **7**, e1000238.

53. Tan, P.-H., Bay, B.-H., Yip, G., Selvarajan, S., Tan, P., Wu, J., Lee, C.-H. and Li, K.-B. (2005) Immunohistochemical detection of Ki67 in breast cancer correlates with transcriptional regulation of genes related to apoptosis and cell death. *Mod. Pathol.*, **18**, 374–381.

54. Brizova, H., Kalinova, M., Krskova, L., Mrhalova, M. and Kodet, R. (2010) A novel quantitative PCR of proliferation markers (Ki-67, topoisomerase IIalpha, and TPX2): an immunohistochemical correlation, testing, and optimizing for mantle cell lymphoma. *Virchows Arch.*, **456**, 671–679.

55. Baek, D., Villén, J., Shin, C., Camargo, F.D., Gygi, S.P. and Bartel, D.P. (2008) The impact of microRNAs on protein output. *Nature*, **455**, 64–71.

56. el-Deiry, W.S., Tokino, T., Velculescu, V.E., Levy, D.B., Parsons, R., Trent, J.M., Lin, D., Mercer, W.E., Kinzler, K.W. and Vogelstein, B. (1993) WAF1, a potential mediator of p53 tumor suppression. *Cell*, **75**, 817–825.

57. Ellisen, L.W., Ramsayer, K.D., Johannessen, C.M., Yang, A., Beppu, H., Minda, K., Oliner, J.D., McKeon, F. and Haber, D.A. (2002) REDD1, a developmentally regulated transcriptional target of p63 and p53, links p63 to regulation of reactive oxygen species. *Mol. Cell*, **10**, 995–1005.

58. Okamura, S., Arakawa, H., Tanaka, T., Nakanishi, H., Ng, C.C., Taya, Y., Monden, M. and Nakamura, Y. (2001) p53DINP1, a p53-inducible gene, regulates p53-dependent apoptosis. *Mol. Cell*, **8**, 85–94.

59. Hasan, K., Cheung, C., Kaul, Z., Shah, N., Sakaushi, S., Sugimoto, K., Oka, S., Kaul, S.C. and Wadhwa, R. (2009) CARF Is a vital dual regulator of cellular senescence and apoptosis. *J. Biol. Chem.*, **284**, 1664–1672.

60. Abbas, T. and Dutta, A. (2009) p21 in cancer: intricate networks and multiple activities. *Nat. Rev. Cancer*, **9**, 400–414.

61. Karginov, F.V., Conaco, C., Xuan, Z., Schmidt, B.H., Parker, J.S., Mandel, G. and Hannon, G.J. (2007) A biochemical approach to identifying microRNA targets. *Proc. Natl. Acad. Sci. U.S.A.*, **104**, 19291–19296.

62. Miranda, K.C., Huynh, T., Tay, Y., Ang, Y.S., Tam, W.L., Thomson, A.M., Lim, B. and Rigoutsos, I. (2006) A pattern-based method for the identification of MicroRNA binding sites and their corresponding heteroduplexes. *Cell*, **126**, 1203–1217.

63. Schoenemeyer, A., Barnes, B.J., Mancl, M.E., Latz, E., Goutagny, N., Pitha, P.M., Fitzgerald, K.A. and Golenbock, D.T. (2005) The interferon regulatory factor, IRF5, is a central mediator of toll-like receptor 7 signaling. *J. Biol. Chem.*, **280**, 17005–17012.

64. Takaoka, A., Yanai, H., Kondo, S., Duncan, G., Negishi, H., Mizutani, T., Kano, S., Honda, K., Ohba, Y., Mak, T.W., et al. (2005) Integral role of IRF-5 in the gene induction programme activated by Toll-like receptors. *Nature*, **434**, 243–249.

65. Bianchi, M.E. and Manfredi, A.A. (2007) High-mobility group box 1 (HMGB1) protein at the crossroads between innate and adaptive immunity. *Immunol. Rev.*, **220**, 35–46.

66. Yanai, H., Ban, T., Wang, Z., Choi, M.K., Kawamura, T., Negishi, H., Nakasato, M., Lu, Y., Hangai, S., Koshiba, R., et al. (2009) HMGB proteins function as universal sentinels for nucleic-acid-mediated innate immune responses. *Nature*, **462**, 99–103.

67. Yoneyama, M., Kikuchi, M., Natsukawa, T., Shinobu, N., Imaizumi, T., Miyagishi, M., Taira, K., Akira, S. and Fujita, T. (2004) The RNA helicase RIG-I has an essential function in double-stranded RNA-induced innate antiviral responses. *Nat. Immunol.*, **5**, 730–737.

68. Pandey, A.K., Yang, Y., Jiang, Z., Fortune, S.M., Coulombe, F., Behr, M.A., Fitzgerald, K.A., Sassetti, C.M. and Kelliher, M.A. (2009) NOD2, RIP2 and IRF5 play a critical role in the type I interferon response to Mycobacterium tuberculosis. *PLoS Pathog.*, **5**, e1000500.

69. Liu, H., Adler, A.S., Segal, E. and Chang, H.Y. (2007) A transcriptional program mediating entry into cellular quiescence. *PLoS Genet.*, **3**, e91.

70. Fensterl, V. and Sen, G.C. (2009) Interferons and viral infections. *Biofactors*, **35**, 14–20.

71. O'Donnell, K.A., Wentzel, E.A., Zeller, K.I., Dang, C.V. and Mendell, J.T. (2005) c-Myc-regulated microRNAs modulate E2F1 expression. *Nature*, **435**, 839–843.

72. Lee, B.-K., Bhinge, A.A., Battenhouse, A., McDaniell, R.M., Liu, Z., Song, L., Ni, Y., Birney, E., Lieb, J.D., Furey, T.S., et al. (2012) Cell-type specific and combinatorial usage of diverse transcription factors revealed by genome-wide binding studies in multiple human cells. *Genome Res.*, **22**, 9–24.

73. Marson, A., Levine, S.S., Cole, M.F., Frampton, G.M., Brambrink, T., Johnstone, S., Guenther, M.G., Johnston, W.K., Wernig, M., Newman, J., et al. (2008) Connecting microRNA genes to the core transcriptional regulatory circuitry of embryonic stem cells. *Cell*, **134**, 521–533.

74. Mao, D.Y., Watson, J.D., Yan, P.S., Barsyte-Lovejoy, D., Khosravi, F., Wong, W.W., Farnham, P.J., Huang, T.H. and Penn, L.Z. (2003) Analysis of Myc bound loci identified by CpG island arrays shows that Max is essential for Myc-dependent repression. *Curr. Biol.*, **13**, 882–886.

75. Kime, L. and Wright, S.C. (2003) Mad4 is regulated by a transcriptional repressor complex that contains Miz-1 and c-Myc. *Biochem. J.*, **370**, 291–298.

76. Marcotte, R., Chen, J.M., Huard, S. and Wang, E. (2005) c-Myc creates an activation loop by transcriptionally repressing its own functional inhibitor, hMad4, in young fibroblasts, a loop lost in replicatively senescent fibroblasts. *J. Cell. Biochem.*, **96**, 1071–1085.

77. Taylor-Papadimitriou, J., Balkwill, F., Ebsworth, N. and Rozengurt, E. (1985) Antiviral and antiproliferative effects of interferons in quiescent fibroblasts are dissociable. *Virology*, **147**, 405–412.

78. Barnes, B.J., Kellum, M.J., Pinder, K.E., Frisancho, J.A. and Pitha, P.M. (2003) Interferon regulatory factor 5, a novel mediator of cell cycle arrest and cell death. *Cancer Res.*, **63**, 6424–6431.

79. Mori, T., Anazawa, Y., Iiizumi, M., Fukuda, S., Nakamura, Y. and Arakawa, H. (2002) Identification of the interferon regulatory factor 5 gene (IRF-5) as a direct target for p53. *Oncogene*, **21**, 2914–2918.

80. Li, Q., Tang, L., Roberts, P. C., Kraniak, J.M., Fridman, A.L., Kulaeva, O.I., Tehrani, O.S. and Tainsky, M.A. (2008) Interferon regulatory factors IRF5 and IRF7 inhibit growth and induce senescence in immortal Li-Fraumeni fibroblasts. *Mol. Cancer Res.*, **6**, 770–784.

81. Ho, A. and Dowdy, S.F. (2002) Regulation of G(1) cell-cycle progression by oncogenes and tumor suppressor genes. *Curr Opin Genet Dev*, **12**, 47–52.

82. Sachdeva, M., Zhu, S., Wu, F., Wu, H., Walia, V., Kumar, S., Elble, R., Watabe, K. and Mo, Y.Y. (2009) p53 represses c-Myc through induction of the tumor suppressor miR-145. *Proc. Natl. Acad. Sci. U.S.A.*, **106**, 3207–3212.

83. Elyakim, E., Sitbon, E., Faerman, A., Tabak, S., Montia, E., Belanis, L., Dov, A., Marcusson, E.G., Bennett, C.F., Chajut, A., et al. (2010) hsa-miR-191 is a candidate oncogene target for hepatocellular carcinoma therapy. *Cancer Res.*, **70**, 8077–8087.

84. Shi, X., Su, S., Long, J., Mei, B. and Chen, Y. (2011) MicroRNA-191 targets N-deacetylase/N-sulfotransferase 1 and promotes cell growth in human gastric carcinoma cell line MGC803. *Acta Biochim. Biophys. Sin. (Shanghai)*, **43**, 849–856.

85. Qin, S., Zhu, Y., Ai, F., Li, Y., Bai, B., Yao, W. and Dong, L. (2013) MicroRNA-191 correlates with poor prognosis of colorectal carcinoma and plays multiple roles by targeting tissue inhibitor of metalloprotease 3. *Neoplasma*, 10.4149/neo_2014_005.

86. He, Y., Cui, Y., Wang, W., Gu, J., Guo, S., Ma, K. and Luo, X. (2011) Hypomethylation of the hsa-miR-191 locus causes high expression of hsa-mir-191 and promotes the epithelial-to-mesenchymal transition in hepatocellular carcinoma. *Neoplasia*, **13**, 841–853.

87. Nagpal, N., Ahmad, H.M., Molparia, B. and Kulshreshtha, R. (2013) MicroRNA-191, an estrogen-responsive microRNA, functions as an oncogenic regulator in human breast cancer. *Carcinogenesis*, **34**, 1889–1899.

88. Lena, A.M., Mancini, M., Rivetti di Val Cervo, P., Saintigny, G., Mahé, C., Melino, G. and Candi, E. (2012) MicroRNA-191 triggers keratinocytes senescence by SATB1 and CDK6 downregulation. *Biochem. Biophys. Res. Commun.*, **423**, 509–514.

89. Kim, D., Pertea, G., Trapnell, C., Pimentel, H., Kelley, R. and Salzberg, S.L. (2013) TopHat2: accurate alignment of transcriptomes in the presence of insertions, deletions and gene fusions. *Genome Biol.*, **14**, R36.

90. Tabas-Madrid, D., Nogales-Cadenas, R. and Pascual-Montano, A. (2012) GeneCodis3: a non-redundant and modular enrichment analysis tool for functional genomics. *Nucleic Acids Res.*, **40**, W478–83.

91. Nogales-Cadenas, R., Carmona-Saez, P., Vazquez, M., Vicente, C., Yang, X., Tirado, F., Carazo, J.M. and Pascual-Montano, A. (2009) GeneCodis: interpreting gene lists through enrichment analysis and integration of diverse biological information. *Nucleic Acids Res.*, **37**, W317–22.

92. Carmona-Saez, P., Chagoyen, M., Tirado, F., Carazo, J.M. and Pascual-Montano, A. (2007) GENECODIS: a web-based tool for finding significant concurrent annotations in gene lists. *Genome Biol.*, **8**, R3.

93. Antonov, A.V., Knight, R.A., Melino, G., Barlev, N.A. and Tsvetkov, P.O. (2013) MIRUMIR: an online tool to test microRNAs as biomarkers to predict survival in cancer using multiple clinical data sets. *Cell Death Differ*, **20**, 367.

94. He, L., He, X., Lim, L.P., de Stanchina, E., Xuan, Z., Liang, Y., Xue, W., Zender, L., Magnus, J., Ridzon, D., et al. (2007) A microRNA component of the p53 tumour suppressor network. *Nature*, **447**, 1130–1134.

95. Gottwein, E., Corcoran, D.L., Mukherjee, N., Skalsky, R.L., Hafner, M., Nusbaum, J.D., Shamulailatpam, P., Love, C.L., Dave, S.S., Tuschl, T., et al. (2011) Viral microRNA targetome of KSHV-infected primary effusion lymphoma cell lines. *Cell Host Microbe*, **10**, 515–526.

96. Leung, A.K.L., Young, A.G., Bhutkar, A., Zheng, G.X., Bosson, A.D., Nielsen, C.B. and Sharp, P.A. (2011) Genome-wide identification of Ago2 binding sites from mouse embryonic stem cells with and without mature microRNAs. *Nat. Struct. Mol. Biol.*, **18**, 237–244.

97. Colamaio, M., Borbone, E., Russo, L., Bianco, M., Federico, A., Califano, D., Chiappetta, G., Pallante, P., Troncone, G., Battista, S., et al. (2011) miR-191 Down-Regulation Plays a Role in Thyroid Follicular Tumors through CDK6 Targeting. *J Clin Endocrinol Metab*, **96**, E1915–24.

98. Patnaik, S.K., Kannisto, E. and Yendamuri, S. (2010) Overexpression of microRNA miR-30a or miR-191 in A549 lung cancer or BEAS-2B normal lung cell lines does not alter phenotype. *PLoS ONE*, **5**, e9219.

99. Romano, G. and Giordano, A. (2008) Role of the cyclin-dependent kinase 9-related pathway in mammalian gene expression and human diseases. *Cell Cycle*, **7**, 3664–3668.

100. Fan, X., Mikolaenko, I., Elhassan, I., Ni, X., Wang, Y., Ball, D., Brat, D.J., Perry, A. and Eberhart, C.G. (2004) Notch1 and notch2 have opposite effects on embryonal brain tumor growth. *Cancer Res.*, **64**, 7787–7793.

101. Koch, U. and Radtke, F. (2007) Notch and cancer: a double-edged sword. *Cell. Mol. Life Sci.*, **64**, 2746–2762.

102. Smith, J.A., Poteet-Smith, C.E., Xu, Y., Errington, T.M., Hecht, S.M. and Lannigan, D.A. (2005) Identification of the first specific inhibitor of p90 ribosomal S6 kinase (RSK) reveals an unexpected role for RSK in cancer cell proliferation. *Cancer Res.*, **65**, 1027–1034.

103. Kang, S., Dong, S., Gu, T.-L., Guo, A., Cohen, M.S., Lonial, S., Khoury, H.J., Fabbro, D., Gilliland, D.G., Bergsagel, P.L., et al. (2007) FGFR3 activates RSK2 to mediate hematopoietic transformation through tyrosine phosphorylation of RSK2 and activation of the MEK/ERK pathway. *Cancer Cell*, **12**, 201–214.

104. Di Leva, G., Piovan, C., Gasparini, P., Ngankeu, A., Taccioli, C., Briskin, D., Cheung, D.G., Bolon, B., Anderlucci, L., Alder, H., et al. (2013) Estrogen mediated-

activation of miR-191/425 cluster modulates tumorigenicity of breast cancer cells depending on estrogen receptor status. *PLoS Genet.*, **9**, e1003311.

105. Lee, D. and Shin, C. (2012) MicroRNA-target interactions: new insights from genome-wide approaches. *Ann. N. Y. Acad. Sci.*, **1271**, 118–128.

106. Chen, H.-Y., Lin, Y.-M., Chung, H.-C., Lang, Y.-D., Lin, C.-J., Huang, J., Wang, W.-C., Lin, F.-M., Chen, Z., Huang, H.-D., et al. (2012) miR-103/107 promote metastasis of colorectal cancer by targeting the metastasis suppressors DAPK and KLF4. *Cancer Res.*, **72**, 3631–3641.

107. Lim, L., Balakrishnan, A., Huskey, N., Jones, K.D., Jodari, M., Ng, R., Song, G., Riordan, J., Anderton, B., Cheung, S.-T., et al. (2013) MiR-494 within an oncogenic MicroRNA megacluster regulates G1/S transition in liver tumorigenesis through suppression of MCC. *Hepatology*, **59**, 202–215.

108. Romano, G., Acunzo, M., Garofalo, M., Di Leva, G., Cascione, L., Zanca, C., Bolon, B., Condorelli, G. and Croce, C.M. (2012) MiR-494 is regulated by ERK1/2 and modulates TRAIL-induced apoptosis in non-small-cell lung cancer through BIM down-regulation. *Proc. Natl. Acad. Sci. U.S.A.*, **109**, 16570–16575.

109. Yamanaka, S., Campbell, N.R., An, F., Kuo, S.C., Potter, J.J., Mezey, E., Maitra, A. and Selaru, F.M. (2012) Coordinated effects of microRNA-494 induce $G_2$/M arrest in human cholangiocarcinoma. *Cell Cycle*, **11**, 2729–2738.

110. Zhang, Y., Chen, X., Lian, H., Liu, J., Zhou, B., Han, S., Peng, B., Yin, J., Liu, W. and He, X. (2014) MicroRNA-503 acts as a tumor suppressor in glioblastoma for multiple antitumor effects by targeting IGF-1R. *Oncol. Rep.*, **31**, 1445–1452.

111. Yang, Y., Liu, L., Zhang, Y., Guan, H., Wu, J., Zhu, X., Yuan, J. and Li, M. (2014) MiR-503 targets PI3K p85 and IKK-β and suppresses progression of non-small cell lung cancer. *Int. J. Cancer*, 10.1002/ijc.28799.

112. Li, N., Zhang, F., Li, S. and Zhou, S. (2014) Epigenetic silencing of MicroRNA-503 regulates FANCA expression in non-small cell lung cancer cell. *Biochem. Biophys. Res. Commun.*, **444**, 611–616.

113. Zhou, B., Ma, R., Si, W., Li, S., Xu, Y., Tu, X. and Wang, Q. (2013) MicroRNA-503 targets FGF2 and VEGFA and inhibits tumor angiogenesis and growth. *Cancer Lett.*, **333**, 159–169.

114. Xiao, F., Zhang, W., Chen, L., Chen, F., Xie, H., Xing, C., Yu, X., Ding, S., Chen, K., Guo, H., et al. (2013) MicroRNA-503 inhibits the G1/S transition by downregulating cyclin D3 and E2F3 in hepatocellular carcinoma. *J Transl Med*, **11**, 195.

115. Cerami, E., Gao, J., Dogrusoz, U., Gross, B.E., Sumer, S.O., Aksoy, B.A., Jacobsen, A., Byrne, C.J., Heuer, M.L., Larsson, E., et al. (2012) The cBio cancer genomics portal: an open platform for exploring multidimensional cancer genomics data. *Cancer Discov*, **2**, 401–404.

116. Polioudakis, D., Bhinge, A.A., Killion, P.J., Lee, B.-K., Abell, N.S. and Iyer, V.R. (2013) A Myc-microRNA network promotes exit from quiescence by suppressing the interferon response and cell-cycle arrest genes. *Nucleic Acids Res.*, **41**, 2239–2254.

117. Bracken, C.P., Gregory, P.A., Kolesnikoff, N., Bert, A.G., Wang, J., Shannon, M.F. and Goodall, G.J. (2008) A double-negative feedback loop between ZEB1-SIP1 and the microRNA-200 family regulates epithelial-mesenchymal transition. *Cancer Res.*, **68**, 7846–7854.

118. Johnston, R.J., Chang, S., Etchberger, J.F., Ortiz, C.O. and Hobert, O. (2005) MicroRNAs acting in a double-negative feedback loop to control a neuronal cell fate decision. *Proc. Natl. Acad. Sci. U.S.A.*, **102**, 12449–12454.

119. Nelson, P.T., Wang, W.-X., Mao, G., Wilfred, B.R., Xie, K., Jennings, M.H., Gao, Z. and Wang, X. (2011) Specific sequence determinants of miR-15/107 microRNA gene group targets. *Nucleic Acids Res.*, **39**, 8163–8172.

120. Kwek, S.S., Roy, R., Zhou, H., Climent, J., Martinez-Climent, J.A., Fridlyand, J. and Albertson, D.G. (2009) Co-amplified genes at 8p12 and 11q13 in breast tumors cooperate with two major pathways in oncogenesis. *Oncogene*, **28**, 1892–1903.

121. Hafner, M., Landthaler, M., Burger, L., Khorshid, M., Hausser, J., Berninger, P., Rothballer, A., Ascano, M., Jungkamp, A.-C., Munschauer, M., et al. (2010) PAR-CliP--a method to identify transcriptome-wide the binding sites of RNA binding proteins. *J Vis Exp*.

122. Xu, Y.-Y., Wu, H.-J., Ma, H.-D., Xu, L.-P., Huo, Y. and Yin, L.-R. (2013) MicroRNA-503 suppresses proliferation and cell cycle progression of endometrioid ndometrial cancer via negatively regulating cyclin D1. *FEBS J.*, **280**, 3768–3779.

123. Forrest, A.R.R., Kanamori-Katayama, M., Tomaru, Y., Lassmann, T., Ninomiya, N., Takahashi, Y., de Hoon, M.J.L., Kubosaki, A., Kaiho, A., Suzuki, M., et al. (2010) Induction of microRNAs, mir-155, mir-222, mir-424 and mir-503, promotes monocytic differentiation through combinatorial regulation. *Leukemia*, **24**, 460–466.

124. Zhou, J. and Wang, W. (2011) Analysis of microRNA expression profiling identifies microRNA-503 regulates metastatic function in hepatocellular cancer cell. *J Surg Oncol*, **104**, 278–283.